Adv Polym Sci (2011) 239: 85–166
DOI: 10.1007/12_2010_96

Published online: 31 July 2010

Rubber–Clay Nanocomposites: Some Recent Results

Amit Das, De-Yi Wang, Klaus Werner Stöckelhuber, René Jurk, Juliane Fritzsche, Manfred Klüppel, and Gert Heinrich

Abstract In order to produce high-performance elastomeric materials, the incorporation of different types of nanoparticles such as layered silicates, layered double hydroxides (LDHs), carbon nanotubes, nanosilica, etc. into the elastomer matrix is now a growing area of rubber research. However, the reflection of the "nanoeffect" on the properties and performance can be realized only through a uniform and homogeneous dispersion of filler particles in the rubber matrix. Generally, the properties and the performance of a reinforced elastomeric composite predominantly depend on the crosslinking chemistry of the rubbers, the nature of the fillers, the physical and chemical interaction of the fillers with the rubber matrix and, especially, on the degree of filler dispersion in the rubber matrix. This article is therefore aimed exclusively at addressing the prevailing problems related to the filler dispersion, intercalation, and exfoliation of layered clays in various rubber matrices and compositions to produce advanced high-performance elastomeric nanocomposites. The effect of two chemically distinct layered nanofillers, namely montmorillonite and LDH, on the curing behavior, mechanical, thermo-mechanical, and dielectric properties, etc. are systematically discussed with respect to various elastomeric systems. Different attempts, such as melt interaction, master batch

A. Das (✉), K.W. Stöckelhuber, and R. Jurk
Leibniz-Institut für Polymerforschung Dresden e.V., Hohe Strasse 6, 01069 Dresden, Germany
e-mail: das@ipfdd.de

D.-Y. Wang
Center for Degradable and Flame-Retardant Polymeric Materials (ERCEPM-MoE), College of Chemistry; State Key Laboratory of Polymer Materials Engineering, Sichuan University, 610064 Chengdu, China

J. Fritzsche and M. Klüppel
Deutsches Institut für Kautschuktechnologie e.V., Eupener Strasse 33, 30519 Hannover Germany

G. Heinrich
Leibniz-Institut für Polymerforschung Dresden e.V., Hohe Strasse 6, 01069 Dresden, Germany
Technische Universität Dresden, Institut für Werkstoffwissenschaft, 01069 Dresden, Germany

dilution techniques, and further chemical modification of the organoclay, have been taken into consideration and a major portion of this paper will be dedicated to these works.

Keywords Layered double hydroxides · Layered silicates · Nanocomposites · Organic modification · Reinforcement · Rubber · Rubber curatives

Contents

1 Introduction

Filler, in general, can be defined as finely divided particles that are often used to enhance the performance and various desirable properties of the host matrix, depending on a typical application. A great deal of research endeavors have been dedicated to the development and the use of different fillers with a dimension at the nanometer level. In rubber technology the term “nano” is not unfamiliar to a rubber specialist. Since the start of the twentieth century, carbon black and silica have been utilized as effective reinforcing agents in various rubber formulations for a variety of applications. The primary particle sizes of these fillers remain in the nanometer range. However, with these conventional fillers the dispersion toward individual

primary particles is significantly difficult to achieve. Nowadays, with the help of modern techniques and methods, particles such as layered silicates, layered double hydroxide (LDH), sol–gel silica, carbon nanotubes, polyoligo sesquesiloxane (POSS), graphene, etc. can be dispersed in a polymer matrix as single isolated particles. For example, organic modification of clay particles could offer totally exfoliated clay layers in some polymer matrices. The outcome of such a technique has been realized by observing a significant improvement in the physical properties of the composites containing a very small amount of nanofiller. Nevertheless, the main advantages of nanofillers are not only to reinforce the rubber matrix but also to impart a number of other properties such as barrier properties, flammability resistance, electrical/electronic and membrane properties, polymer blend compatibility, etc. In spite of tremendous research activities in the field of polymer nanocomposites during the last two decades, elastomeric nanocomposites are still at a stage of infancy as far as their application is concerned. The major challenge in this regard is the replacement of carbon black and silica, which are mostly used in bulk amounts in rubber compositions, by a small amount of nanofillers such as layered silicates in order to achieve a desirable combination of properties. In typical polymer–clay nanocomposites, the filler concentration hardly exceeds 10 wt%, whereas in common rubber composites the reinforcing fillers are often incorporated to above 30 wt%. Therefore it is of great interest to meet desired combinations of different properties in an elastomeric nanocomposite at a very small concentration of filler. The major problem associated with nanoparticles is the degree of dispersion in the rubber matrix. Due to the extraordinarily high viscosity of the rubber matrix, the dispersion of any foreign materials is an extremely challenging task. In order to achieve the desired dispersion of the nanoparticles, various methods have been taken into consideration, such as in situ polymerization, solution casting, latex coagulation, melt compounding, etc. Though rubber is an amorphous material, high temperature shear mixing could be a promising method because it is economical, more flexible in formulation, and the existing facility for compounding and extrusion can be utilized without any complication. This review will discuss rubber nanocomposites based on different rubbers and clays prepared by different compounding techniques.

Layered silicates are now being used widely for preparation of rubber-based nanocomposites. These layered silicates are a class of inorganic materials that have a naturally layered structure. The technique to convert this individually layered structure into a single silicate sheet ($\sim$1 nm thick) in the polymer matrix was first reported by the Toyota group [1]. Among natural clays, montmorillonite (MMT) is the most commonly used layered silicate in nanocomposite preparation due to its high cation exchange capacities, large surface area, good surface reactivity and surface adsorptive properties. Beyond MMT, other clay minerals have been used, such as hectorite, synthetic fluoro-hectorite, sepiolite and synthetic micas [2]. MMT belongs to the 2:1 family of phyllosilicate clay minerals, where each crystal layer is composed of a silica tetrahedral layer sandwiched between two octahedral sheets of aluminum and magnesium hydroxides. In MMT, the isomorphous substitution of Al^{3+} by Mg^{2+}, Fe^{2+}, etc. in the octahedral sheets results in a net negative charge

in the sandwiched layers (Fig. 1). As a result, cations (Na^+, K^+, etc.) and water molecules are intercalated in the interlayer region of MMT. The ideal dispersion of the layered silicate is realized if all the layers are sufficiently separated from one another in the polymer matrix. Unfortunately, the space between two successive layers is too small to allow polymer molecules into it. Organic modification is one of the techniques that can be used to overcome this problem by enhancing the gap distance between the layers. In this method, the cations (present in the gallery to counterbalance the excess charge) are replaced by some quaternary ammonium compound with a long hydrophobic tail. However, organic modification is not a sufficient step to obtain intercalated and exfoliated structures in the rubber matrix. This means that incorporating an organomodified layered silicate in an amorphous rubber medium does not always result in markedly improved mechanical properties of the rubber vulcanizates. This may be due to the inability of a substantial portion of the layered material to dissociate into individual layers. This has also been attributed, in part, to a lack of affinity between organic polymers and the inorganic layered silicates. For most purposes, complete exfoliation of the clay platelets (i.e., separation of platelets from one another and dispersed individually in the polymer matrix) is the desired goal of the formation process. However, this ideal morphology is frequently not achieved, and varying degrees of dispersion are more common. Compared with thermoplastics, the dispersion of organoclay in rubber is more difficult; high viscosity, amorphous nature, and low surface energy of the rubber polymers being the main causes. Significant attention has already been paid to preparation of rubber–clay nanocomposites, characterization of their fundamental behavior, and their use in a wide variety of applications. This review paper is a humble effort by the authors to summarize the outcome of a research project while working on a related project.

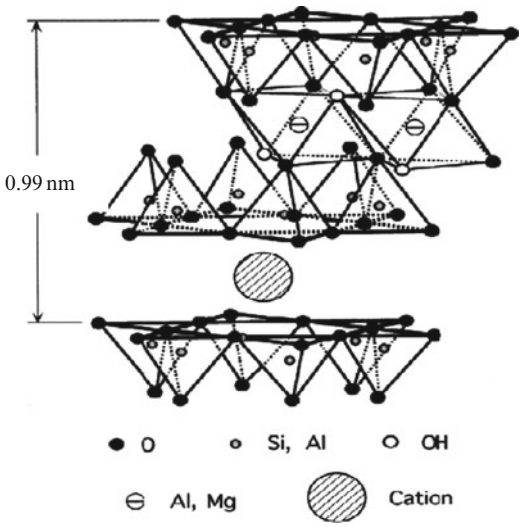

Fig. 1 Chemical structure of MMT showing tetrahedral layer sandwiched between two octahedral sheets

2 Preparation and Properties

2.1 Carboxylated Nitrile Rubber

Carboxylated nitrile rubber (XNBR), a high-performance elastomer, is remarkable for providing vulcanizates that exhibit enhanced tensile strength, elastic modulus, hardness, and improved resistance to tear, abrasion, and the deleterious action of oil. On the other hand, XNBR, being a polar rubber, is expected to interact with layered silicate more efficiently in comparison to other diene rubbers. Only a few reports could be found in the literature concerning the utilization of layered silicate in XNBR. Very recently, it was reported that in the presence of layered silicate the tensile properties of the XNBR vulcanizates were decreased to a considerable extent [3]. The explanation given for this undesired effect is a reduction of the amount of ionic crosslinking due to the consumption of ionic clusters formed by the metal and carboxylic groups by the layered silicates. Successful preparation of layered silicate nanocomposites by a latex coagulation method was also reported [4]. However, this method and the physical properties are not very acceptable for practical applications. On the other hand, direct polymer intercalation and subsequent exfoliation from the melt using various types of polymer compounding equipment provides a straightforward commercial process, but may not be completely effective. Thus, for compounding of nanocomposites, conditions such as the rotor speed (which governs the mixing intensity and heat generation), mixing temperature, and mixing time should still be optimized. Preferred conditions would generally feature a long mixing time at low mixing temperature to avoid undesirable degradation of the materials [5]. The effect of temperature on the intercalation–exfoliation process of the layered silicate in the XNBR matrix has been studied, keeping the other parameters of the internal mixer such as rotor speed and mixing time fixed. In this study, a clay was selected that had been modified with quaternary ammonium salt, and the basal spacing of this organoclay was 2.98 nm. In order to optimize the mixing temperature for this particular compound, the mixing temperature of the internal mixer was selected at 40, 80, 120, and 160°C for four different batches [6]. The amount of organoclay was also varied between 2.5 and 10 phr (part per hundred parts rubber).

As can be seen from the rheometric data summarized in Table 1, the maximum rheometric torque (R_∞) is slightly higher for those mixes derived from the internal mixer at 160°C compared to the curing torque produced by the gum. In most cases, the maximum rheometric torque increases with increasing filler amount. The compounds mixed at 40, 80, and 120°C show lower torque compared to the gum. Additionally, the effect on the curing time of the incorporation of organoclay is negligible. The preliminary rheometric study shows that the compounds mixed at 160°C exhibit better curing activity compared to the compounds mixed at lower temperatures.

XNBR shows excellent physical properties, even in the gum form. Nevertheless, it is expected that with the addition of a reinforcing filler, the properties of XNBR

Table 1 Formulations and curing characteristics of organoclay-filled XNBR vulcanized at 160°C

Mix number[a]	Mixing temperature (°C)	Organoclay loading (phr)	R_∞ (dNm)	Scorch time t_2 (min)	Optimum cure time t_{90} (min)
1	40	0	8.53	1.1	16.4
2	40	2.5	7.84	1.1	16.6
3	40	5	7.82	1.0	16.9
4	40	7.5	7.12	1	16.1
5	40	10	8.17	0.9	16.5
6	80	2.5	7.05	0.8	16.0
7	80	5	7.47	0.8	15.7
8	80	7.5	7.22	0.7	15.5
9	80	10	7.36	0.7	15.8
10	120	2.5	7.23	0.8	15.3
11	120	5	7.44	0.9	16.6
12	120	7.5	7.49	0.8	15.4
13	120	10	7.73	0.7	15.5
14	160	2.5	8.59	0.9	16.8
15	160	5	8.91	0.9	15.9
16	160	7.5	9.39	0.9	16.1
17	160	10	9.31	0.8	15.8

[a]All the mixes were vulcanized with 3 phr ZnO, 2 phr stearic acid, 1.4 phr sulfur, 1.7 phr CBS and 2 phr DPG

will be enhanced. It has been found that even a very small amount of organoclay, like 5 phr, enhances the XNBR physical properties to a remarkable extent.

In Fig. 2, the stresses at 100% elongation (the so-called 100% modulus) are plotted against loading of the clay mixed at different temperatures. It is evident from this figure that with the increase of clay loading, the values rise gradually and the effect is much more pronounced with a higher mixing temperature. A sharp increase in the 100% modulus can be found from 2.5 to 5 phr loading at 160°C mixing temperature. At 5 phr content of organoclay, the 100% modulus was increased by 72% compared to the vulcanizates mixed at 40 and 160°C. It can be said that at elevated temperatures the extent of the intercalation–exfoliation process is facilitated. At lower loading of organoclay (e.g., 2.5 and 5 phr), the addition of the filler mixed at a low temperature like 40°C does not produce any significant change in the rubber matrix in terms of the 100% elongation compared to the gum value. However, in high temperature mixes, the difference is quite remarkable. Obviously, at low loadings and low temperatures, no proper dispersion of the organoclay can take place, which explains the indifferent nature of the physical properties. Also in Fig. 2, the modulus at 300% elongation is plotted against loading of the organoclay and, as observed, a high mixing temperature has a strong effect on the physical properties. For example, at 10 phr organoclay loading, an increment of 39% in the 300% modulus was found for those vulcanizates mixed at 160°C as compared to 40°C. In addition, it can be seen from Fig. 3 that, with the same loading of organoclay, the tensile strength increases quite sharply with increasing temperature.

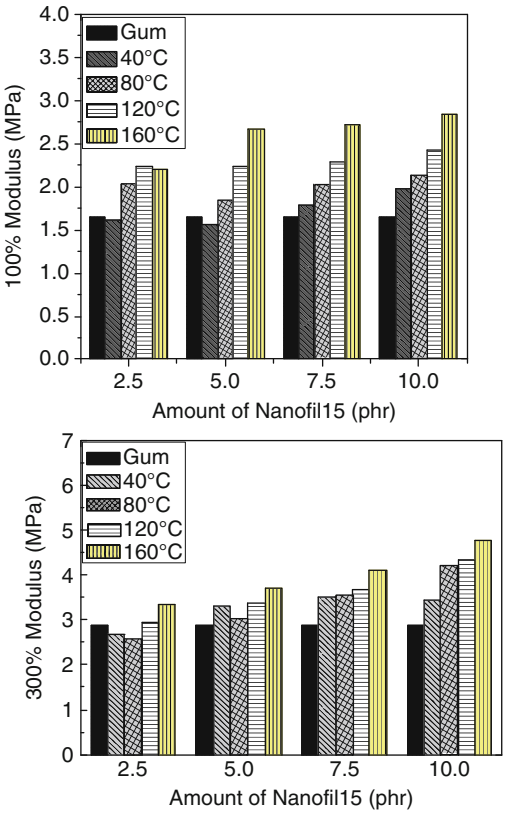

Fig. 2 Variation of 100% (*top*) and 200% (*bottom*) modulus values of XNBR–organoclay composites mixed at different temperatures

The maximum tensile strength was found for the vulcanizates containing 7.5 phr organoclay mixed at 160°C. Here, the increment of the tensile properties is 120% compared to the gum without filler. This type of strong reinforcement is only possible with such a low concentration of inorganic filler if exfoliation and intercalation occur to a considerable extent. In this context, a mechanical scheme is shown in Fig. 4 to explain the exfoliation–intercalation process. It is assumed that at higher mixing temperature, a reaction between the silanol (–OH) groups on the edge of the clay and carboxylic (–COOH) groups of the XNBR takes place, forming an ester-type bond. This type of chemical bond between clay and rubber (first step) is formed under the conditions of high shearing force (internal mixer) and at a high temperature such as 160°C. So, it is expected that the strong shearing force can be transferred from the rubber to the layered silicate and delaminate the staged layers by overcoming the force between two adjacent silicate layers, and ultimately results in an exfoliated clay structure in the rubber matrix. However, the exfoliation and intercalation processes have no significant effect on the elongation at break values, as seen from Fig. 3. The tensile experiment can also be depicted as stress versus strain curves. The stress–strain curves obtained from different mixing temperatures

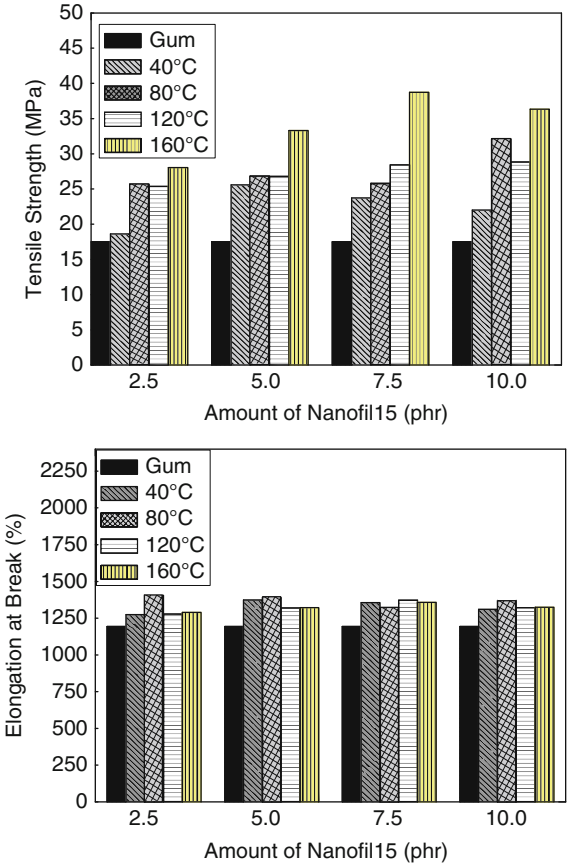

Fig. 3 Variation of tensile strength (*top*) and elongation at break (*bottom*) values of XNBR–organoclay composites mixed at different temperatures

at a loading of clay of 5 phr are shown in Fig. 5. In the low strain region (0–300% elongation), the curves are steeper with the increase of mixing temperature at 5 phr filler loading. So, it can reasonably be said that the reinforcing efficiency of organoclay increases with the increase of mixing temperature, as well as with the shearing forces given on the silicate layers, which also supports the scheme in Fig. 4. It is also interesting to discuss the nature of the stress–strain plot at higher elongation. It is surprising to note the three crossovers of the gum over the 40, 120, and 140°C mixed vulcanizates (circled in Fig. 5). It can be assumed that at low temperature mixing (40–120°C), there may exist some clusters of organoclay in a local filler–filler network. These local networks do not exist in a continuous fashion over the whole rubber matrix but in discrete zones, which affects the homogeneity in the rubber matrix and ultimately deteriorates the reinforcement. At higher elongation, the stress cannot be transferred from one side of the clay cluster to the other side and, as a consequence, the initiation of cracks takes place. On the other hand, for the 160°C mixing temperature, such cluster or aggregate formation

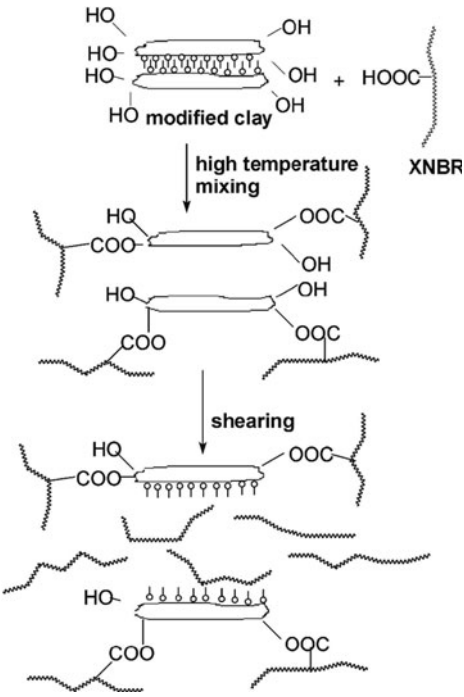

Fig. 4 Mechanism of exfoliation and intercalation of layered silicate in XNBR matrix

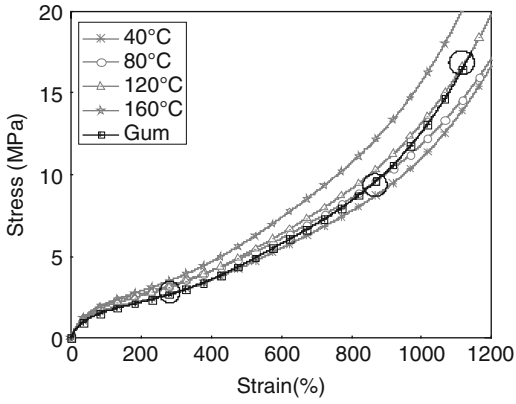

Fig. 5 Stress–strain diagram of rubber composite mixed at different temperatures containing 5 phr organoclay in a XNBR matrix. *Circles* indicate crossover points

of the filler, which can deteriorate the stress at the same strain, is absent. Obviously, this is the possible reason for the strange behavior of the filled vulcanizates. This behavior also supports a better degree of dispersion (through the intercalation–exfoliation process) of the vulcanizates mixed at 160°C.

2.2 Acrylonitrile Butadiene Rubber

Nitrile rubber (NBR) is a copolymer of acrylonitrile and butadiene and is mainly made by emulsion polymerization. This rubber is one of the most-used commercial rubbers for manufacturing technical rubber goods. By selecting an appropriate acrylonitrile content, one can tailor the different properties in order to use NBR for different applications like roll covers, hydraulic hoses, conveyor belting, oil field packers, seals for all kinds of plumbing and appliances, and also for oil-, fuel-, and chemically resistant materials. It has also excellent temperature resistance properties with a wide short- and long-term operating temperature range (as much as −40°C to +125°C). Like most unsaturated thermoset elastomers, NBR requires formulating with added ingredients, and further processing to make useful articles. Additional ingredients typically include reinforcement fillers, plasticizers, weather protectants, and vulcanization packages. Plenty of literature can be found describing where layered silicate has been used as nanofiller in NBR [7–9]. Nanocomposites of intercalated and exfoliated organosilicates in NBR have been prepared by solution-blending methods and dramatic enhancement in the mechanical and thermal properties of NBR are found by the incorporation of very small amount of organosilicates. The degradation temperature for NBR with 10 phr loading of organosilicate was found to be 25°C higher than that of pure NBR [10]. Reactive mixing intercalation was also used for the preparation of NBR–clay composites. Resorcinol and hexamethylenetetramine were used for the reactive mixing process. It was proposed that rubber and organoclay were chemically attached by the help of the resorcinol–tetramine complex. It was also noticed that the *d*-spacing of the layered silicate increased substantially when the resorcinol–tetramine complex was added to the rubber compounds [11]. Layered silicate was modified by *N*,*N*′-dimethylalkyl-(*p*-vinylbenzyl)-ammonium chloride, an ammonium compound containing a vinyl group, and this organoclay was used for the preparation of NBR–clay composites [12]. The mechanical properties as well as gas barrier properties were improved considerably when the organic modifier contained vinyl groups. Measurements of the X-ray diffraction (XRD) of modified clay showed that, as the alkyl chain length was varied from 7, 11, to 17 carbon atoms, the *d*-spacing of the organoclay increased from 1.8, 2.3, to 2.7 nm, respectively. These enhancements probably result from strong interactions between NBR and clay, promoted by the alkyl chains and, possibly, from extra crosslinking of the vinyl groups with rubber molecules. A silane-coupling agent, 3-(mercapto propyl) trimethoxy silane, was added during the preparation of organoclay–NBR composites and it was observed that the silane-coupling agent established a chemical interaction between the silanol group of the silicate layers and the rubber chains [13]. Elastomer nanocomposites consisting of NBR latex and layered silicates were prepared by a modified latex shear blending process aided by ball milling [7]. A schematic presentation is shown in Fig. 6. A partly exfoliated and partly intercalated morphology of the layered silicate was found when the concentration of the layered silicate was less than 7.5%. The tensile and tear strength of NBR–clay increased by 200% and 60%,

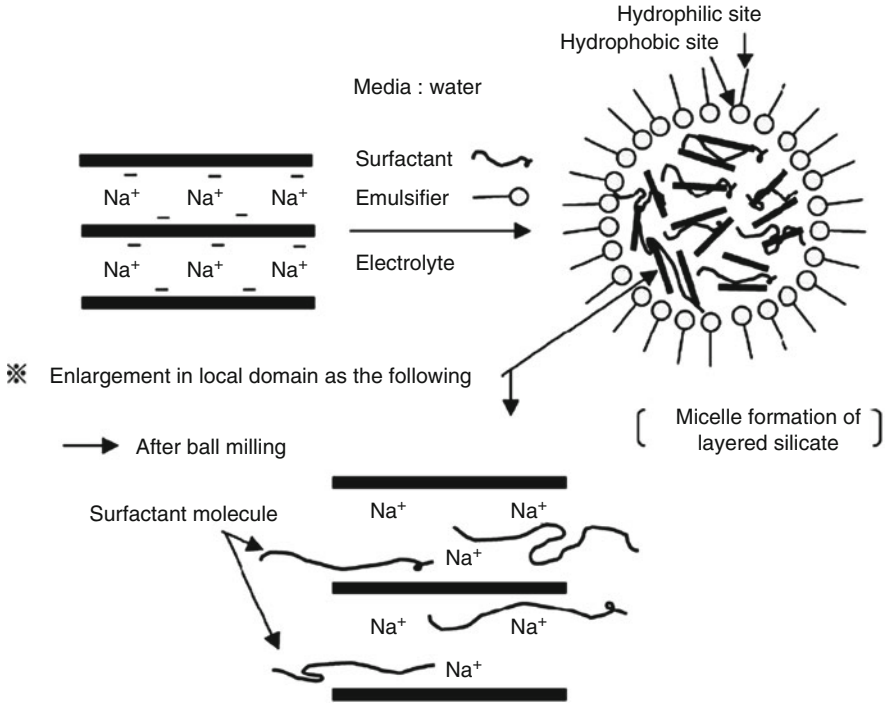

Fig. 6 Latex blending of NBR-layered silicate composites (reprinted from [10], with the permission from Elsevier)

respectively. But there are very few reports [14–18] concerned with the interactions of different types of rubber additives with the layered silicate or with organomodified layered silicate. The understanding of these interactions is very important to exploit layered silicate as potential filler in practical rubber goods. Studies have been done with different kinds of rubber vulcanization packages in order to find the suitability of those ingredients for the reinforcement process by layered silicates. The detailed formulations and processing methods are given in Table 2.

The rheometric study was done at 160°C and the obtained data are shown in Table 3. It can be seen that the addition of 5 phr organoclay in the NBR matrix has a profound effect in raising the ultimate torque for all cases, as compared with gum and the filled systems (comparing mix 1 with mixes 2–5, and mix 6 with mixes 7, 8). This observation indicates that the NBR matrix becomes harder and stronger with the addition of only 5 phr organoclay. The increment of torque with respect to gum is remarkably higher in the case of a peroxide-cured system compared with sulfur-cured systems (Fig. 7a). Here, it can be said that the presence of organoclay in the NBR matrix facilitates the extent of cure (difference between maximum and minimum rheometric torque) of NBR. Among the sulfur-cured systems, the torque decreases with the increase of stearic acid content (Fig. 7b). This behavior is

Table 2 Formulation of NBR filled with organoclay and carbon black

Mix	Accelerator[b]	Organoclay loading (phr)	DCP[c] (phr)	Stearic acid (phr)	ZnO (phr)
1. Gum, sulfur	ZDMC	–	–	1	5
2. Filled, sulfur	ZDMC	5	–	1	5
3. Filled, sulfur	ZDMC	5	–	2	5
4. Filled, sulfur	ZDMC	5	–	4	5
5. Filled, sulfur	ZDP	5	–	2	5
6. Gum, peroxide	–	–	2	–	–
7. Filled, peroxide	–	5	2	–	–
8. Filled, peroxide, sulfur	ZDMC	5	2	2	5
9. Filled, peroxide, ZnO	–	5	2	–	2
10. Filled, peroxide, ZDMC	ZDMC	5	2	–	–
11. Filled, carbon black[a], sulfur	ZDMC	–	–	2	5

[a]Carbon black N330 loading was 5 phr
[b]ZDMC (zinc dimethyldithiocarbamate) and ZDP (zinc dithiophosphate) were used as conventional and multifunctional accelerators, respectively
[c]dicumyl peroxide

Table 3 Physical properties of NBR filled with layered silicate and carbon black

Mix	Maximum rheometric torque (R_∞) (dNm)	Scorch time (t_2) (min)	Cure time (min)	100% modulus (MPa)	Tensile strength (MPa)	Elongation at break (%)	Hardness (Shore A)
1	4.22	0.3	5.4	0.96	2.86	650	49
2	5.14	0.3	4.8	1.48	5.03	586	56
3	4.52	0.3	4.5	1.31	4.58	747	55
4	4.71	0.2	5.8	1.52	8.58	794	59
5	4.45	0.4	23.8	1.38	12.79	1,211	57
6	5.94	0.7	19.1	0.84	2.85	693	47
7	7.75	0.7	18.3	1.51	8.64	826	56
8	6.43	0.2	6.6	1.47	4.86	551	57
9	7.38	0.7	19.6	1.43	7.95	826	56
10	3.10	1.0	24.8	0.90	8.25	1,931	47
11	4.56	0.2	3.6	1.17	5.49	786	52

expected if one considers the softening effect of stearic acid. Generally, 2 phr is the optimum dose of stearic acid in diene rubbers such as natural rubber (NR), styrene butadiene rubber (SBR), polybutadiene rubber, etc. In our study, we varied the stearic acid content to see the effect of this long chain fatty acid on the intercalation–exfoliation process. It is reported that an excess amount of stearic acid in ethylene-propylene-diene monomer (EPDM)–clay nanocomposites facilitated the intercalation process of clay layers [17]. The explanation behind this observation is the chemical interaction between the acid group of stearic acid with the silanol group of silicate. These interactions help the intercalation of the polymer into the

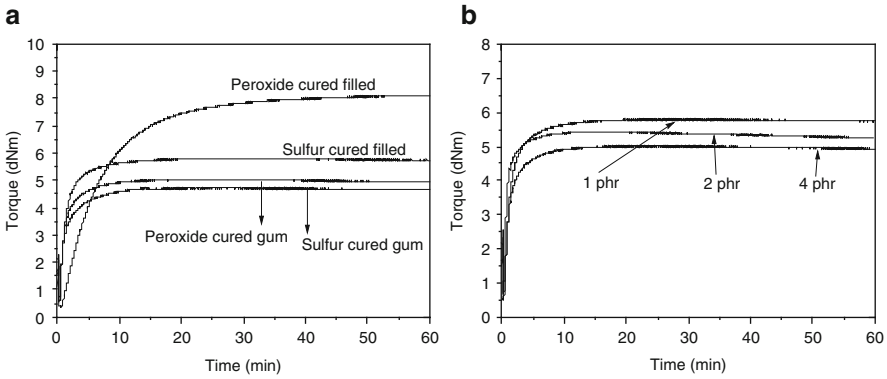

Fig. 7 Rheographs of the layered-silicate-filled NBR cured at 160°C in the presence of sulfur and peroxide (**a**), and different amounts of stearic acid (**b**)

gallery. Here, it is important to note the adverse effect of zinc dimethyl dithiocarbamate (ZDMC) by decreasing the rheometric torque (Table 3) when this additive is added in the peroxide curing (mix 10). It has also been reported that ZDMC-type curatives can help the exfoliation–intercalation process of layered silicates by providing free radicals to the layered silicate–EPDM system [14].

Unfortunately, it was found that, in the presence of peroxide, ZDMC does not facilitate the intercalation process of the clay minerals. On the contrary, it seems that ZDMC consumes the free radicals generated from peroxide and that the rubber matrix remains in the under-cured state with a very low "maximum rheometric torque" value. As far as the scorch time is concerned, there is no such considerable difference between filled and gum compounds. However, prolonged cure time has been observed where ZDP (zinc dithiophosphate, a multifunctional rubber accelerator) has been used as an accelerator in the sulfur curing packages. The stress–strain curves of the crosslinked NBR–silicate nanocomposites are shown in Fig. 8a–c. Figure 8a shows that layered silicate particles can improve the tensile properties significantly, irrespective of their curing type (peroxide or sulfur). This means that it is immaterial to consider the effect of curing type on the reinforcement process since in both cases the nature of the stress–strain curves is identical. It is also evident from Fig. 8a that NBR filled with 5 phr organoclay gives stronger vulcanizates, even compared with NBR loaded with 5 phr carbon black. This behavior can only be explained from the nanoscale distribution phenomenon of layered silicate in the rubber matrix. In this study, a carbon black (N330) with a primary particle size of 28–36 nm was also used. However, the reinforcing efficiency of this black filler at 5 phr loading is much lower than with layered silicate. Obviously, the high aspect ratio (in our case 100–500) of layered silicate is responsible for adding such reinforcing capability to a rubber matrix. The mechanical properties of the NBR vulcanizates are shown in Table 3. In the case of peroxide-cured vulcanizates containing layered silicates, we observed a 179% increment of the 100% modulus

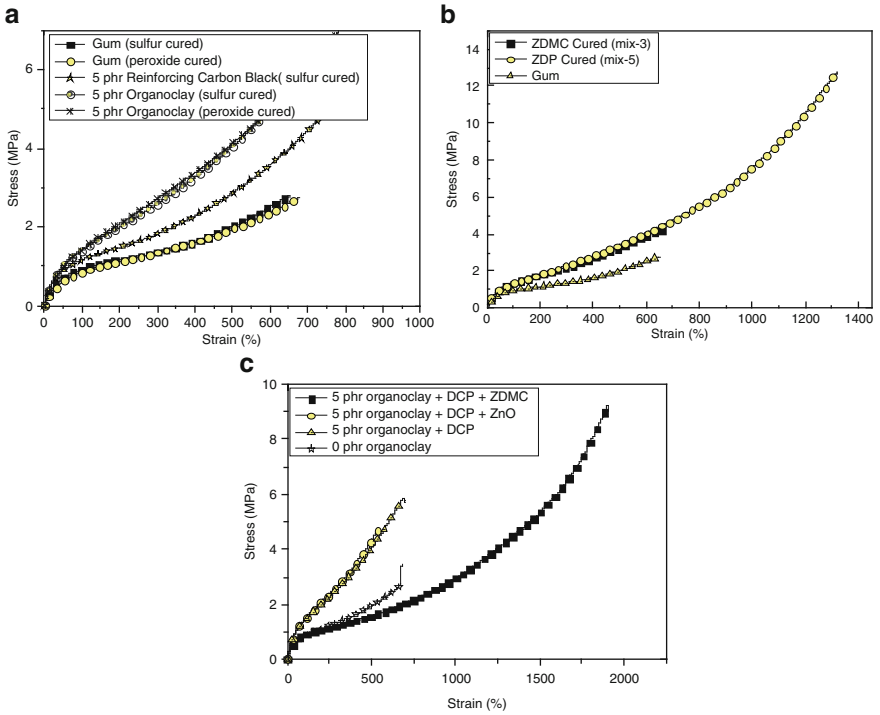

Fig. 8 Stress–strain plots of layered-silicate-filled NBR cured by sulfur and peroxide (**a**), sulfur in the presence of different zinc organic salts (**b**), and peroxide in the presence of different vulcanizing ingredients (**c**)

and 216% increment of the 300% modulus with respect to gum rubber. The tensile strength is about 3–4 times higher, as compared with the corresponding gum vulcanizates, and the Shore A hardness increased by 9 points. These observations indicate that the layered particles are distributed very uniformly and dispersed in intercalated and exfoliated form. The variation of stearic acid content does not affect the modulus of the vulcanizates significantly, but the tensile strength has been increased to a considerable extent with higher elongation at break values. Therefore, it can be concluded that the physical properties in terms of tensile strength can be increased to a considerable extent by a stearic acid content up to 4 phr. This may be due to the fact that stearic acid helps to intercalate rubber chains into the space between two clay layers and thus the reinforcing capability of the given amount of layered silicate is increased and reflected in the higher tensile strength. Ma et al. [17] also found that the tensile strength increased from 4.3 MPa with 2 phr stearic acid to 20.1 MPa with 10 phr stearic acid, without effecting stress values up to 350% elongation in EPDM rubber. Very interesting observations were also noticed when the effect of ZDP was analyzed. About a fivefold increment of tensile strength was achieved with the help of 5 phr organoclay in the ZDP-cured

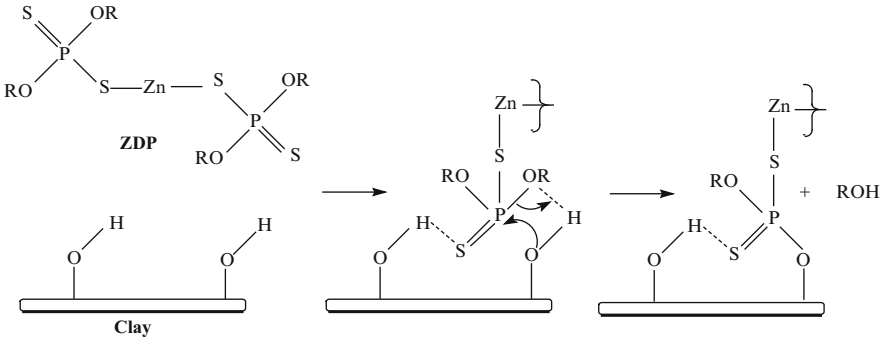

Scheme 1 Probable chemical interaction between ZDP and silanol group of clay surface

vulcanizates (Fig. 8b). Based on the above observations, a reaction mechanism has been proposed (Scheme 1). The ZDP contains active alkoxy (–OR) groups attached to a five-valent phosphorus atom (Scheme 1). This –OR group can interact with the silanol groups of silica to form a Si-O-P linkage [19, 20]. On the other hand, it is an established fact that the thiophosphoryl additive can form a pendant accelerator moiety on the NBR rubber backbone. In our study, it can be imagined that the fragment of accelerator group might interact with the silanol groups of the layered silicate and, thus, the ultimate chemical linkage between layered silicate particle and rubber could offer a higher compatibility between them. It is also evident from Fig. 8b that the ZDP-cured vulcanizates behave at low strains similarly to the ZDMC-cured vulcanizates, but that the stress increases dramatically at high strain. Therefore, it can be reasonably assumed that for NBR vulcanizates that include ZDP, a remarkable increase in stress in the high-strain region results from the effect of molecular chain orientation, together with the resultant orientation of layered silicates brought about by the rubber molecule orientation. Such characteristics of ZDP-cured layered silicate nanocomposites indicate a good possibility for ZDP application in producing rubber-layered silicate nanocomposites. A very peculiar behavior is observed in Fig. 8c: the vulcanizates including ZDMC and peroxide show a much smaller modulus at small strain, but at higher elongation the rubber matrix becomes stronger. The tensile strength and elongation at break values are surprisingly high (elongation at break value 2,000%) as compared to other systems.

2.3 Chloroprene Rubber

Chloroprene rubber (CR) is well known for its high gum vulcanizate strength arising from strain-induced crystallization. The uncured rubber also shows storage hardening due to slow crystallization. It has excellent physical properties, weather

resistance, thermal resistance, and retain able properties at low temperature. Owing to the presence of halogen in the rubber molecule, chloroprene resists burning inherently better than exclusively hydrocarbon rubbers. The durability of chloroprene rubber components is largely dependent on the tear and tensile strength of the matrix. Incorporation of layered silicate into the CR rubber was reported to show an improvement of tear strength of such composites [21]. CR–clay nanocomposites were also prepared by co-coagulating the rubber latex and an aqueous suspension of clay, and a significant improvement of physical properties like hardness, modulus, tensile and tear strength were noticed [22].

How the physical properties of CRs are influenced by the presence of organo-layered silicate was also studied. In this work, different kinds of nanofillers were incorporated and the resulted properties were compared in order to find the most suitable nanofillers for CR [23]. For this reason, LDH in modified and unmodified form both were selected. In fact, LDH is a typical anionic clay, i.e., a host–guest material consisting of positively charged metal hydroxide sheets with intercalated anions and water molecules. It can be represented by a general formula, $[M^{2+}{}_{1-x}M^{3+}{}_{x}(OH)_2]^{x+}A_{x/n}{}^{n-}\ yH_2O$, where M^{2+} and M^{3+} are divalent and trivalent metal cations such as Mg^{2+}, Zn^{2+}, Ca^{2+}, etc. and Al^{3+}, Co^{3+}, Fe^{3+}, respectively, A^{n-} are interlayer anions such as $CO_3{}^{2-}$, Cl^- and $NO_3{}^-$. The anions occupy the interlayer region of these layered crystalline materials. The most common naturally occurring LDH clay is hydrotalcite (Mg-Al type) with the chemical formula $Mg_6Al_2(OH)_{16}CO_3{\cdot}4H_2O$, with a structure represented in Fig. 9.

In principle, the intercalated anions in the gallery of LDHs can be exchanged with wide varieties of anionic species, both of organic and inorganic origin. This gives LDH a great advantage over layered silicates because, for layered silicates, the interlayer species can only be exchanged with a limited range of positively charged cations, mostly based on alkyl-ammonium. This makes LDH a suitable precursor for polymer nanocomposite preparation [24, 25]. In this section, rubber–LDH nanocomposites are described, including the synthesis and characterization of organomodified LDH, preparation of rubber–LDH nanocomposites and their special properties. Details of work on rubber–LDH nanocomposites is discussed at the end of this review in Sect. 6.

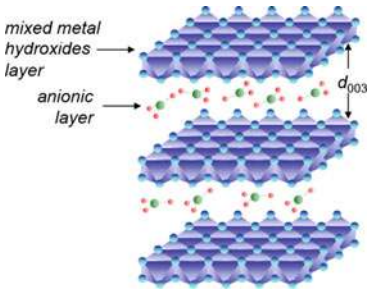

Fig. 9 Representation of LDH crystal structure

The compounding of CR with fillers and vulcanization ingredients was done by a laboratory size open two-roll mixing mill. All the weights are given in parts per hundred parts of rubber and the recipe for the CR compounds is given in Table 4.

The influence of clay and modified clay on the physical properties of the CR vulcanizates at 5 phr filler concentration is given in Table 5. As is obvious, the modulus values (stresses at 100%, 200% and 300% elongation) increase in all cases after filler loading. Again, the extent of improvement depends on the nature of the nanofillers. In the case of unmodified clay, the increase in 100% and 300% modulus is more with LDH, whereas MMT shows similar enhancement as that observed with

Table 4 Formulation of chloroprene rubber compounds

Sample code[a]	CR (g)	Filler (5 g)
CR gum	100	–
CR-LDH	100	LDH
CR-MMT	100	MMT
CR-OLDH	100	OLDH
CR-OMMT	100	OMMT
CR-N220	100	Carbon black

LDH layered double hydroxide, *MMT* montmorillonite, *OLDH* organomodified LDH, *OMMT* organomodified MMT

[a]Each sample contain 4 g MgO, 5 g ZnO, 0.5 g stearic acid and 1 g ethylene thiourea

Table 5 Curing characteristics and physical properties of CR vulcanizates reinforced with different types of clay

Compounds	100% modulus (MPa)	300% modulus (MPa)	Tensile strength (MPa)	Elongation at break (%)	Hardness (Shore A)
CR gum	1.08	1.80	15.65	1,406	52
	(1.20)	(2.12)	(6.19)	(846)	(54)
	+11	+17	−60	+40	
CR-LDH	1.45	2.72	14.99	1,053	54
	(1.51)	(2.97)	(8.21)	(736)	(56)
	+4	+9	−45	−30	–
CR-MMT	1.37	2.45	16.35	1,085	54
	(1.53)	(2.80)	(9.04)	(731)	(57)
	+11	+12	−44	−32	–
CR-OLDH	1.43	2.62	17.16	617	55
	(1.48)	(2.71)	(5.02)	(520)	(56)
	+3	+3	−70	−16	–
CR-OMMT	2.23	3.92	21.22	1,088	62
	(2.41)	(4.23)	(15.02)	(842)	(63)
	+8	+8	−29	−23	–
CR-N220	1.30	2.49	22.72	1,107	54
	(1.56)	(3.34)	(13.04)	(742)	(58)
	+16	+34	−42	−33	–

Data in parenthesis represent the mechanical properties after aging. Data with (+) or (−) signs are the retention values of the mechanical properties

carbon black at the same filler concentration. The organic modification influences the reinforcing efficiency of the clay to a different extent. Whereas organically modified MMT (OMMT) gives significant improvement in modulus values compared to the MMT filled vulcanizates, organically modified LDH (OLDH) gives no significant change. A typical stress–strain plot of these vulcanizates is shown in Fig. 10, where the highly reinforcing nature of OMMT at low strain can be seen. It is apparent that the nature of the surfactants and the net inorganic content of the modified clays play an important role in enhancing the mechanical properties of the CR vulcanizates. It is the inorganic fraction that provides mechanical reinforcement, and the higher its content in the modified clay, the better are the mechanical properties. OMMT contains about 65% of its weight as inorganic layers, whereas OLDH has about 56 wt%. Again, a part of the surfactant in the modified clay might impart plasticizing effects, facilitating polymer chain slippage. As a result, the CR-OMMT vulcanizate shows better mechanical properties than CR-OLDH vulcanizate. Higher surfactant content in OLDH could be a potential cause of lower hardness and elongation at break in CR-OLDH. These values are significantly higher in the case of CR-OMMT among all the CR compounds studied. It can be mentioned here that the considerable decrease of elongation at break of CR-OLDH and the higher elongation at break of CR-MMT cannot be explained solely in terms of the plasticity effect of the surfactant. Other factors like topological constraints, nature of the crosslinks, and crosslinking density also determine the overall physical properties. However, critical discussion of those results is out of the scope of this paper.

Chloroprene rubber also generally offers good compression set properties. A higher percent of the compression set means a permanent deformation of the rubber matrix in a compressed form. The filled vulcanizates show a marked

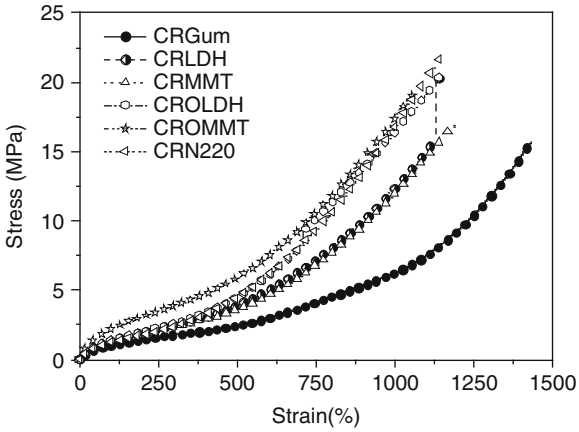

Fig. 10 Stress–strain behavior of CR gum, CR–clay (*CRLDH* and *CRMMT*), CR–modified clay (*CROLDH* and *CROMMT*), and CR–carbon black (*CRN220*) composites

difference in compression set values in comparison to the gum vulcanizate. The compression set values for all these composites are given in Fig. 11. It is evident that addition of nanofiller in the rubber matrix deteriorates the compression set, as expected. This can be explained by the volume fraction of the filler in the rubber matrix. In the study, 5 phr filler was used in all cases, but their volume fractions were different from each other and depend on the density of the related filler. A higher volume fraction means a higher dilution effect with respect to volume and, hence, lowers the compression properties [26]. Of the unmodified nanofillers, LDH gives a higher compression set, whereas MMT and carbon black (N220) produce comparable set properties. Interestingly, organic modification has no influence on the set properties in the case of LDH, whereas OMMT affects the compression set property of the vulcanizates to a considerable extent. The clays impart mechanical reinforcement of a elastomer thorough different mechanism before and after organic modification. The unmodified clays (both LDH and MMT) have polar –OH groups on the edges of the layered particles, which can form hydrogen bonds with the electronegative chlorine atoms in CR. On the other hand, organically modified clays have a higher interlayer distance, which make them suitable for intercalation of polymer chains in their gallery space. Such polymer–filler interaction always helps in better stress transfer through the interface and, hence, result in improved mechanical properties (Table 5). However, the vulcanizate containing the reinforcing carbon black still shows higher tensile strength than the clay-filled vulcanizates.

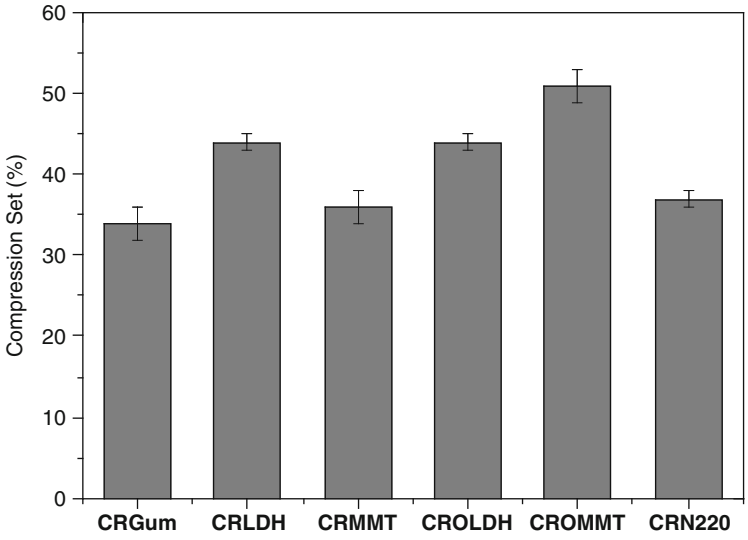

Fig. 11 Compression set properties of CR gum, CR–clay (*CRLDH* and *CRMMT*), CR-modified clay (*CROLDH* and *CROMMT*), and CR–carbon black(*CRN220*) compounds

2.4 Styrene Butadiene Rubber

Increasing attention has been paid to the use of precipitated silica as a reinforcing filler for green tire tread formulations to produce high-performance tires, showing improved rolling resistance and wet grip behavior. Here, the development of advanced coupling silanes provides a better compatibility between rubber and silica, resulting in reduced rolling resistance and improved fuel economy. Solution styrene butadiene rubber (S-SBR) is widely used nowadays as a tire tread, especially in tires of passenger cars where low rolling resistance and high wet grip are the challenging properties. Some literature [27–30] has been found concerning emulsion styrene butadiene rubber (E-SBR) in combination with nanofillers, but the mechanical properties are too poor to consider these systems as potential candidates for practical applications. Ma et al. [27] reported a preparation method using a latex compounding technique, but in this work the ultimate mechanical properties were not described. Mousa et al. [28] describe nanocomposites of SBR and organoclay mixed by a two-roll mill that showed a tensile strength of more than 12 MPa at 10 phr silicate content, but without any direct evidence of formation of a nanocomposite (as shown by XRD or TEM studies). With the help of the latex-compounding technique, layered silicate was dispersed in SBR latex and 3-aminopropyltrietoxysilane was simultaneously intercalated into clay galleries during the co-coagulating procedure [29]. Hexamethoxy methylmelamine (HMMM) has been used as a dispersion agent in the preparation of SBR-layered silicate nanocomposites [30]. According to that study, HMMM swelled the clay gallery, thus facilitating the intercalation of the rubber chain (as revealed by wide-angle X-ray diffraction, WAXD). HMMM in the presence of organoclay enhanced the elastic modulus with minor effects on tensile strength and further modified the ultimate elongation through either a change in the degree of reinforcement or through matrix plasticization. It was also observed that the pristine clay (Na-MMT) is less effective in enhancing the physical properties of the composites because of its narrower gallery height, stronger interplatelet forces, and higher polar surface. In order to improve the interfacial interaction between clay and SBR, unsaturated organic ammonium chloride *N*-allyl-*N*,*N*-dimethyl-octadecylammonium chloride was introduced for in situ modification of MMT before latex compounding. The SBR nanocomposites thus obtained showed a dramatic improvement of tensile strength (from 4 to 18 MPa) [31]. The same group of researcher also successfully utilized hexadecyl trimethyl ammonium bromide and 3-aminopropyl triethoxy silane in SBR–clay nanocomposite preparation. They found that partly rubber-intercalated and partly modifier-intercalated structures were developed during rubber compounding and curing. The tensile strength and the 300M of modified SBR–clay nanocomposites were found to be three times higher than those of gum compounds [32] SBR–clay was prepared by the surface modification of pristine clay by allylamine, and very interesting properties were found for these nanocomposites [33]. The allylamine molecules served here as a coupling agent between the SBR chain and the surface of the clay

platelets. SBR with different styrene contents were considered for the preparation of rubber–clay nanocomposites. The styrene content of rubber had a pronounced effect on the properties of the nanocomposites and it was found that with increasing styrene content, the physical properties increased [34]. It was also observed that systems cured with peroxide and/or sulfur displayed similar strength, but higher elongation, and that slightly lower modulus values were obtained with the sulfur-cured system. Rubber compounds based on SBR/BR blends containing layered silicate and bis(triethoxysilylpropyl-tetrasulfan) (TESPT) were prepared and characterized by Ganter et al. [35]. The results obtained from those nanocomposites were compared with composites containing commercially available silica. It was found that organoclay vulcanizates exhibited enhanced hysteresis when compared to silica compounds. This observation was related to orientation and sliding of anisotropic silicate layers, as determined by online wide-angle X-ray scattering (WAXS) measurements during cyclic tensile testing. The origin of the higher hysteresis could be explained by reorientation of aggregates in systems with matrix–filler coupling, and by irreversible orientation and sliding of silicate layers for systems with intercalated structure. Preparation and properties of SBR–clay have been discussed by considering different organic amines with different chain lengths as the organic modifier of the clay. With increasing chain length of the amine, there was an increase in tensile strength. A sudden increase in modulus was observed when the chain length of the amine contained ten carbon atoms [36]. Recently, it has been reported that organoclay-based S-SBR polymer nanocomposites could be prepared by using XNBR as a vector to transfer layered silicate into the S-SBR matrix. The rubber matrix obtained in such a way provided a significant improvement of physical properties with only small amounts of filler in the rubber matrix [37, 38]. In that study, the highly polar XNBR was used as a vector to transfer layered silicate into S-SBR. A large amount of organomodified clay was blended into a XNBR matrix at high temperatures (160°C) by an internal mixer and, subsequently, the obtained product was used as a master batch and mixed into the S-SBR. In this way, attempts were made to obtain a good degree of exfoliated clay in the nonpolar S-SBR matrix. This process was described as a new preparation method for S-SBR–clay nanocomposite by a melt compounding route [37, 38].

The contents of the master batch are presented in Table 6. The torque and temperature behavior against time recorded during the mixing process is shown in Fig. 12a, b. The temperature during the mixing process increased up to 180°C. For loadings up to 30 phr organoclay, the torque during mixing of XNBR and organoclay remained constant. In contrast to higher loadings, the torque increased significantly. This effect might be an indication of the intercalation process. The formulations and cure characteristics for the mixing of the master batch with S-SBR are given in Table 7. The curing additives were chosen according to a typical silica-filled green tire formulation. In the samples SB-00 to SB-14 (Table 7), different loadings of master batches were used in various combinations. The samples SB-15 and SB-16 were formulated to obtain the effect of an unfilled XNBR in the composite. Concerning the XNBR content, these mixes are equivalent to SB-12

Table 6 Preparation of the XNBR master batch

Master batch	XNBR (g)	Organoclay (g)
M-30	100	30
M-40	100	40
M-50	100	50
M-60	100	60

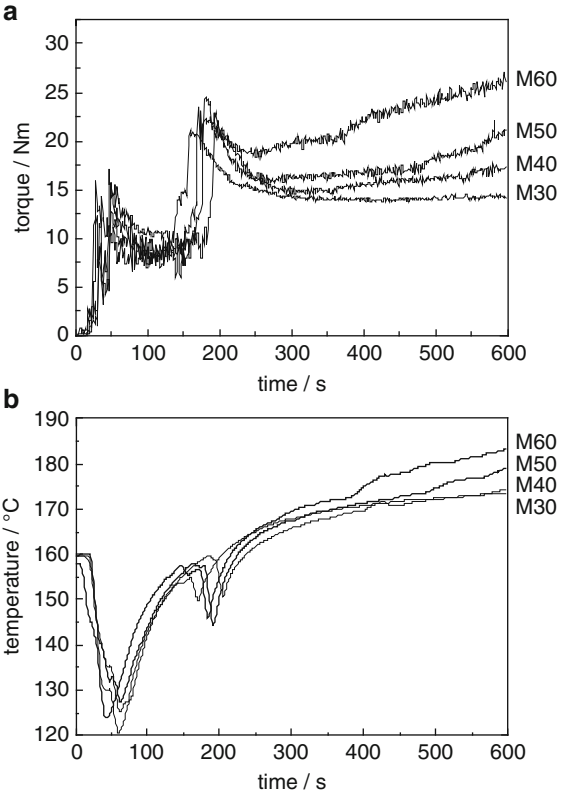

Fig. 12 Time–torque curves for master batch preparations with XNBR and organoclay in the internal mixture at 160°C and 50 rpm rotor speed (**a**). Time–temperature curves for master batch preparations with XNBR and organoclay in the internal mixture at 160°C and 50 rpm rotor speed (**b**)

and SB-14, respectively. It is evident from the table that samples of pure S-SBR and XNBR (SB-00 and XN-00) have higher "maximum rheometric torque" (R_∞) than the XNBR-containing SBR samples. However, for every single master batch system, the torque decreases with the increasing amount of master batch. Evidently, the presence of two different kinds of rubber with different polarities provides less torque than expected. The scorch safety seems to be independent of master batch content as well as filler loading. The cure times (listed in Table 7) decrease for the XNBR/S-SBR blend as compared to the pure rubber samples SB-00 and XN-00. For every single master batch system, the cure time increases with the amount of

Table 7 Recipes for the S-SBR vulcanizates

Mix number	SBR (g)	M-30 (g)	M-40 (g)	M-50 (g)	M-60 (g)	XNBR (g)	Maximum rheometric torque (R_∞) (dNm)	Scorch time (t_2) (min)	Optimum cure time (t_{90}) (min)
SB-00	100	–	–	–	–	–	7.05	1.72	9.59
SB-01	100	5	–	–	–	–	6.40	1.09	8.83
SB-02	100	10	–	–	–	–	6.28	1.24	8.99
SB-03	100	15	–	–	–	–	5.87	1.67	9.00
SB-04	100	–	5	–	–	–	6.45	1.24	8.50
SB-05	100	–	10		–	–	6.40	1.27	9.20
SB-06	100	–	15	–	–	–	6.18	1.27	10.17
SB-07	100	–	–	5	–	–	6.66	1.18	7.61
SB-08	100	–	–	10	–	–	6.37	1.26	8.51
SB-09	100	–	–	15	–	–	6.22	1.25	9.29
SB-10	100	–	–	–	5	–	6.91	1.15	9.14
SB-11	100	–	–	–	10	–	6.78	1.30	9.60
SB-12	100	–	–	–	15	–	6.40	1.28	11.44
SB-13	100	–	–	–	20	–	5.48	1.31	11.59
SB-14	100	–	–	–	30	–	5.49	1.34	14.72
SB-15	100	–	–	–	–	9.37	5.87	1.49	8.11
SB-16	100	–	–	–	–	18.75	4.99	1.53	10.21
XN-00	–	–	–	–	–	100	8.53	1.12	16.47

master batch due to the increasing XNBR to S-SBR ratio. For different master batches, the cure time decreases with the amount of organoclay in the master batch, except for the M-60 containing samples; here the cure time is higher than expected. It is also worth mentioning that without organoclay the cure time of an XNBR/S-SBR blend is lower. The results are not quite understood; probably different acceleration effects are taking place due to the well-known interaction of Zn ions with carboxylic groups and the presence of ammoniums salts and organoclay. Results of tensile tests are shown in Fig. 13.

In Fig. 13a, the stress values at 200% elongation are plotted against the amount of clay and compared to the samples without clay, which are plotted against the amount of XNBR. It is evident from this figure that with an increase of filler amount, the modulus increases with a linear tendency. In contrast, in the unfilled samples containing S-SBR and XNBR the corresponding physical values are very low. These observations prove that the obtained higher rigidity of the rubber matrix is not caused by the XNBR part, and support the suggestion of reinforcement caused by the organoclay. Concerning tensile strength, the above-mentioned result is also reflected in Fig. 13b. For the samples with around 5 phr loading, sevenfold higher values in tensile strength are obtained compared to the gum. It is also found from the polynomial fit curve in Fig. 13b that there is a maximum of tensile strength at around 5–8 phr organoclay. At higher loading, the clay particles aggregate and obviously do not contribute to the ultimate strength of the composite. Stress–strain plots are shown in Fig. 13d for some composites. In these stress–strain curves,

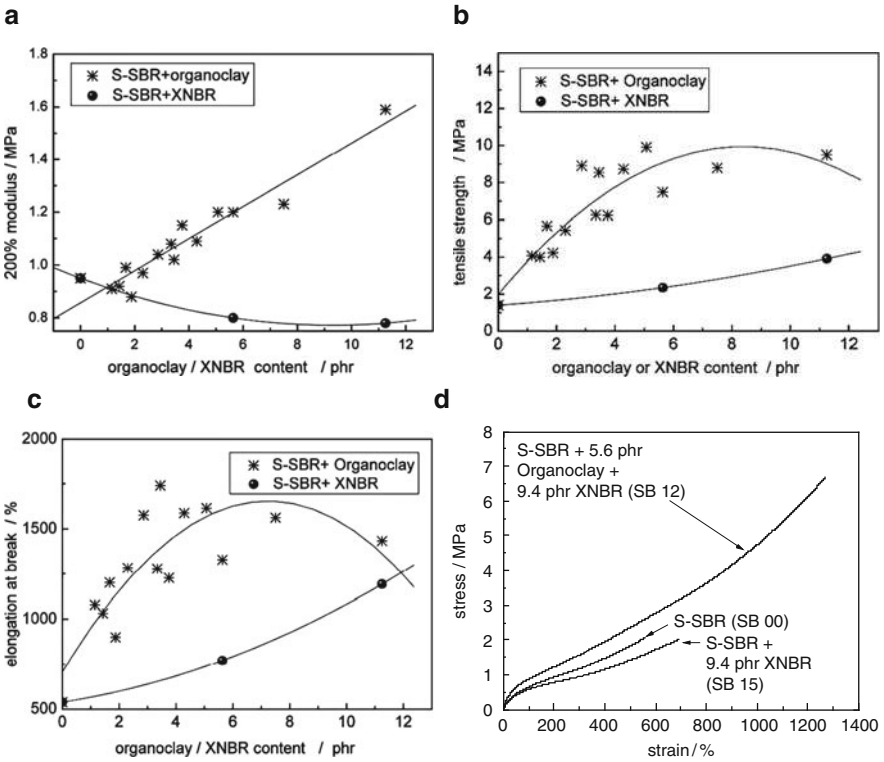

Fig. 13 Variation of 200% modulus (**a**), tensile strength (**b**), and elongation at break (**c**) with the amount of organoclay and XNBR. Stress–strain diagram of the organoclay–rubber composites (**d**)

a remarkable effect of the organoclay is observed. The mechanical properties of the nanocomposites become enhanced at higher elongations due to the presence of a small amount of organoclay (4.6 phr) in the rubber matrix. In contrast, an equivalent amount of XNBR without any filler deteriorates the corresponding mechanical properties of the composites. Therefore, it can be stated that the organomodified nanoclay not only provides excellent reinforcement effects to the rubber matrix, but also acts as a compatibilizer between polar and nonpolar rubber, as mentioned before. The investigated types of rubber nanocomposites also showed very high elongation at break values, as presented in Fig. 13c. High elongation at break values are otherwise found in silica-filled rubber compounds [19], with a direct chemical bonding between polymer and silica. In the rubber nanocomposites made of XNBR, S-SBR, and organoclay it can be assumed that the surface silanol groups of the layered silicates react with the carboxyl groups of the XNBR and, thus, direct rubber–filler bonds are formed. In this way, the high elongation properties can be explained.

3 Characteristics of the Nanocomposites

3.1 Dynamic Mechanical Properties

3.1.1 Temperature Dependencies

The dynamic mechanical thermal analyzer (DMTA) is an important tool for studying the structure–property relationships in polymer nanocomposites. DMTA essentially probes the relaxations in polymers, thereby providing a method to understand the mechanical behavior and the molecular structure of these materials under various conditions of stress and temperature. The dynamics of polymer chain relaxation or molecular mobility of polymer main chains and side chains is one of the factors that determine the viscoelastic properties of polymeric macromolecules. The temperature dependence of molecular mobility is characterized by different transitions in which a certain mode of chain motion occurs. A reduction of the tan δ peak height, a shift of the peak position to higher temperatures, an extra hump or peak in the tan δ curve above the glass transition temperature (T_g), and a relatively high value of the storage modulus often are reported in support of the dispersion process of the layered silicate.

The DMTA measurements were done with organoclay-filled XNBR rubber (Fig. 14). The glass transition process was detectable at $-10°C$ and the tan δ maximum decreased slightly with increasing filler content. An additional relaxation process at high temperatures was confirmed, and a shift to a higher temperature of this process with incorporation of organoclay was also noticed [39]. When a temperature sweep was done against the dynamic properties, at constant strain

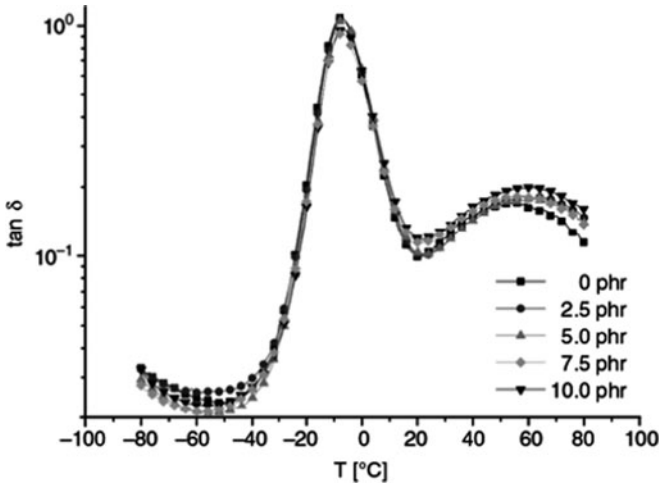

Fig. 14 Tan δ versus temperature of the XNBR vulcanizates containing different amounts of organolayered silicate

and frequency, the vulcanizates of CR showed two different transitions. At low temperature, the relaxation is correlated to the polymer glass transition, and at high temperature another relaxation occurs due to the melting of the crystalline domains in chloroprene rubber [23].

Figure 15 depicts the tan δ versus temperature plots of the CR vulcanizates containing different types of nanofiller. All the samples show the same T_g irrespective of their filler type. But the peak height is maximum for OLDH and minimum for OMMT. It is well known that the smaller the tan δ peak, the higher is the reinforcing efficiency of the related filler. Reduced chain mobility owing to physical and chemical adsorption of the CR molecules on the filler surface causes a height reduction of the tan δ peak during dynamic mechanical deformation. So, the presence of only 5 phr OMMT reinforces the CR to a great extent. For better understanding the reinforcement process, the storage tensile modulus (E') is plotted against temperature. Very interesting information can be derived from Fig. 16a.

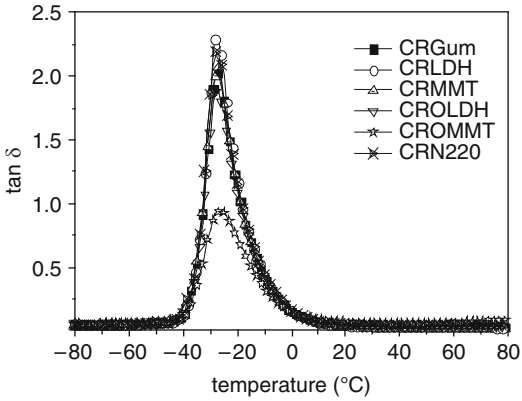

Fig. 15 Effect of different kinds of nanofiller on the dynamic loss tangent of CR vulcanizates with temperature

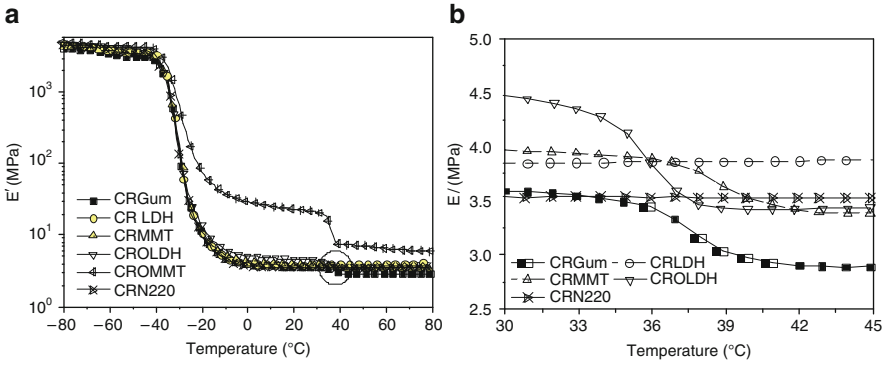

Fig. 16 Variation of storage modulus with temperature in CR vulcanizates containing different kinds of nanofillers (**a**). Circled region is shown in more detail in (**b**)

At room temperature, the storage modulus is increased about fivefold in OMMT-filled vulcanizates. The increment of this value in CR-OLDH is much smaller, whereas unmodified clays give hardly any change at room temperature.

Figure 16a also depicts the influence of nanofillers on the crystallization behavior of the CR vulcanizates. The modified nanofillers facilitate crystal formation, which is reflected in a loss in storage modulus value in the melting region of the crystal domains. This loss is very strong in the case of CR-OMMT, indicating that CR molecules crystallize better in the presence of OMMT. The unmodified MMT also behaves similarly but to a lesser extent (Fig. 16b), which is very similar to the behavior observed in the gum vulcanizates. But, unmodified LDH and N220 completely suppress the crystallization process, resulting in no change in the storage modulus value in this temperature range. This effect is important as it can be utilized to control the storage stability of CR compounds.

A strong influence of the organoclay on the dynamic mechanical properties of S-SBR has also been noticed [38]. Figure 17a, b displays the storage shear modulus G' and the mechanical loss factor tan δ as a function of temperature for the samples that contain the organoclay–XNBR master batch. The sample with 5 phr master batch (SB-10) and the unfilled S-SBR sample (SB-00) show no significant difference in G' at room temperature. In contrast, the samples with higher loadings show strong reinforcement effects, resulting in higher G' values. For example, in the case of SB-11 (10 phr master batch) the increment was 1.65 times compared with S-SBR gum. Additionally, it is interesting to discuss the effect of XNBR on the dynamic mechanical performance of the SBR vulcanizates. The vulcanizate containing 9.37 phr XNBR (SB-15) without filler, equivalent to SB-12 concerning the amount of XNBR, shows a smaller G' value at room temperature, indicating a lack of compatibility between the two different rubbers. Therefore, it can be stated that organophilic layered silicates not only reinforce the rubber matrix, but also act as a compatibilizer between the different phases. Figure 17b shows the tan δ plot of the nanocomposites. Usually, the tan δ peak indicates the compatibility of two

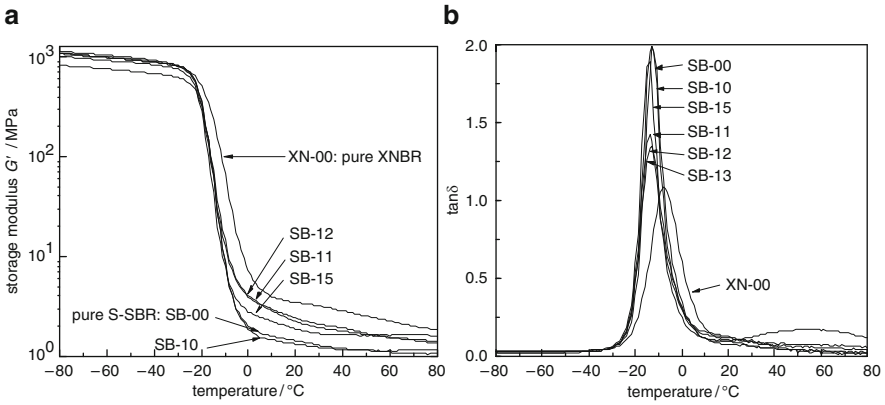

Fig. 17 Temperature dependence of G' (**a**) and tan δ (**b**) of the organoclay-filled S-SBR rubber composites

polymers in a rubber blend for all nanocomposites. Here, the small amount of XNBR in the samples does not contribute enough thermal relaxation to show a peak broadening due to heterogeneity, hence, a single tan δ peak is obtained. For pure XNBR (XN-00), a second broad tan δ peak appears at higher temperatures (40–80°C). In the cure recipe, zinc oxide was used, which can establish a metallic carboxylate linkage by ionic crosslinking in the rubber matrix. Consequently, these ionic rubber chain segments form ionic clusters, as discussed for the multiple cluster model [40]. The mobility of the rubber chain is restricted in the vicinity of these associated multiples, and this type of ionic force or Columbic attraction force opposes the polymer chain mobility. Therefore, a secondary transition appears at higher temperatures.

It is also interesting to compare the height of the tan δ peak of the composites. It is noteworthy that the smaller the tan δ peak, the higher the reinforcing efficiency of the related filler. Accordingly, for the sample with 5 phr master batch (SB-10) no reinforcement effects can be detected, in contrast to the vulcanizates containing higher loadings of organoclay. Here, a sharp decrease in height of the tan δ peak was observed for SB-11 and SB-12 composites. Especially for SB-11, the peak height was decreased to 32%. The peak height for the sample containing S-SBR and XNBR without organoclay is only slightly decreased, confirming the results for G'.

3.1.2 Strain Dependencies

The interaction between two fillers particles can be investigated by measuring the "Payne effect" of a filled rubber compounds. In this measurement, dynamic properties are measured with strain sweep from a very small deformation to a high deformation. With the increased strain, the filler–filler network breaks and results in a lower storage modulus. This behavior is commonly known as the Payne effect [41]. To study this behavior, strain sweep measurements were done with the filled chloroprene rubber vulcanizates. Figure 18 shows the variation in the storage modulus, G', with the double strain amplitude of the cured rubber sample. There is apparently no change in the nature of variation in the storage modulus in the vulcanizates with increasing double strain amplitude. So, it can be said that no Payne effect can be observed in any of the vulcanizates. This indicates that at such a low filler concentration (5 phr) there exists no significant filler–filler network structure. However, the absolute value of G' is always higher for the filled vulcanizates than for the gum. The OMMT gives maximum increase in G' value among the vulcanizates, showing again its superior reinforcing nature. Taking the absolute value of G'as a measure of reinforcement by the nanofiller, the nanofillers can be ranked according to their reinforcing efficiency, i.e., OMMT > OLDH > LDH > MMT > carbon black (N220).

The strain dependence of the elastic storage modulus of clay-filled NBR has been measured and the results compared with those of unfilled vulcanizates. The corresponding data are shown in Fig. 19. From this figure it is revealed that there is no Payne effect, because the G' values do not decrease with the increase in strain

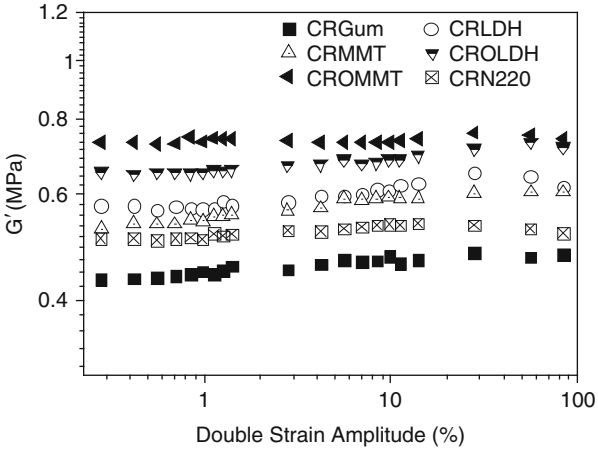

Fig. 18 Strain dependence of G' of CR vulcanizates filled with different kinds of nanofillers. The measurements were done by a moving die rheometer (Scarabaeus SIS V50) applying sinusoidal strain at constant frequency of 0.1 Hz at 60°C

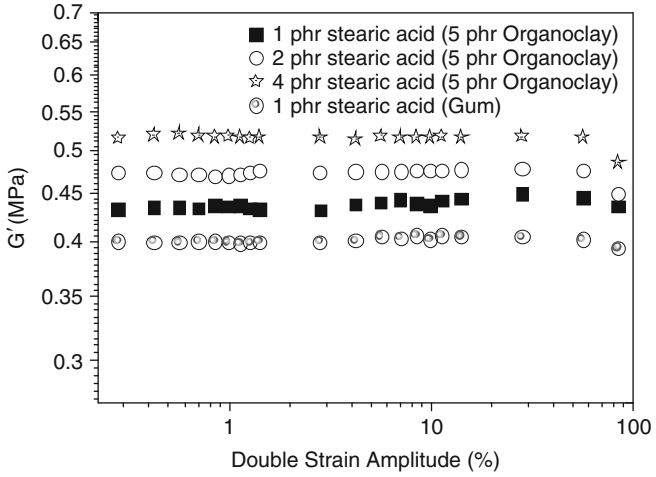

Fig. 19 Strain dependence of G' for NBR vulcanizates filled with organoclay

amplitude. Although the absolute value of G' is not large at this small filler loading, there is some effect on the absolute value of G' from the stearic acid content in the curing packages. With increasing stearic acid content, the absolute value of G' also increases. That means that stearic acid supports the exfoliation–intercalation process of the layered silicate, leading to dissociation into very fine nanometer-sized particles. It may be speculated that stearic acid first enters into the gallery gap and

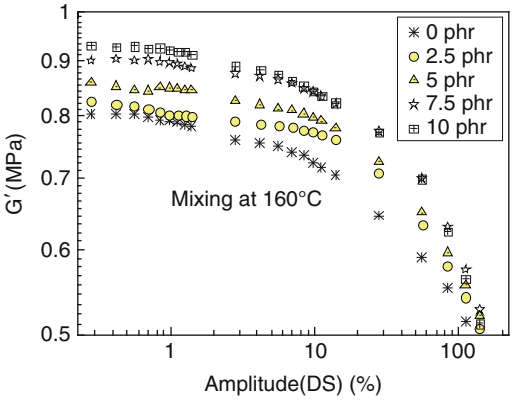

Fig. 20 Strain dependence of G' for XNBR vulcanizates filled with organoclay

opens up the layered silicate cluster, thus paving the way for intercalation of other macromolecular chains. The dynamic property measurements at low strain amplitude were also discussed for the filler–filler network as well as for the rubber–filler network at low loading of nanoclay fillers in XNBR matrix. The plots of G' versus double strain amplitude of the 160°C mixed vulcanizates are shown Fig. 20. It is evident from this figure that up to 10% strain amplitude, the values of G' are remaining constant in all cases and thereafter a significant decrease in the values is observed. This decrease in G' is due to slippage of the moving die during the measurements at higher amplitude and not due to the breaking of the filler–filler networks since the same observation is made in the case of the unfilled rubber. The G' value increases with the increase of filler loading, which is attributed to the hydrodynamic effect of rigid solid particles. At high-temperature mixing (ca. 160°C) the silicate layers are more homogeneously distributed, mainly through the exfoliation process, which enhances the reinforcing capability of the filler significantly. With the increase of filler amount, the formation of bound or trapped rubber (dead rubber) is enhanced. Subsequently, the effective volume of the filler is increased substantially, thereby raising the modulus of the rubber matrix.

3.2 Dielectric Analysis

Dielectric relaxation study is a powerful technique for obtaining molecular dipolar relaxation as a function of temperature and frequency. By studying the relaxation spectra, the intermolecular cooperative motion and hindered dipolar rotation can be deduced. Due to the presence of an electric field, the composites undergo ionic, interfacial, and dipole polarization, and this polarization mechanism largely depends on the time scales and length scales. As a result, this technique allowed us to shed light on the dynamics of the macromolecular chains of the rubber matrix. The temperature as well as the frequency window can also be varied over a wide

range. The effect of clay addition on the polymer chain dynamics has been well studied [42]. Rao et al. observed from dielectric spectra that addition of clay in the polymer matrix affected the mobility of polymer chains significantly [43]. Hernandez et al. studied the effects of clay proportion and nanoscale dispersion on the dielectric response of poly(vinyl alcohol)–bentonite nanocomposites [44]. They observed that better clay dispersion promotes chain mobility for the low-temperature secondary relaxations with a plasticization effect. Page and Adachi [45] have reported the dielectric relaxation behavior of nanocomposites based on Na-MMT with a series of polymers. They observed that all the nanocomposites exhibited an additional relaxation process at a temperature below the T_g of the pure polymer, which was assigned to the segmental motion of the chains intercalated in the MMT interlayers. The dielectric response of layered-silicate-reinforced natural and polyurethane rubber nanocomposites was studied by Psarras et al. [46]. They observed that both the α-relaxation and β-relaxation were less affected by the presence of the layered silicates in the polyurethane rubber nanocomposites. In addition to these relaxations, they also observed interfacial polarization present in the nanocomposites.

Due to its carboxyl groups and the nitrile content, the high polarity of XNBR provides large values for the dielectric loss ε''. Examples of the results obtained for the dielectric loss ε'' in dependence of temperature and frequency for the unfilled sample and the sample filled with 10 phr organoclay are given in Fig. 21. In all measurements the glass transition process (α-process) due to the cooperative segmental motion of the chain is observable, forming a characteristic temperature- and frequency-dependent Vogel–Fulcher behavior. At low temperatures, the Arrhenius-activated β-process can be observed in all samples, which is due to local fluctuations of chain segments or side groups. At high temperatures, the value of ε'' increases extremely with increasing temperatures probably due to conductivity effects or

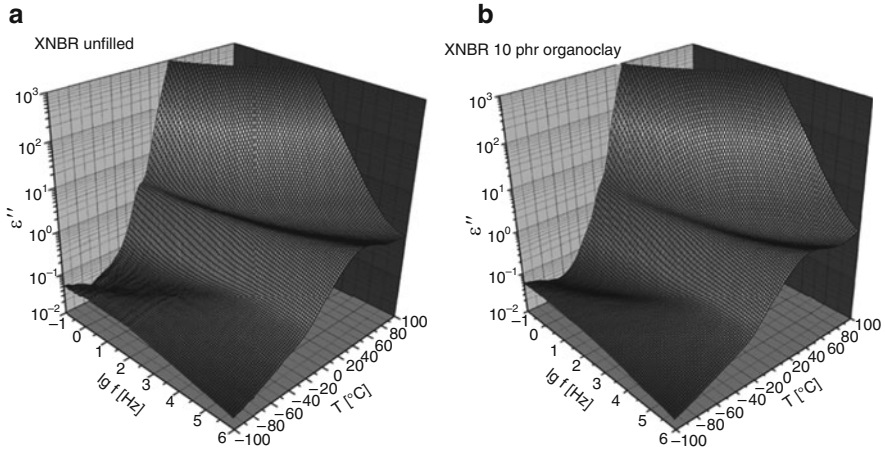

Fig. 21 Temperature and frequency dependence of dielectric loss ε'' for the unfilled XNBR sample (**a**) and the sample filled with 10 phr organoclay (**b**)

electrode polarization. To analyze the high temperature part of the spectra, the analyzing procedure developed by Steeman and van Turnhout [47] was applied to the measured data, which has been reviewed by Wübbenhorst and van Turnhout [48] This method is based on the Kramers–Kronig relation (**1**), saying that both ε' and ε'' carry the same information about relaxation processes and are related by a Hilbert transformation:

$$\varepsilon''(\omega_0) = \frac{\sigma_{dc}}{\varepsilon_0 \omega_0} + \frac{2}{\pi} \int_0^\infty \varepsilon'(\omega) \frac{\omega_0}{\omega^2 - \omega_0^2} d\omega, \tag{1}$$

where σ_{dc} is the direct current conductivity, ε_0 the permittivity of space, and ω the alternating current frequency.

In this procedure, the derivation of ε' denoted as ε''_{deriv} (2) is used in order to obtain narrow and sharp peaks and to eliminate conductivity effects due to the independence of ε' from ohmic conductivity:

$$\varepsilon''_{deriv} = -\frac{\pi}{2} \frac{\partial \varepsilon'(\omega)}{\partial \ln \omega} \approx \varepsilon''. \tag{2}$$

In the case of broad relaxation peaks like those of the α-transition, (2) is almost exact and the derivative reproduces the measured frequency-dependent ε'' data. By contrast, for narrow Debye-like processes a peak sharpening is observed and $\varepsilon''_{deriv} \sim \omega^{-2}$ is obtained for large frequencies instead of $\varepsilon'' \sim \omega^{-1}$ [48]. This opens the interesting possibility of obtaining more information about low-frequency relaxation processes of dipolar origin, which are often obscured by strong electrode polarization due to ionic conduction. In the XNBR samples under consideration, ionic conductance probably results from mobile protons due to the presence of carboxylic groups and other ions obtained from the addition of the processing agents zinc oxide and stearic acid. The blocking of ions at the metallic electrodes leads to the pronounced relaxation process at high temperatures and low frequencies (as observed in Fig. 22). This electrode polarization refers typically to sharp Debye-like processes and therefore the application of the derivative considered in (2) is expected to sharpen this undesired peak. As a consequence, other processes of dipolar origin may become visible in the spectrum. The spectrum of the XNBR sample filled with 10 phr is shown in Fig. 23 after applying the derivative method (2). Interestingly, the resulting spectra now show an additional relaxation process at higher temperatures in all investigated samples, which obviously was obscured in the original spectra by the strong electrode polarization. Though this process is still partly covered by electrode polarization, its location and activation behavior can be evaluated. The plot of ε''_{deriv} against temperature at 0.5 kHz given in Fig. 23 shows an increase of the dielectric loss with increasing content of organoclay. Additionally, a reasonable shift to higher temperatures of this process from the unfilled sample to the filled samples is detectable. This shifting indicates different processes in the unfilled and the filled samples.

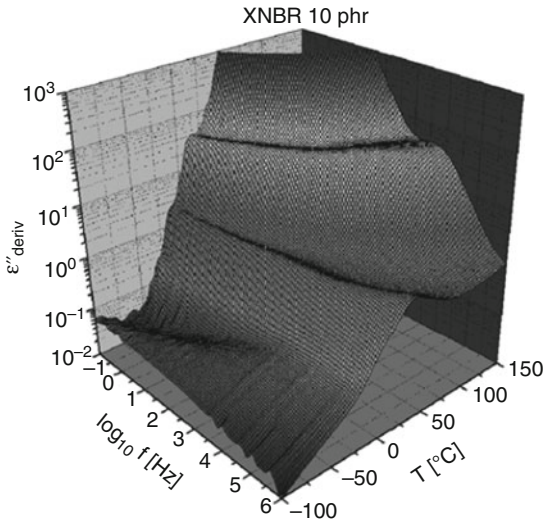

Fig. 22 Temperature and frequency dependence of ε''_{deriv} after applying the analyzing procedure (2) for the XNBR filled with 10 phr organoclay

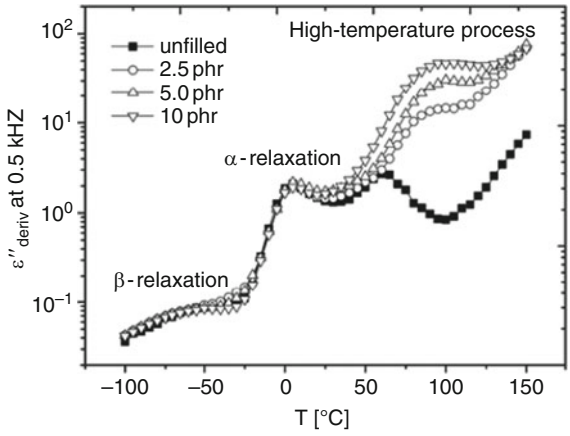

Fig. 23 Plot of ε''_{deriv} against temperature at 0.5 kHz for XNBR samples

3.3 XRD Studies

X-ray diffraction is a powerful tool for obtaining a preliminary understanding of the intercalation–exfoliation phenomena of a nanocomposite containing layered silicates. However, though it is a necessary study, it is still not sufficient to establish nanoscale dispersion. Insufficient amount of clay, preferred orientation of clay (especially in the case of rubber processing and molding) and peak broadening always lead to a wrong interpretation of the disappearance of a basal peak like that of the <001> plane of a MMT-type clay [49, 50].

Morphological characteristics of LDH, MMT and their modified forms (OLDH and OMMT) have been discussed with respect to their WAXS patterns [23] (Fig. 24). The 2θ-values along the x-axis can be converted to layer spacing values (d) by the Bragg relationship ($\lambda = 2d \sin \theta$, where λ is the wavelength of the radiation). The interlayer distance (d-value) calculated using Bragg's equation from the first-order basal reflection <001> of the unmodified clays is 0.76 nm in LDH and 1.32 nm in MMT. The higher d-value in the case of MMT is due to the difference in the thickness of the crystal layer, which is about 1.0 nm in MMT and 0.48 nm in LDH. The intercalation of organic molecules in the interlayer space causes shifting of the <001> reflection to the lower 2θ value (Fig. 24). This shifting corresponds to an enlargement of the d-value to 2.96 nm in OLDH and 2.98 nm in OMMT. The two nanofillers were incorporated into CR and different intercalation behaviors were noticed.

After incorporation of modified and unmodified clay into the CR matrix. very interesting X-ray scattering patterns can be noticed (see Fig. 25). It is evident from this figure that in every case, three very sharp common peaks appear at 1.41, 0.93, and 0.70 nm. Because these peaks are present even in the gum without any filler, it means that rubber additives (like ZnO and MgO along with stearic acid and organic accelerator, or the intermediate products arising from the vulcanization reaction) are responsible for this scattering. However, it is surprising to observe that no peak corresponding to the <001> plane of layered silicate in the lower angle region appears for the OMTT-filled CR matrix. Here, we can say that CR, being a polar rubber, finely distributes the layers in the exfoliated form, at least under the area where the measurement was done. It was also noticed that in the presence of OMMT and MMT the peak at 1.41 nm became broader than the gum peak. The broad peak, which merges with the gum rubber peak at 1.41 nm, may come from some crystalline phase of CR itself. In our dynamic mechanical study it is suggested that CR undergoes partial crystallization in the presence of nanofillers, especially in

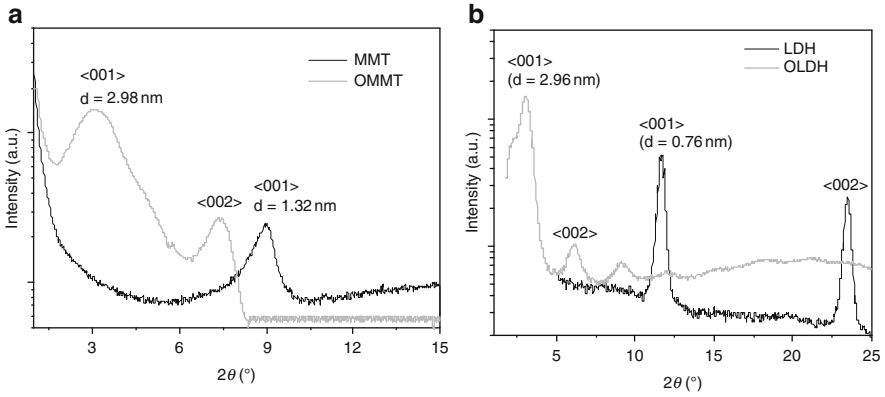

Fig. 24 WAXD analysis of two types of clays and their organically modified forms: MMT and OMMT (**a**), LDH and OLDH (**b**)

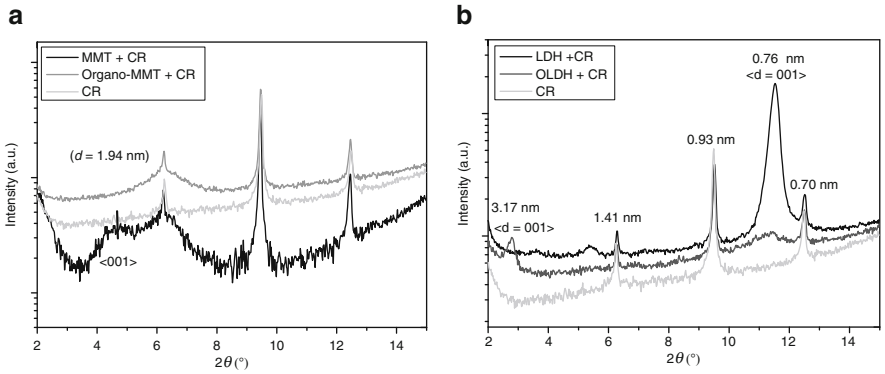

Fig. 25 WAXD analysis of clay-filled nanocomposites: MMT and OMMT in CR matrix (**a**), LDH and OLDH in CR matrix (**b**)

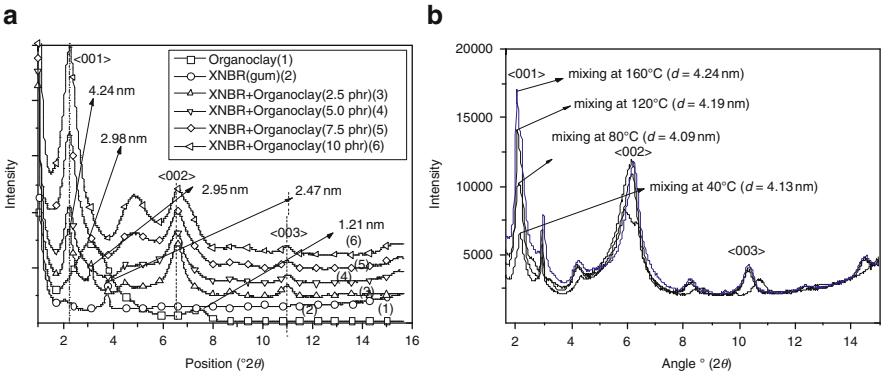

Fig. 26 WAXD patterns of XNBR reinforced with different amounts of organoclay (**a**), and 2.5 phr organoclay-filled XNBR vulcanizates processed at different temperatures (**b**)

the presence of OMMT. So, the presence of these crystalline state responses in the XRD, and the broad peak, coincide with the gum rubber diffraction seen at 1.41 nm.

The WAXS patterns of unmodified clay (MMT) also provide one broad peak in the CR matrix around the *d*-spacing of about 1.94 nm. So, the expansion of the gallery gap takes place from 1.32 to 1.94 nm. This small increment of the *d*-spacing might arise due to partial distortion of the layered silicate, especially in the edge area of a stack of layered silicate. As far as the XRD traces of LDH and OLDH in CR matrix are concerned, it is observed that the reflection from the <001> plane of OLDH comes at 3.17 nm, whereas the pure OLDH has a reflection of the same plane at 2.96 nm. Here, some sort of interaction of the CR chain is also taking place. However, in the case of pure LDH there is no change in the peak position after incorporation of the LDH in the CR matrix.

As far as the XRD patterns of organoclay-filled XNBR are concerned (Fig. 26a), the reflection from the <001> plane is shifted towards a lower angle for all vulcanizates,

which were prepared under different mixing conditions. In each case, the interlayer spacing increased to about 4 nm. This observation supports the suggestion that intercalation takes place for all the vulcanizates containing organoclay. The appearance of other peaks can also be seen at higher angles, and the intensities of these entire peaks rise with the increase of organoclay. This observation signifies that a higher amount of organoclay in the rubber matrix results in an ordering of the clay particles and that the particles are rearranged into a more coherent symmetrical form. It is also evident from Fig. 26a that at 2.47 nm, a sharp peak appears in the XNBR gum compound. The presence of this sharp peak can also be observed in the 2.5 phr organoclay-containing XNBR sample, but the position is shifted toward lower angles and the corresponding spacing value is 2.95 nm. Moreover, the same peak has disappeared or merged with the main scattering coming from organoclay at relatively higher loading of organoclay and may be due to the in situ formation of zinc stearate. At higher loading of organoclay, the excess zinc oxide might be adsorbed on the surface of clay whereby the in situ formation is hindered. For organoclay, the main peak appears at 2.98 nm and there is also another reflection at 1.21 nm. So, XRD studies indicates that intercalation is a common process for 2.5–10 phr organoclay mixed at 160°C.

The effect of mixing temperature on the microstructure has also been analyzed by WAXS experiments. The X-ray scattering patterns were taken from 2.5 phr organoclay-filled XNBR matrix at different mixing temperatures. It is observed from Fig. 26b that in all vulcanizates the space gap increases to some extent from low temperature mixing to high temperature mixing. It can also be seen from this figure that the peak intensity becomes more intense in the high temperature mixed compound. Here, higher peak intensity means a higher number of intercalated layered species under the X-ray beam. The maximum number of intercalated layered silicate species appears in the rubber matrix from the aggregated mass of the organoclay. In the case of low temperature mixing, a fewer number of intercalated clay layers makes the reflection of X-rays less intense from the corresponding <001> plane.

Figure 27 shows the XRD patterns for the rubber compounds of S-SBR with organomodified layered silicate. A broad peak appears for unmodified clay at about 1.32 nm, and this peak is shifted to 2.98 nm for organoclay. For SB-10, SB-11, and SB-12 the corresponding values are 4.43, 4.01, and 3.82 nm, respectively. The diffraction peak of organoclay is obviously shifted toward the low angle direction, indicating the effective expansion of the interlayer distance of the clay. However, the interlayer spaces decrease with an increase of clay content. Obviously, with increasing filler loading, not enough space is available for the clay layers to occupy their positions without sacrificing the gallery gap.

3.4 Transmission Electron Microscopy

TEM pictures give direct visual evidence about the nanoscale dispersion of the layered silicate in the rubber matrix. Figure 28a shows the XNBR matrix filled with

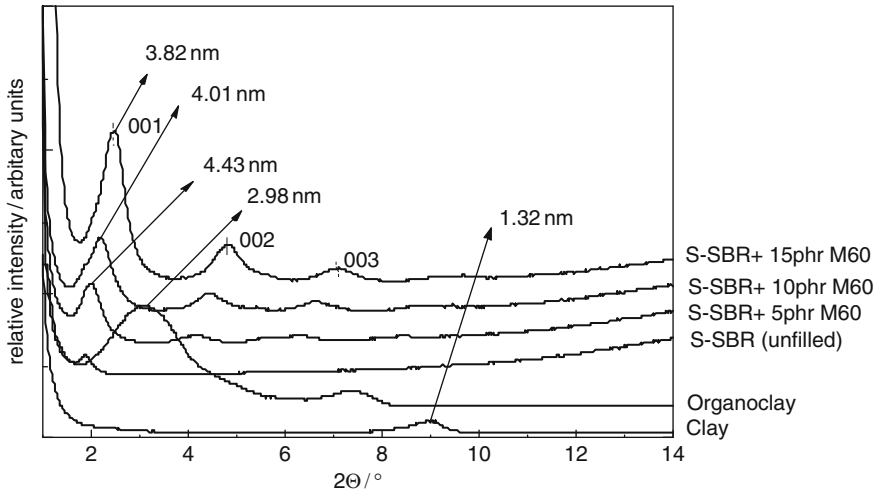

Fig. 27 XRD spectra of S-SBR reinforced with OMMT. Note that the spectra of the related clays and organoclays are also shown. The position of the (001), (002), and (003) reflexes are indicated

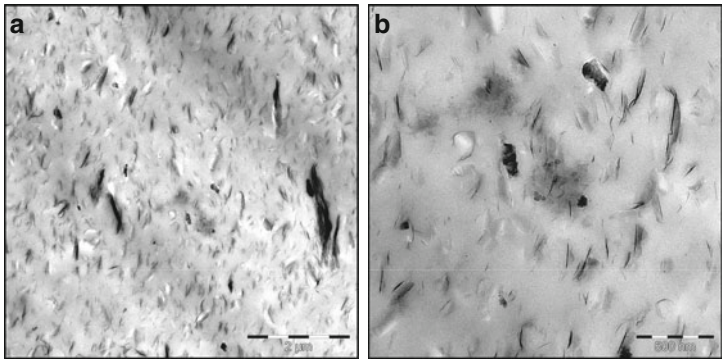

Fig. 28 TEM image of the XNBR nanocomposite containing 5 phr organoclay (**a**), and magnification of a selection (**b**)

5 phr organoclay mixed at 160°C, where most of the clay layers are oriented towards the north–south direction. The silicate layers in the rubber matrix are oriented preferably during the processing, which is quite common for layered silicate–rubber nanocomposites [51]. A closer look shows the simultaneous existence of intercalated and exfoliated structures. Nevertheless, there are still a few agglomerated staged silicate layers, so total exfoliation and intercalation are not achieved through melt processing. Figure 28b is a magnified selection from Fig. 28a. Here, most of the visible silicate layer thickness is around a few nanometers and the length is some multiple of a hundred nanometers. Therefore, it may

be considered that most of the silicate layers are not monolayers but couples of layers attached together.

TEM pictures have been taken from the SBR vulcanizates containing 1.8 phr organoclay. Figure 29a shows the TEM picture of SBR matrix in which the layered silicate was dispersed by using XNBR as a carrier of the organoclay.

It is observed from this figure that there are a lot of small dark lines preferably oriented in a north–south direction. Here, the organoclay is distributed evenly in the whole rubber matrix. Some small dark clusters are shown enlarged in Fig. 29b. These structures are formed due to the separation of the polar XNBR phase from the nonpolar S-SBR matrix. Furthermore, exfoliated layers of organoclay are visible in the interface between the two polymer phases, which obviously promotes a better compatibility between XNBR and S-SBR phases. Figure 29c displays the TEM

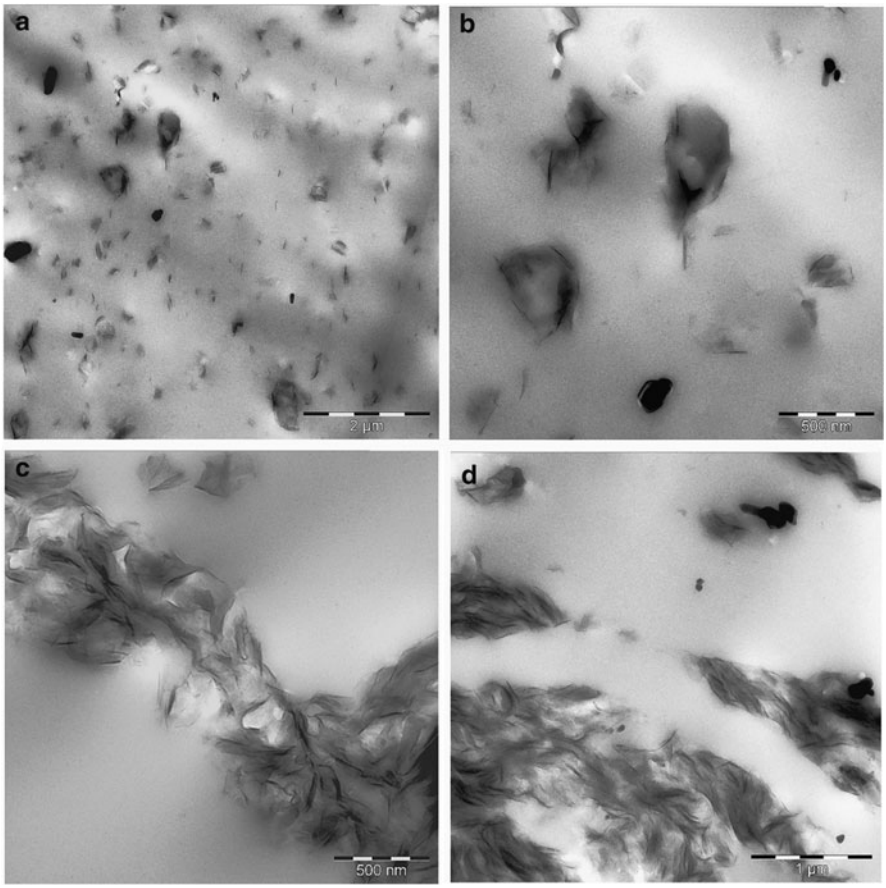

Fig. 29 TEM images of the SBR nanocomposites containing 1.8 (**a**), 1.8 (**b**), 3.7 (**c**), and 5.6 (**d**) phr of organoclay

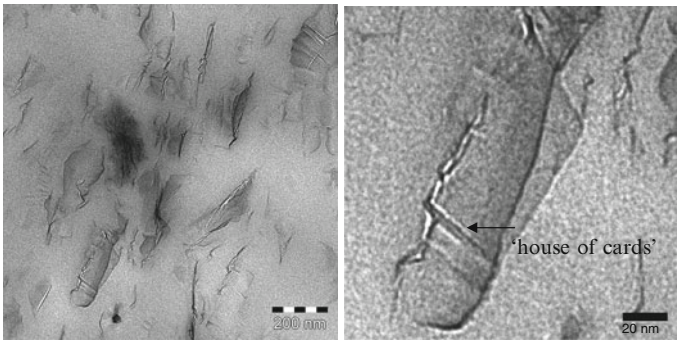

Fig. 30 TEM images of organoclay-filled CR. Image on the *right* is a magnified selection

image of SBR in which the organoclay concentration was 3.7 phr. Here, layered silicates form local network-like structures remaining in the exfoliated and intercalated state. The rise of such network structures is also seen in the vulcanizate containing a higher amount of organoclay (~5.6 phr, Fig. 29d). No considerable amount of staged (tactoid) layered silicates is observed. Therefore, we conclude that most of the layered silicates are either exfoliated or intercalated and that the rubber matrix is sufficiently reinforced.

A good state of dispersion of the organoclay has been found in the CR matrix. The exfoliated structure can be directly observed from the TEM of the OMMT-filled CR composite (left-hand image in Fig. 30). It is noticed from this micrograph that all silicate layers are exfoliated and distributed very nicely throughout the whole rubber matrix. It is also observed that some of the exfoliated clay platelets form a "house of cards" structure (right-hand image in Fig. 30).

3.5 Infrared Spectroscopy

Fourier transform infrared spectroscopy (FTIR) can give useful information on chemical changes occurring in the system. However, the detection of such changes can be challenging because often the new species produced are present in small amounts and they are chemically similar to the initial material, so their absorption peaks are masked.

However, such spectroscopic techniques are sometimes used to more fully understand rubber–clay interaction. For example, XNBR filled with organoclay gave very interesting results with IR studies.

The attenuated total reflection infrared (ATR-IR) spectra taken from organoclay, pure XNBR, and the vulcanizates filled with 5 phr clay and mixed at 160°C temperature, are depicted in Fig. 31. From the spectra, the principal peaks for the pure organoclay are observed at 2,846 cm^{-1} and 2,920 cm^{-1} due to the presence of

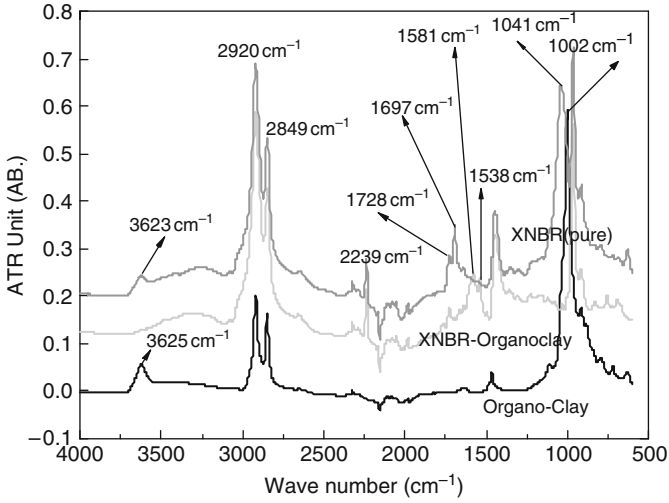

Fig. 31 ATR-IR spectra of organoclay, pure XNBR (gum), and 5 phr organoclay-filled XNBR vulcanizates mixed at 160°C

aliphatic $–CH_2$ groups in the hydrophobic tails of the quaternary amine modifier. The broad peak at around 3,625 cm^{-1} of this material can be attributed to the presence of –OH groups on the surface. The characteristic absorbance for –Si–O–Si– in the clay is seen at 1,002 cm^{-1}.

The pure XNBR gives rise to peaks at 2,920 and 2,849 cm^{-1} due to the $–CH_2$ groups on the rubber backbone. The characteristic absorbance for –C–N of XNBR can be observed at 2,239 cm^{-1}. Peaks in the range of 1,500–1,700 cm^{-1} result from the >C=O group of the carboxylic part in the rubber. The absorption at 1,040 cm^{-1} arises on account of the asymmetric stretching of the –C–OH in the carboxylic functionality.

A careful study of the spectra for the composites shows that the peaks at 1,695 and 1,728 cm^{-1} disappear in the cured XNBR matrix, being replaced by two new ones at 1,538 and 1,581 cm^{-1}, respectively. These can be assigned to the >C=O stretching in different chemical environments. The former peak corresponds to the stretching in the tetra-coordinated zinc–carboxylate complex, whereas the latter peak corresponds to that in a hexa-coordinated complex. The peak at 3,625 cm^{-1} on the pure organoclay spectrum disappears in the nanocomposite spectrum, probably owing to an interaction with the –COOH groups on the XNBR. Furthermore, a shift in characteristic absorbance of –Si–O–Si– is observed from 1,002 cm^{-1} to around 996 cm^{-1}, i.e., 6 cm^{-1} to the lower energy side. A similar transition has been observed by Katti et al. [52] in their studies on polyamide–MMT nanocomposites. The linkage of the COOH group on XNBR with the silanol–OH on the clay surface that, in turn, is already bonded with the silica tetrahedral of MMT, may have caused this shift of the Si–O stretching band in the composite with respect to the organoclay.

4 Effect of Vulcanization Ingredients

4.1 Effect of Sulfur and Peroxide Curing

It is well known that the presence of an amine compound in the curing recipe provides curing acceleration during the vulcanization process. So, it is easy to speculate that the quaternary ammonium compound (QUAT), which was used for the organic modification of MMT clay, can easily participate in the sulfur curing mechanism. There are some reports about these interactions and, in most cases, they give rise to collapse of the gallery height of the silicate layers [53, 54]. Since in peroxide curing the amine has no role, it is very interesting to compare the clay morphology in the rubber matrix cured by sulfur and with that in matrix cured by peroxide. The XRD peaks at $2\theta = 3.06°$, 5.47°, and 7.55° represent the diffraction of the <001>, <002> and <003> crystal surface of the silicate particle in the sulfur-cured NBR vulcanizate (Fig. 32a), corresponding to a *d*-spacing of 4.35, 1.97, and 1.34 nm, respectively. This indicates that a relatively large gallery expansion in layered silicates has taken place during the melt mixing and curing at 160°C. In the case of peroxide-cured systems (Fig. 32b), there were three diffraction peaks of the <001>, <002>, and <003> crystal surface at 2θ equal to 3.38°, 5.68° and 7.80°, respectively, corresponding to a *d*-spacing of 3.69, 1.88, and 1.26 nm, respectively. Here, the gallery gap between two parallel plates of silicate particles has also been increased to a considerable extent. However, the extent of space increment is higher in the case of the sulfur-cured system as compared with the *d*-spacing from the master batch (Fig. 32c). It is also interesting to note that the peak intensity of diffracted X-ray obtained from peroxide-cured compounds is much higher than for sulfur-cured systems (Fig. 32a, b). In this case, the higher peak intensity might come from higher orientations in a particular direction of the layer structure [55]. Higher orientation could be due to the fact that the alignment of layered silicates particles are probably uniformly distributed towards one direction, i.e., highly ordered orientation of clay platelets in peroxide-cured matrix. In contrast, there is no such orientation effect in the sulfur-cured matrix, though both of them are processed through the same procedures. This behavior can be directly justified by TEM. Figure 33a, b displays the TEM pictures of sulfur- and peroxide-cured vulcanizates. It is evident from Fig. 33b that a large number of parallel dark lines are oriented in one direction, and that these dark lines represent the silicate particles in the rubber matrix. On the other hand, Fig. 33a does not show a special orientation of the silicate particles in the rubber matrix. It is also observed that in both cases the particles are distributed very uniformly in the whole visual region. The orientation of the layered silicate in the rubber matrix is expected in the direction of flow during the processing of the rubber compound [51]. This type of spatial distribution should, apparently, be observed irrespective of the curing type because, in both cases (sulfur or peroxide), the rubber compounds were processed by the same procedure. However, sulfur-cured rubber matrix shows an isotropic arrangement of the silicate particles. Therefore, it was assumed

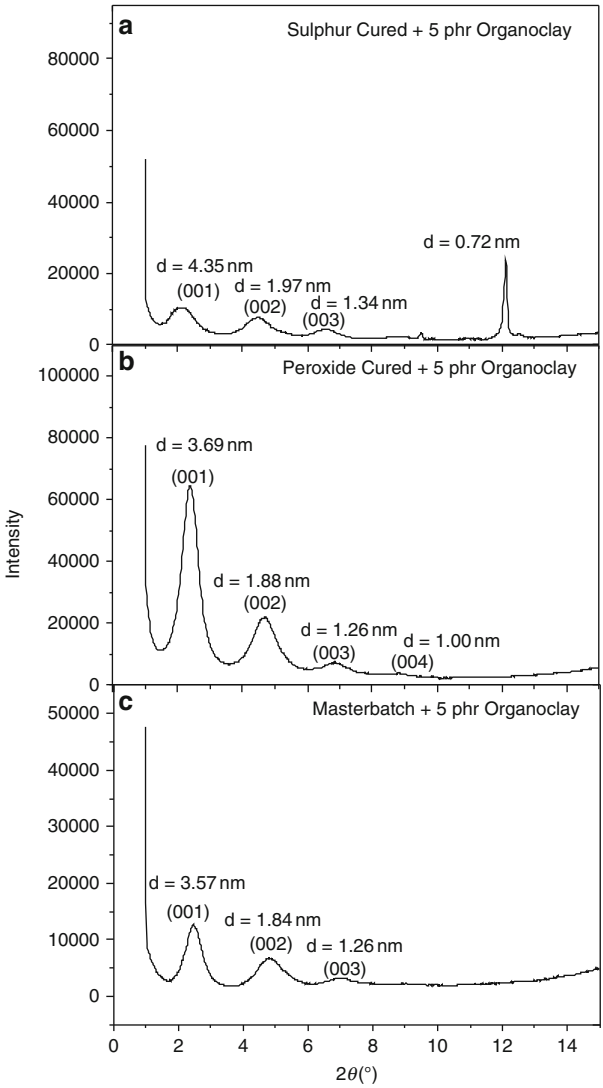

Fig. 32 WAXD patterns of NBR compounds reinforced with 5 phr organoclay and cured by sulfur (**a**), peroxide (**b**), and NBR master batch (**c**) (without curatives and uncrosslinked)

as a working hypothesis that alignment of the clay layers comes from the mixing direction of the two-roll mill during mixing the rubber with the other rubber additives. This orientation of the clay layers is affected by some of the rubber additives when these curatives are added during the mixing cycle. The clay particles seem to be surrounded by stearic acid and other additives and, hence, the shearing force from the mill is not properly transferred to the clay layers due to slippage

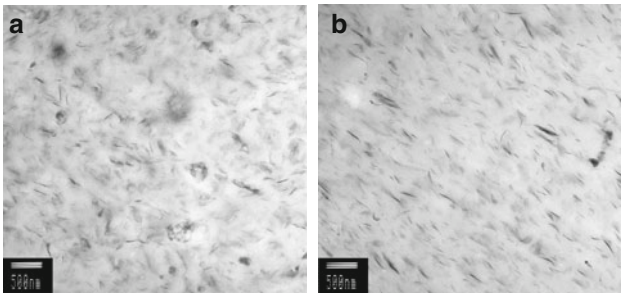

Fig. 33 TEM images of NBR vulcanizates cured by sulfur (**a**), and peroxide (**b**)

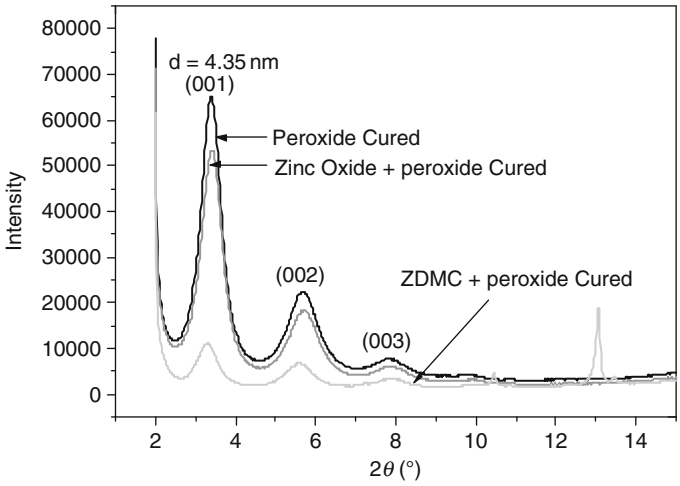

Fig. 34 WAXD patterns of 5 phr organoclay-filled peroxide-crosslinked NBR in the presence of different vulcanizing ingredients

between the clay layers and rubber chains, whereby the particles no longer remain in the oriented form. On the other hand, in the peroxide-cured system, the shearing force is, more or less, transferred to the particles and the layers are forced to maintain the anisotropy. To explore this in more detail, the individual effect of vulcanization ingredients on this type of anisotropic behavior of the layered silicates was studied, with special on two different peroxide vulcanization systems.

In addition to dicumyl peroxide (DCP), in two different batches zinc oxide (ZnO) or a conventional organic accelerator (ZDMC) were used. Figure 34 depicts the corresponding XRD pattern. In both cases, the peak positions are almost the same as that of the pure peroxide-cured vulcanizates. However, the intensity of the XRD pattern was significantly reduced in the case of ZDMC, and there is only a little effect of ZnO. Obviously, the sulfur-containing zinc salt influences and promotes dispersion and reorientation of the layered

silicates uniformly toward all directions [16]. Detailed studies are required to unravel the mechanism behind this.

4.2 *Effect of Accelerator Type*

Usuki et al. [14] from Toyota, Japan reported that the use of thiuram- and dithiocarbamate-type accelerators in EPDM rubber curing could enhance the exfoliation process of layered silicate. They proposed that when the zinc salt of ZDMC-types of accelerators were used in rubber curing, then the rubber backbone was modified with the grafted and accelerator moiety, and thus the rubber molecules became polar. They also described that this grafting of accelerators took place in a free radical fashion. As a result, this polar rubber molecule intercalated more easily into the gallery gap by virtue of the hydrogen bonds between the polar groups of rubber and the silanol groups of layered silicates.

It has also been reported that the use of silane-coupling agents, e.g., TESPT, can increase the reinforcing ability of clay by virtue of chemical linkage between the silanol group of silicates and the polymers [56, 57]. This type of coupling agent has two types of chemical groups: one that interacts with the hydroxyl groups of silicate and another that is responsible for the attachment with the rubber matrix. ZDP [20, 58] is also a type of multifunctional rubber additive that has the capability to act as a silane-coupling agent like TESPT as well as acting as a rubber-vulcanizing accelerator like ZDMC. The effect of this type of multifunctional rubber additive on the exfoliation–intercalation process of layered silicates was also investigated. A shift of the intensity peak in XRD to lower diffraction angles indicates that intercalation is a common phenomenon for both ZDMC- and ZDP-cured systems, and that ZDP-cured vulcanizates show a higher gallery gap between two successive layers of silicate particles (Fig. 35). There is also a significant reduction of peak intensity of the (002) and (003) crystal faces, with a peak broadening effect that signifies the uneven and irregular fashion of intercalation. Ultimately, it can be assumed that ZDP enhances the intercalation process of the layered silicate. This substance, being a multifunctional rubber additive, plays a special role as compatibilizer between organic polymers and inorganic silicates by providing an extra interaction as proposed in Scheme 1. The scheme shows how ZDP is grafted onto the surface of clay layers, and how this compound acts as a sulfur-crosslinking precursor to the rubber chains, bringing out some sort of compatibility between the clay and rubber. It is also noteworthy to mention that all sulfur-cured gum compounds containing ZDMC show one sharp peak around $d = 0.72$ nm. It is easily understandable that this scattering comes from sulfur vulcanization ingredients or from the in situ formation of some crystalline product from those sulfur curatives. Pure peroxide-cured rubber and the master batch compound did not show any scattering in this area since it did not contain any other crystalline substances.

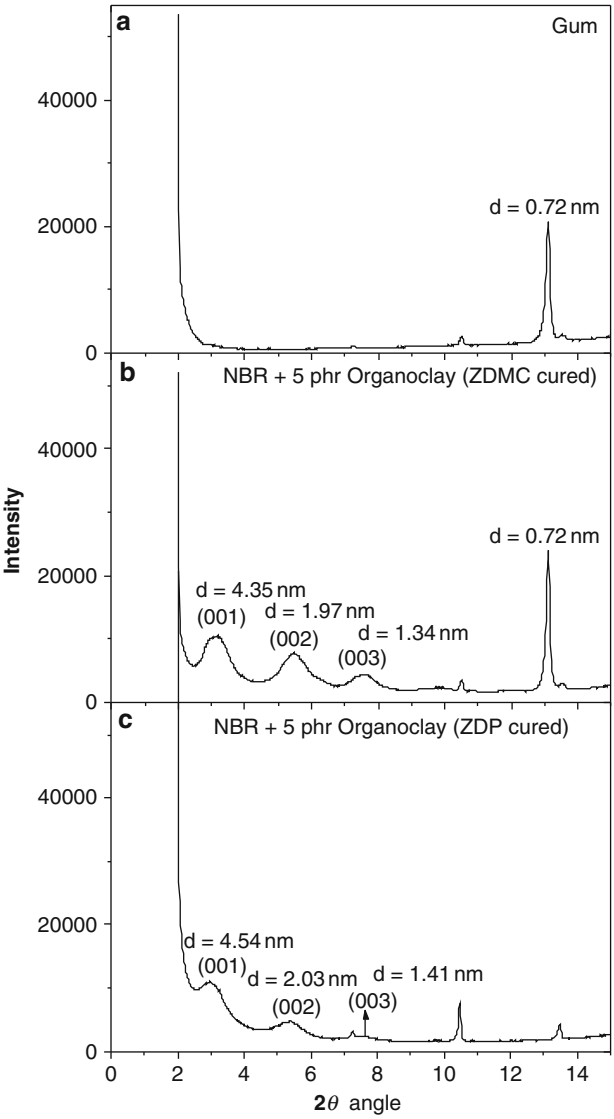

Fig. 35 WADX patterns of sulfur- and ZDMC-cured NBR gum (**a**), sulfur- and ZDMC-cured organoclay-filled NBR (**b**), sulfur- and ZDP-cured organoclay-filled NBR (**c**)

4.3 Effect of Stearic Acid

Many of the classical processing additives that had been introduced in the early years of rubber technology still remain in common use in various rubber products.

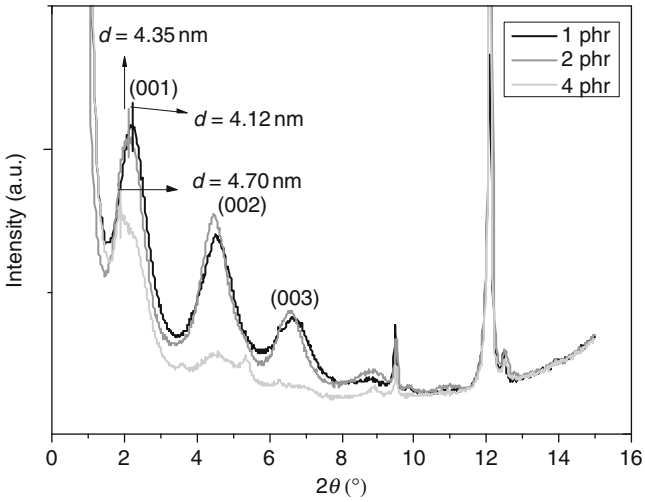

Fig. 36 WADX patterns of 5 phr organoclay-filled NBR, cured by sulfur in the presence of 1, 2, and 4 phr stearic acid

Stearic acid is one of these classical additives that are used as activators in the sulfur vulcanization process. Stearic acid [octadecanoic acid, $CH_3(CH_2)_{16}COOH$] is a long chain fatty acid consisting of 18 carbon atoms without double bonds. Recently, it was observed that stearic acid has a beneficial effect on the intercalation–exfoliation process of nanoclay in nitrile rubber [18]. The effect of stearic acid on the exfoliation–intercalation process of the layered silicate has been understood by XRD experiments. For this study, different amounts of stearic acid were taken in sulfur-curing packages. Very interesting XRD patterns have been received from these compounds and the corresponding WAXD patterns are given in Fig. 36. The interlayer distances of the silicate particles in the NBR matrix containing 1, 2, and 4 phr stearic acid are 4.12, 4.35 and 4.70 nm, respectively, whereas in the master batch compound the interlayer distance between two adjacent silicate layers was 3.57 nm. This means that the interlayer distance increased during sulfur mixing and/or curing, and that an excess amount of stearic acid favors the extent of intercalation. With increase of the stearic acid content, the corresponding scattered X-ray peak from the <001> crystal face of silicate particles shifts toward lower angles with a higher space gap. Ultimately, at 4 phr stearic acid content the diffraction curves show an almost exfoliated type of scattering pattern at higher order reflections such as <002>, <003>, etc. with very few intercalated structures. As a conclusion, a higher amount of stearic acid is recommended for the preparation of rubber-layered silicate nanocomposites. Very recently, Ma et al. [17] also reported that stearic acid increases the gallery gap. However, they did not find any change in the gallery gap after adding the stearic-acid-treated organoclay into the rubber matrix. The space gap between two clay layers was confined to 3.9 nm.

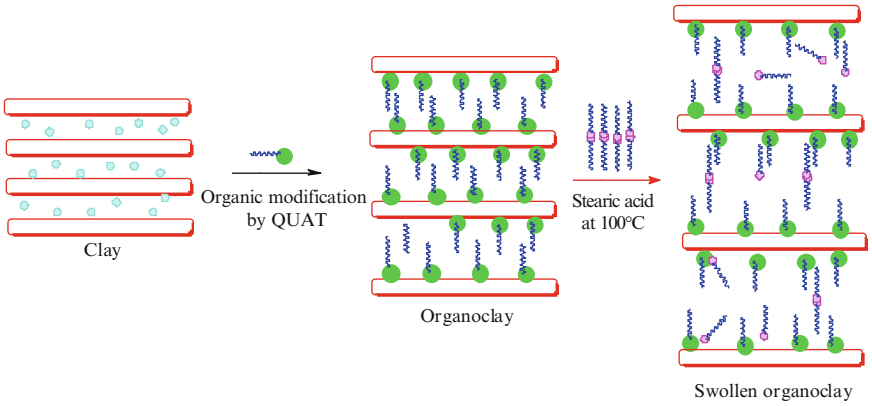

Fig. 37 Illustration of the gradual modification of MMT clay

It was suggested that stearic acid, which consist of small molecules, enters into the gallery of the layered silicate structure during the mixing and vulcanization processes, thus paving the way for intercalation of the rubber chains.

In order to prove the importance of the delaminated layer structure in the direct (melt) intercalation, the intercalation of stearic acid molecules into the clay galleries has been studied by premixing them with organoclay and then successfully incorporating this modified clay into the rubber matrix [59]. A schematic presentation of such modification of clay is given in Fig. 37.

After modification of the organoclay by stearic acid, the interlayer spacing increases from 2.98 to 3.96 nm (Fig. 38). So, the enhancement of the *d*-space has taken place due to the intercalation of stearic acid into the galleries and this pre-intercalation seems to make penetration of the rubber molecules easier and pave the way for nanostructure formation of the final composites.

Several kinds of rubber were taken into account to find the intercalation–exfoliation behavior of swollen clay. It is observed from Fig. 39a that the change in modulus at 50% elongation is always higher for all composites (except NBR) containing swollen clay as compared with compounds containing only organoclay. A very remarkable change was shown in polybutadiene rubber (BR): after addition of 10 phr clay the improvement in the 50% modulus was not observed, but as soon as 20 phr swollen clay was incorporated, the modulus increased significantly.

Figure 39b illustrates the improvement of tensile strength with respect to the respective gum compound. It is evident from this figure that improvement of tensile strength is seen for all vulcanizates filled with 10 phr activated clay (except XNBR and NBR), whereas incorporation of only 10 phr organoclay leads to rather small improvements. XNBR and NBR, being polar rubbers, do not undergo further intercalation by activated organoclay since it has already been intercalated by normal mechanical melt mixing and, due to this fact, further improvement of properties could not be achieved. The changes in elongation at

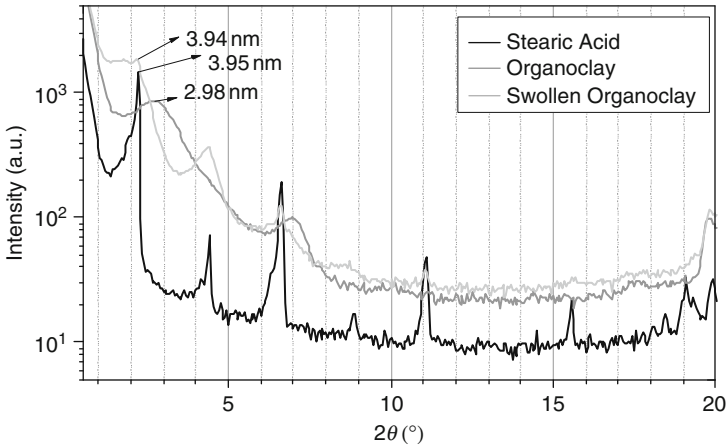

Fig. 38 WAXD patterns of stearic acid, clay, and swollen clay. The swollen clay was prepared by mixing stearic acid and organically modified clay (Nanofil-15) at the ratio of 1:1

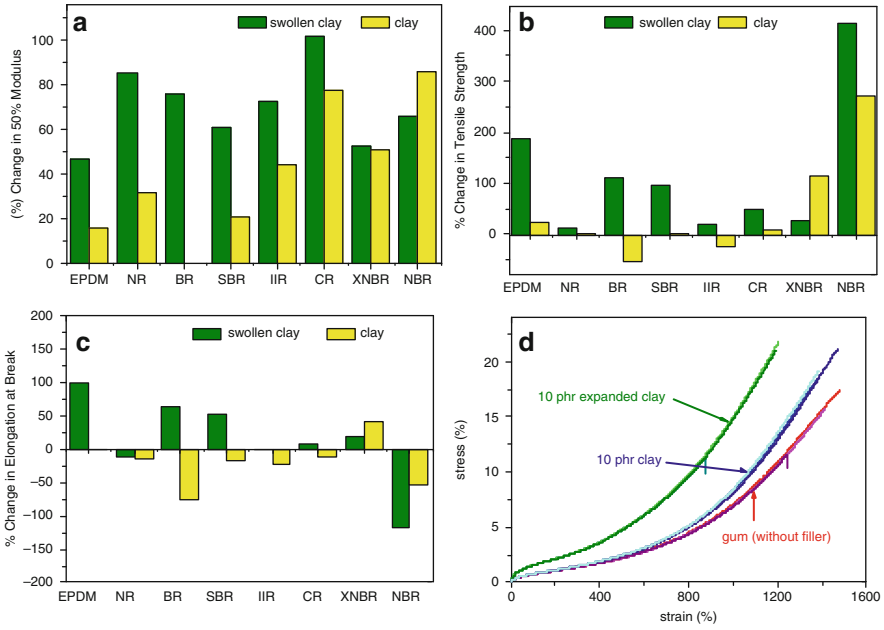

Fig. 39 Improvement of physical properties of various rubbers through incorporation of clay or swollen clay: 50% modulus (**a**), tensile strength (**b**), elongation at break (**c**), and the stress–strain plots for natural rubber (**d**). The strain was measured on the basis of clamp distance measurements

break after incorporation of clay and of swollen clay can be seen in Fig. 39c. None of the rubber vulcanizates having swollen clay in their matrix (except XNBR) show higher elongation at break values compared with their respective gum. In the

presence of a small amount of swollen clay, the vulcanizates offer higher modulus values, as shown in Fig. 39a. This finding can be explained by the higher effective volume fraction of the swollen clay, leading to a decrease of the elongation at break.

It will be very interesting to discuss the nature of the stress–strain curve obtained from the vulcanizates. The stress–strain curves obtained from NR compounds are shown in Fig. 39d. It is evident from this figure that the nature of the curves from the compounds containing swollen clay are much steeper and stronger than those from the sample containing only organoclay. It is worth mentioning that a similar type of approach was considered for preparation of rubber–nanoclay composites [17, 59]. However, they did not find any significant reinforcement in mechanical properties. Those composites were prepared by mixing of the compounds at room temperature. Hence, stearic acid possibly did not melt at that mixing condition and the rubber chains could not find space in the gallery by replacing the solid crystal of stearic acid. In our study, the mixing was done above the melting point of stearic acid and at this temperature the rubber chains enter into the layered galleries

The $d_{(001)}$ values of the clay in different rubber matrices are given in Table 8. It is clear that after incorporation in the rubber matrix the space gap between two successive layers has been increased in all cases. However, the enhancement of the $d_{(001)}$ values is marginal as compared with the swollen clay. As can be seen in Fig. 40, the peak positions are not changed to a large extent, but the peaks have altered height and broadened width. The intercalation of the rubber chains by pushing the platelets apart and by losing the order of the stacks (changing the crystallinity) are the causes behind these observations. A rough idea about the extent of such a delamination process can be obtained by analysis of the XRD peak area measurements [60]. It can be easily understood that the lower the peak area, the greater the delamination of the clay. Table 8 summarizes the results obtained from such observations over a wide range of rubber systems. Larger areas under the curves have been found from EPDM, XNBR, and BR and smaller areas have been calculated for CR, NR, and butyl rubber (IIR). A very interesting correlation was found between this trend and the improvement of the 50% modulus (stress at 50% elongation) of the swollen-clay-filled vulcanizates. CR, NR, and IIR

Table 8 Analysis of XRD and DMA data obtained from different rubber vulcanizates containing expanded organoclay

Rubber	XRD	
	$d_{(001)}$ value (nm)	Area under the (001) peak from X-ray pattern (a.u.)
EPDM	4.00	26,899
NR	3.95	5,484
BR	4.19	19,795
S-SBR	4.19	18,676
IIR	4.50	9,422
CR	4.12	1,741
XNBR	4.06	21,102
NBR	4.68	18,346

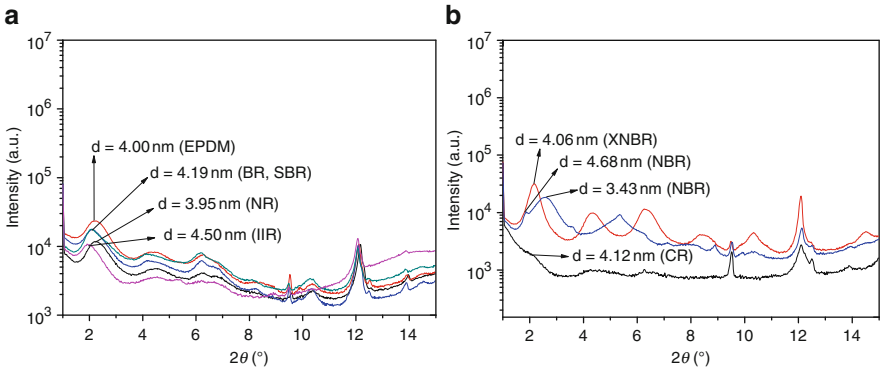

Fig. 40 WAXD patterns of non-polar rubbers (**a**) and polar rubbers filled with 20 phr swollen clay (**b**). All the vulcanized rubbers contain some curing ingredients like organic accelerator, zinc oxide, etc

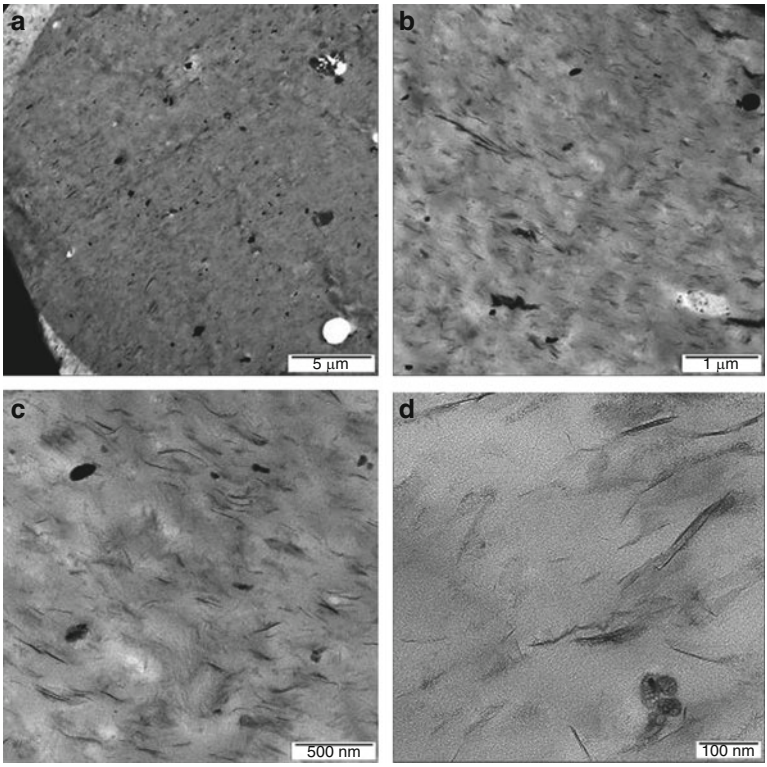

Fig. 41 TEM images (**a**–**d**), at different magnifications, of 10 phr swollen-clay-filled NR

show significant improvement (CR 100%, NR 107%, and IIR 73%) in enhancing the stress at 50% elongation parallel with a higher degree of delamination of the clay layers. In contrast, EPDM shows a poor enhancement (48%, from Fig. 39) of these properties after loading with 20 phr swollen organoclay. This correlation between the calculated areas under the XRD pattern with the enhancement of modulus indicates a nice agreement with each other. However, for XNBR a large area under the XRD was noticed. It was previously reported that XNBR, being a polar rubber, does not offer better physical properties after addition of swollen clay as compared with organoclay because it is already reinforced by organoclay. Most probably the complex crystalline morphology arising from metal-carboxylate (Zn–OOC) [6] clusters contribute to the X-ray reflection and results in the higher peak area. The higher physical properties of the swollen-clay-containing rubber vulcanizates and the expansion of the $d_{(001)}$ spacing directly lead us to the conclusion that intercalation of rubber chains through the gallery gap is becomes easier with swollen clay than with organoclay.

TEM images also directly corroborate the above conclusion by showing mostly intercalated and some exfoliated silicate clay layers in different rubber matrices. Figure 41 shows TEM images of swollen-clay-filled NR at different magnifications. The overall distribution of clay particles can be observed in Fig. 41a, b. It can be seen from these pictures that there is no big agglomeration of the clay particles. Even at higher magnification (Fig. 41c, d), single clay layers can be detected. Though 20 phr swollen organoclay was employed in this work, the clay particles did not form any big clusters or aggregates throughout the rubber matrix.

5 Clay in Rubber Blends

The fundamental justification for blending two or more elastomers is acquisition of the combinatorial and desirable features exhibited by the vulcanizates of the component elastomers in a unique substance. Unfortunately and most commonly, however, it has been found that covulcanization leads to reduction in the mechanical strength of the vulcanizate compared with its expected values. The elastomer blend components that resist gross phase segregation and/or give desirable blend properties are frequently said to have a degree of "compatibility" even though in a thermodynamic sense they are not miscible. Homogeneity of mixing and retention of the compatibility during vulcanization are the most relevant issues pertaining to elastomer blends and microheterogeneity is usually desirable in order to retain the individual properties of the respective elastomer components.

Nevertheless, the compatibility of two rubbers is largely governed by the polarity and the T_g of the corresponding rubbers. It is very difficult to predict the miscibility of two rubbers only by inspecting the above two factors. Determination of the Hildebrand solubility parameter (δ) by calculation of the Hoy molar

attraction constant [61] could be one way to understand the miscibility of the rubbers in a blend. In unfilled rubber compounds, the domain size of a heterogeneous blend is proportional to the difference of δ parameters of the constituent rubbers. With the incorporation of fillers, the δ parameter decreases and, hence, the miscibility of the rubbers can be improved. For instance, the rubber domain sizes in blends of BR and isoprene–butadiene rubber (IBR) are highly reduced by adding 30 wt% of silica or carbon black fillers [62] Here the fillers act like a compatibilizer between two heterogeneous rubbers with two different T_g. However, for blends of dissimilar elastomers, problems can arise in achieving optimum carbon black distribution between the microphases of the final product. In blends of elastomers that differ significantly in terms of unsaturation or viscosity, carbon black tends to locate preferentially in the higher unsaturation or lower viscosity phase [63]. Polarity is also a factor controlling carbon black migration in elastomer blends. Carbon black has been shown to transfer or migrate between EPDM and CR [64]. However, it was reported that migration of fillers can be restricted if a special technique is followed to process heterogeneous rubber blend compounds [65]. There is plenty of literature on the effect of fillers on the phase separation behavior of several immiscible blends [65–68]. In recent years, various reports have been made that describe the use of organically modified clay as a compatibilizer for several types of immiscible polymer blends by effectively reducing the domain size of the polymer phases. It is described that nanoclays are an attractive alternative to traditional compatibilizers because they can be compounded very easily. These nanoclays are also known to stabilize different crystalline phase of polymers and have also been proved to have the ability to improve the mechanical and thermal properties. For example, Vo and Giannelis [66] reported the compatibility and phase separation behavior of poly(vinylidine fluoride)/nylon-6 blends by the use of organically modified nanoclay. Addition of 5 wt% organoclay and maleic-anhydride-grafted polyethylene was found to be effective in reducing the ethylene–octene copolymer phase size in low density polyethylene/ethylene–octene copolymer blends [67]. Poly(ε-caprolactone)/poly(ethylene oxide) blends were prepared in the presence of nanoclay and it was found that exfoliated silicate platelets were preferentially located at the interface between the two blend phases [68]. The effect of organically modified clay on the morphology and properties of poly(propylene)/poly(butylene succinate)-*co*-adipate blends has been studied and the enhancement of physical properties, thermal stability, and rheological behavior was reported [69]. Several research groups also incorporated nanoclay into different type of rubber blends with the aim of improvement in physical properties [70–72]. It is reported that the preferential accumulation of intercalated clay layers on the phase boundary increased the compatibility of two different polymers when they have strong interactions with organoclay surface. Arroyo et al. [73] observed that organoclays give rise to a finer and more homogeneous dispersion of epoxidized natural rubber in the natural rubber matrix. Preferential accumulation of the exfoliated layered silicates is also observed in the interface of poly(ε-caprolactone)/poly(ethylene oxide) blends [68]. Very recently it was observed that organoclay, remaining in a rubber blend, can provide a dual role:

one role is the enhancement of the rubber–rubber compatibility (A. Das, personal communication) and the other is interfering with the interfacial crosslinking between two different rubber phases [74]. In the following sections, the positive and negative roles of organoclay on the compatibility between two different rubbers are discussed.

5.1 CR/EPDM

CR is an extremely versatile synthetic rubber with more than 75 years of proven performance in a broad industry spectrum due to its unique combination of properties: ozone resistance, oil resistance, toughness, dynamic flex life, good adhesion to other materials, and heat resistance up to 100°C [75]. This rubber has been the material of choice for moldings and extrudates of all types, reinforced hoses, roll covers, belting, including conveyor belts, air spring bellows, cable sheathing and insulation for low-voltage cables, sponge rubber, corrosion-resistant linings, sheeting, fabric proofing and footwear, most power belts, boots, hose water suits and water sealant, and numerous other applications. To meet these emerging needs, and for new material development for more demanding applications, improvements in resistance to heat, ozone, and cut growth of CR products are very desirable. The above requirement for CR products could be satisfied by blending with polyolefin elastomers such as ethylene–propylene rubber (EPR) or EPDM, which have better resistance to heat, ozone, and cut growth [76]. However, these CR/EPR or EPDM blends are incompatible [77].

5.1.1 Preparation

A typical mixing procedure was followed to obtain the CR/EPDM blend compounds. First, the clay was treated with stearic acid in a mortar and placed in an oven at 100°C for 30 min. After heating, the mass was thoroughly ground with a pestle (keeping it hot) and again the vessel was kept at 100°C. The hot material was cooled to room temperature and again ground. This compound was used as a filler. The EPDM rubber was mixed with ZnO and the stearic-acid-modified clay was incorporated into it in a two-roll mixing mill for 5 min. This mix was added to the premasticated CR and then the curatives (accelerator and sulfur) were incorporated into the rubber compounds. For gum compounds (without any clay), the stearic acid was added after the addition of ZnO to the EPDM. Finally, the rubber compound was compression molded to prepare samples of ~2 mm thickness.

5.1.2 Characterization

It was already mentioned that an extra amount of stearic acid has a pronounced effect on the intercalation of layered silicate in nitrile rubber. So, a higher amount of

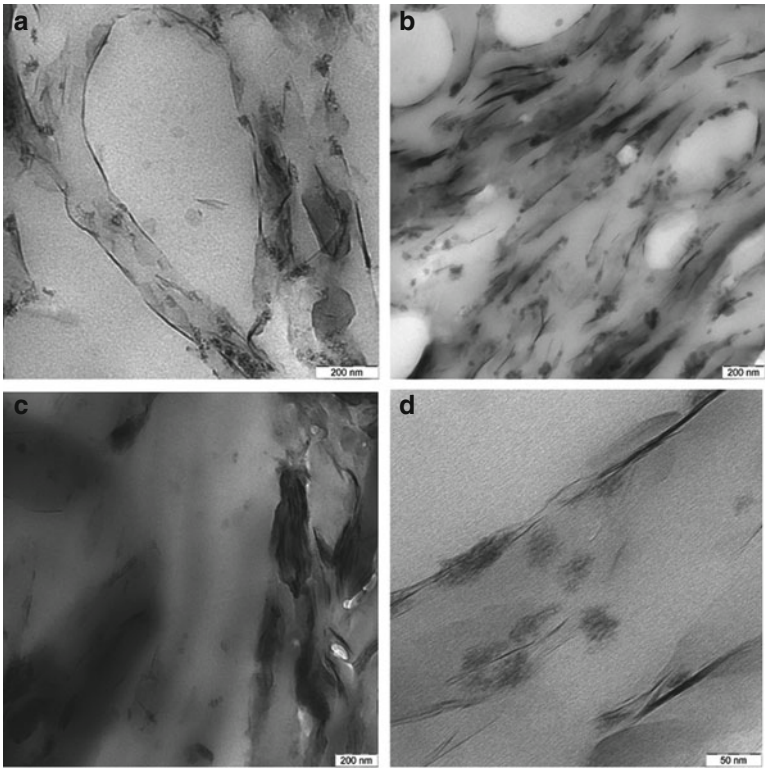

Fig. 42 TEM images of the blends of 25 EPDM/75 CR (**a**), 50 EPDM/50 CR (**b**), 75 EPDM/25 CR (**c**), and 25 EPDM/75 CR filled with 10 phr nanoclay (**d**)

stearic acid (10 phr) was added to the organically modified clay to obtain a higher *d*-space for the organoclay in the swollen state . Because the stearic-acid modified organoclay exhibits a higher *d*-space (2.98–3.96 nm), it is expected that a large portion of the clay will form a good degree of intercalated–exfoliated structures in the rubber matrix.

Figure 42 shows TEM images of CR/EPDM blends at the ratios of 75/25, 50/50, and 25/75, all containing 10 phr clay. Each blend was prepared by incorporating all the clay in the EPDM rubber and, subsequently, mixing the resulting composites with CR. It is obvious from Fig. 42a, b that two phases of CR and EPDM coexist with a large number of exfoliated and intercalated clay platelets at the interfaces. The dark phase is most probably CR phase with a higher electron density due to the presence of chlorine atoms in the rubber chains. Remarkably, it was found that there are almost no clay layers in the bright phase rather than in the dark phase. CR, being a polar rubber, forces migration of the clay particles into it, rendering the EPDM phase poor, despite the fact that all the clay was premixed with EPDM. Migration of inorganic clay layers takes place from nonpolar EPDM to polar CR. As far as

viscosity mismatch (Mooney viscosity) is concerned, the migration is also driven by the viscosity difference because the Mooney viscosity of EPDM is higher than the viscosity of CR.

The migration of clay from EPDM to CR phase can also be explained as a wetting/dewetting process between polymers and filler. Hereby, the driving force of filler particle migration is the difference of the interfacial tensions between the rubbers and clay:

$$\Delta\gamma = \gamma_{F-CR} - \gamma_{F-EPDM}, \tag{3}$$

where $\gamma_{\text{F-EPDM}}$, and $\gamma_{\text{F-CR}}$ are the interfacial tensions between the organoclay filler (subscript F) and EPDM or CR respectively. The interfacial tensions can be calculated using the following equation of Good et al. [78]:

$$\gamma_{\text{sl}} = \gamma_{\text{s}} + \gamma_{\text{l}} - 2\left(\sqrt{\gamma_{\text{s}}^{\text{D}}\gamma_{\text{l}}^{\text{D}}} + \sqrt{\gamma_{\text{s}}^{\text{P}}\gamma_{\text{l}}^{\text{P}}}\right), \tag{4}$$

where γ_{sl} is the interfacial tension between a solid and a liquid, and γ_{s} and γ_{l} are the surface tensions or energies of the liquid or solid, respectively. The superscripts D and P denote their dispersive or polar parts.

Using this equation, the driving force for the filler particle migration, the difference of interfacial tensions $\Delta\gamma$ can be expressed as:

$$\begin{aligned}\Delta\gamma = &\left[\gamma_F + \gamma_{CR} - 2\left(\sqrt{\gamma_F^D\gamma_{CR}^D} + \sqrt{\gamma_F^P\gamma_{CR}^P}\right)\right] \\ &- \left[\gamma_F + \gamma_{EPDM} - 2\left(\sqrt{\gamma_F^D\gamma_{EPDM}^D} + \sqrt{\gamma_F^P\gamma_{EPDM}^P}\right)\right].\end{aligned} \tag{5}$$

The dispersive and polar parts of the surface energies were calculated from contact angle measurements with test liquids of different surface tension and polarity, using a modified Wihelmy technique [79]: Organoclay filler: $\gamma_{\text{F}} = \gamma_{\text{F}}^{\text{D}} + \gamma_{\text{F}}^{\text{P}} = 24.3\ \text{mJ m}^{-2} + 1.0\ \text{mJ m}^{-2}$ EPDM: $\gamma_{\text{EPDM}} = \gamma_{\text{EPDM}}^{\text{D}} + \gamma_{\text{EPDM}}^{\text{P}} = 24.2\ \text{mJ m}^{-2} + 7.6\ \text{mJ m}^{-2}$ CR: $\gamma_{\text{CR}} = \gamma_{\text{CR}}{}^{\text{D}} + \gamma_{\text{CR}}^{\text{P}} = 22.5\ \text{mJ m}^{-2} + 12.8\ \text{mJ m}^{-2}$.

After considering the above values of γ_{F}, γ_{EPDM} and γ_{CR} from contact angle measurements, the difference interfacial energies $\Delta\gamma$ according to (3) has a value of $-3.4\ \text{mJ m}^{-2}$. This negative value leads to the conclusion that the migration of the clay particles from EPDM phase to CR phase is a thermodynamically favorable process. Exactly similar behavior has also been reported by Göldel et al. [80] while working with multiwalled carbon nanotubes in polycarbonate (PC) and polystyrene–acrylonitrile (SAN) blends. The migration of carbon nanotubes from SAN phase to PC phase was also understood in terms of an interfacial energy driven process.

TEM images (Fig. 42a, b) also supported the overall exfoliation of clay in CR for blends with a ratio of 25/75 and 50/50 of EPDM to CR. A striking difference in the dispersion of the clay can be observed if the TEM image of the 75/25 blend is

compared with the 25/75 and 50/50 blends of EPDM and CR. The existence of various large aggregated structures of the clay indicates a poor dispersion at this particular blend ratio, and the effect was reflected in other properties like a low Young's modulus, etc. (discussed at the end of this section).

It is a common phenomenon that the intercalated–exfoliated clay coexists in the bulk and in the interface of a blend. Previous studies of polymer blend–clay systems usually show that the clay resides either at the interface [81] or in the bulk [82]. The simultaneous existence of clay layers in the interface and bulk allows two functions to be attributed to the nanoclay particles: one as a compatibilizer because the clays are being accumulated at the interface, and the other as a nanofiller that can reinforce the rubber polymer and subsequently improve the mechanical properties of the compound. The firm existence of the exfoliated clay layers and an interconnected chain-like structure at the interface of CR and EPDM (as evident from Fig. 42a, b) surely affects the interfacial energy between CR and EPDM, and these arrangements seem to enhance the compatibility between the two rubbers.

The dependence of the storage modulus (E') on the strain amplitude at very low strain gives an understanding of the impact of the filler network within the rubber matrix. Generally, E' remains unaltered with increasing strain for an unfilled rubber system. However, for a filled system, the storage modulus decreases with increasing strain. This nonlinear behavior of a filled rubber system is called the Payne effect [41] and yields information about filler–filler networking in the rubber matrix (see Sect. 3.1.2). In our investigations, the plots of E' versus double strain amplitude of the CR/EPDM blends are shown in Fig. 43a. It is evident from this figure that the gum blend without any filler does not undergo any change in E' with increasing strain. However, a strong dependency can be observed for all filled samples. Here, all rubber blends are filled with only 10 phr of clay and, obviously, these clay particles, being either exfoliated and/or intercalated, build a strong filler–filler network in the rubber matrix. The preferential localization of the clay at the interface fulfills the demand to remain in contact with hydrogen bonding by the virtue of hydroxyl group of clay (end-to-end coupling). Moreover, it is quite interesting to discuss the very high value of E' at the low strain region. A very high E' value ($\sim$45 MPa) at low loading of clay ($<$10 wt%) has not been reported in the literature so far. For example, the value of E' was found to be only $\sim$9 MPa in a natural rubber filled with 20 wt% of nanoclay [83]. These observations can only be explained if a large amount of delaminated silicate particles come out from the nanoclay stacks through the exfoliation process. In the CR/EPDM blend it can be observed that, with the increase of the EPDM content, the filler–filler networking decreases. This can be attributed to relatively smaller space availability (CR phase) of the clay particles at a fixed volume and, consequently, the clay particles are forced to remain in nonintercalated–exfoliated form (Fig. 42c). This figure also indicates the same explanation for these facts. It is observed from this TEM image of the 75 EPDM/25 CR blend that clay particles remain in the agglomerated form and this finding directly corroborates the above observations. Nevertheless, the single exfoliated particles can be seen in Fig. 42d, where several single clay platelets are embedded in the 25 EPDM/75 CR blend

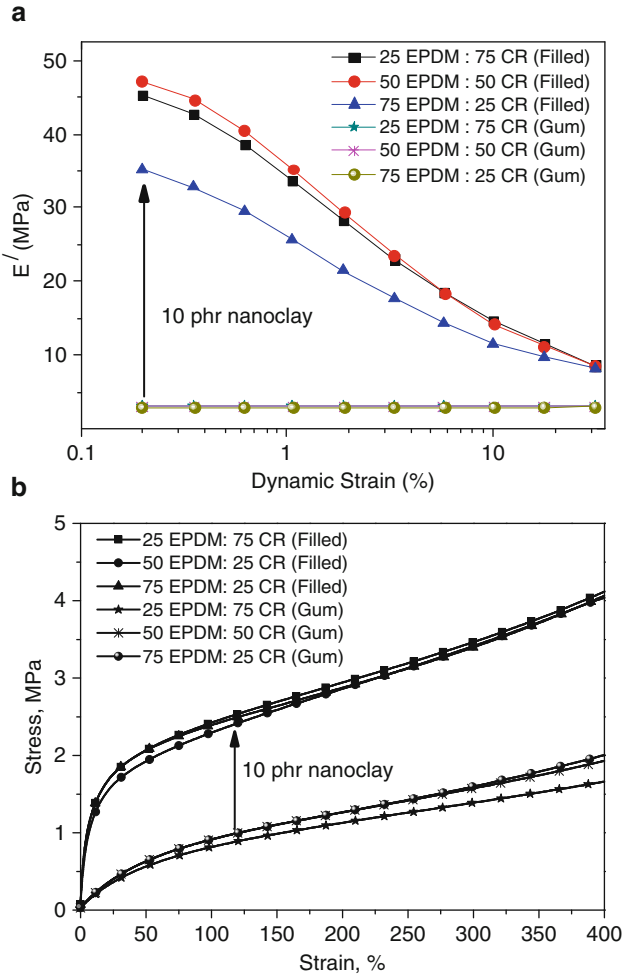

Fig. 43 Effect of dynamic strain amplitude on storage modulus (**a**). Stress–strain behavior of CR/EPDM blend in the absence and presence of nanoclay (**b**). For this experiment, tension mode was selected for the variation of the dynamic strain from 0.01 to 40% at 10 Hz frequency

matrix. But, in the stress–strain experiment, at the low strain regime all blends exhibit the same nature (Fig. 43b).

Dynamic mechanical analysis (DMA) has been carried out to understand the dynamic response of the blend after the addition of clay. The dependency of the storage modulus obtained from oscillatory tension deformation as a function of temperature is given in Fig. 44. All samples show a steep decrease of E' over the temperature range $T = -50$ to $-20°C$ followed by a rubbery plateau (Fig. 44a). The most exciting information, observed in this figure, is the increase of modulus values at room temperature by the addition of clay. The storage modulus increases from 2 MPa to 54 MPa with the addition of only 10 phr clay in the 25 EPDM/75 CR

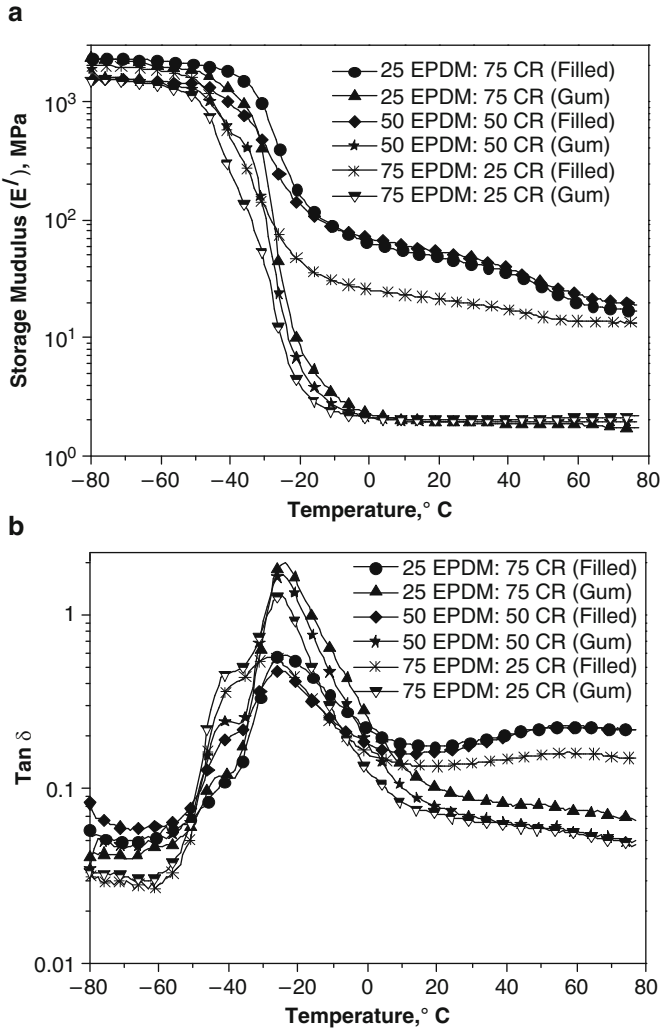

Fig. 44 Storage modulus (E') versus temperature (**a**), and tan δ versus temperature (**b**) plots of CR/EPDM blends in the absence and presence of nanoclay

matrix. A good state of exfoliation of the clay in the CR matrix reinforced the rubber blend very strongly. A sufficiently strong filler–filler interaction as well as the compatibility between CR and EPDM play major roles in giving rise to a very highly reinforced rubber matrix.

The T_g of a rubber or polymer depends on the structure and cooperative mobility of the chain segments. In the case of partially compatible blends, the T_g values of the blend components are expected to be shifted toward each other as compared with the pure components. The T_g values remain largely unaltered for a completely incompatible blend. Fig. 44b shows the tan δ dependencies on the temperature for

Table 9 Glass transition temperature of EPDM/CR rubber blends

Rubber[a]	Glass transition temperature (°C)					
	Without clay			With clay		
EPDM:CR	EPDM peak	CR peak	Separation between two peaks	EPDM peak	CR peak	Separation between two peaks
100:0	−37	*a*	–	−37	*a*	–
75:25	−44	−25	19	−42	−26	16
50:50	−42	−25	17	−41	−27	14
25:75	−40	−24	16	−35	−28	7
0:100	*a*	−24	–	*a*	−24	–

[a]The curing recipe used in this study was 5 phr zinc oxide, 10 phr stearic acid, 7 phr ZDMC, and 1 phr sulfur.
a absent for that particular case

the CR/EPDM blend systems, and the T_g of the corresponding rubbers are listed in Table 9. The two pure vulcanized rubbers show T_g at −37 and −24°C and, even after incorporation of the clay, the values remain unaltered. However, those rubbers remaining in the blend system showed different T_g values. It is clear from Table 9 that the T_g values are closer when the blend matrix is filled with 10 phr clay, which indicates that the clays have a strong capability to increase compatibility between two heterorubbers. A shift of 9°C was observed for the 75 CR/25 EPDM blend. Exactly the opposite type of behavior was found [74] for an incompatible rubber blend, as revealed by the situation when the clay interferes with the compatibility between chloroprene and XNBR during the self-crosslinking reaction.

It is also important to note that even at higher temperatures (40–60°C), a second flat and broad relaxation process is observed for the blends containing clay. Such a process at the same temperature range has been reported for a CR–clay composite [23]. In that work, we proposed that the rubber (especially CR chain segments) is partially crystallized in the presence of organically modified clay. Very recently [84] such a process has been explained by considering the fact that, during the measurement of the dynamic mechanical properties, the anisotropic fillers are arranged in such a way that they have to reorient by following the applied mechanical field and additional energy dissipation sets, resulting in relaxation at higher temperatures [85]. Finally, from stress–stress experiments it was found that the Young's modulus increases from 1.93 MPa to 27.24 MPa with the addition of 10 phr clay along with 10 phr stearic acid. However, it is evident from Fig. 43b that the improvement of tensile properties is not as high as expected from other studies. Insufficient crosslinking of the rubber matrix could be the reason behind this observation.

5.2 CR/XNBR

Various blends of functionally active rubbers are reported to be capable of partial crosslinking at high temperatures in the absence of any curatives. Some of these

self-vulcanizable rubber blends include binary blends of epoxidized natural rubber (ENR)/XNBR, ENR/CR, CR/XNBR, chlorosulfonated polyethylene/XNBR, and ENR/chlorosulfonated polyethylene [86]. For instance, the interfacial crosslinking of CR and XNBR takes place as a result of the reaction of the active tertiary allylic chlorine of CR with the –COOH group of XNBR, with the elimination of hydrochloric acid [87]. However, the T_g of those two rubbers are widely separated and, hence, CR and XNBR are immiscible.

It is also interesting to look into the chemical interactions of organoclay (QUAT-modified MMT) with functionally polar rubbers like XNBR, CR, and their mutual blend. The role of layered silicate on the curing process of CR/XNBR blends was investigated through the study of curing kinetics, mechanical properties, WAXS, and DMA [74].

5.2.1 Preparation

The formulations of the rubber compounds are given in Table 10. For the preparation of CR–organoclay and XNBR–organoclay single rubber composites, those two pure rubbers were individually mixed with organoclay at 180°C by an internal mixer. In order to produce rubber blends, the masticated preblended rubbers were mixed with organoclay at a relatively low temperature of 100°C using an internal mixer. The mixing time was 10 min for all the samples. After taking out the rubber compounds from the internal mixer, the sulfur curatives were added with an open two-roll mixing mill.

Table 10 Formulations and physical properties of CR and XNBR and their blends

Mix[a] no.	CR (%)	XNBR (%)	Organoclay loading (phr)	Swelling index	Crosslinking density[c] (mmol/100 g)
1	100	0	0	–[b]	–[b]
2	75	25	0	3.58	1.39
3	50	50	0	3.70	1.21
4	25	75	0	5.11	0.72
5	0	100	0	–[b]	–[b]
6	100	0	10	–[b]	–[b]
7	75	25	10	2.90	1.01
8	50	50	10	3.22	0.82
9	25	75	10	4.14	0.51
10	0	100	10	–[b]	–[b]

[a]The curative packages contained MgO 4 phr, ZnO 5 phr, stearic acid 2 phr, zinc dithiocarbamate 6 phr, sulfur 1 phr, and ethylene thiourea 1 phr

[b]The crosslinking densities of the 100% pure rubbers (uncrosslinked) have not been measured

[c]The crosslinking density of the filled vulcanisate is calculated considering the organoclay as a coarse spherical particle. If we consider the shape factor, the values of the crosslinking density of the filled sample will be much lower than the present values

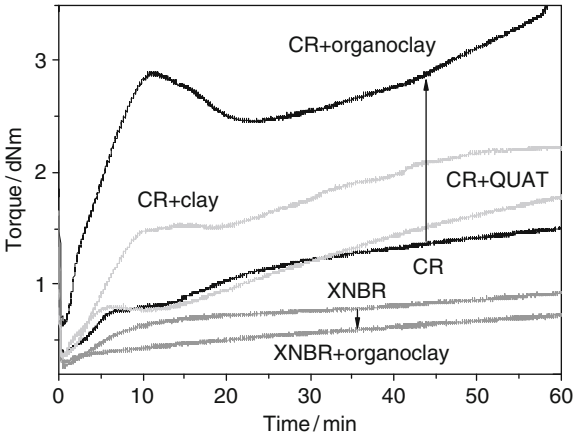

Fig. 45 Rheographs obtained from CR and XNBR in the presence of some additives at 180°C. *Arrows* indicate the influence of organoclay on the torque during heating of pure CR and XNBR

5.2.2 Characterization

Figure 45 depicts the improvement of torque against time at 180°C for CR and XNBR in the presence of clay, organoclay, and the organic modifier. A QUAT compound (di-steryldimethyl ammonium) was used to modify the clay. To see the effect of this amine modifier, an equivalent amount of that amine was mixed with CR and a rheometric study performed at 180°C. It is evident from Fig. 45 that the torque gradually increases for CR under thermal treatment, but for XNBR the response is little in developing the elastic modulus. The presence of 1.4% of the tertiary allylic chlorine atom on the backbone of CR chain is responsible for this thermal crosslinking [88]. In the presence of MMT clay, the extent of crosslinking is higher than for plain CR. So, the clay acts here as a crosslinking catalyst by actively taking part in thermal dehydrohalogenation reactions. The excess metal cations, present on the surface, might react with the chloride to form metal chloride and thus facilitate the crosslinking reactions [89]. This crosslinking acceleration activity is noticed very well when the CR matrix is filled with amine-modified clay. The QUAT, present in the organoclay as a modifier, is supposed to take part in the initial stage of the thermal reaction, but it should be noted that the presence of this QUAT alone is not able to accelerate the crosslinking. Clay together with QUAT increases the ultimate torque to a considerable extent. This interesting behavior of amine-modified MMT clay with respect to the thermal curing of CR can be called cure synergism by functional fillers. Here, it should be noted that curing or crosslinking of CR cannot be promoted by an organic molecule with only one amine group, but only by the organic molecules with at least two amine groups. These two amine groups anchor the two CR rubber chains by the participation of the tertiary allylic carbon atom of the CR chain in an electrophilic substitution reaction with the nitrogen atom of the amine. This mechanism of CR crosslinking is called

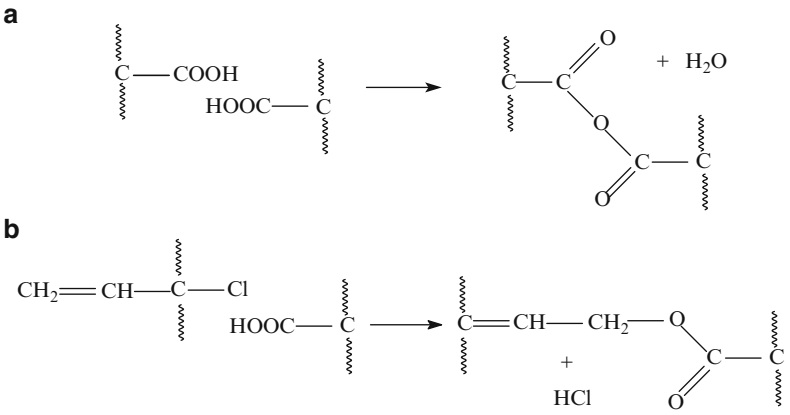

Scheme 2 Formation of carboxylic anhydride at 180°C temperature as a crosslink in the XNBR matrix (**a**), and ester linkage between CR and XNBR produced during heating at 180°C (**b**)

bis-alkylation [90]. In contrast to the above role of organoclay, a negative influence on the thermal crosslinking of XNBR was observed by reducing the ultimate torque. Since the rubbers were heated at 180°C, a dehydration of carboxylic acid may occur, which leads to thermal crosslinking of XNBR. The mechanism is shown in Scheme 2. In the presence of organoclay, the carboxylic group is blocked either by the ammonium compound present on the clay or by the hydrogen bonding between silanol group of clay and carboxylic group of XNBR. Therefore, the carboxylic groups neither undergo a dehydration reaction, nor do they form any acid anhydride crosslinks.

Figure 46 shows the IR spectra of pure XNBR, organomodified layered silicate, and XNBR-layered silicate compound. The XNBR-layered silicate compound was prepared at 180°C in an internal mixer for 10 min . From this figure it can be seen that the out-of-plane vibration of Si–OH (1,002 cm^{-1}) of the organoclay sample has been shifted neatly towards a higher frequency (1,040 cm^{-1}). The silanol groups of silicate particles form a hydrogen bond with the carboxylic group of XNBR, which results in shifting of the Si–OH vibration from lower to higher frequency. However, no significant change in the C=O stretching frequency (not shown in Fig. 46) of the COOH is observed after the incorporation of layered silicate in the XNBR matrix.

It is well established that CR and XNBR undergo a chemical crosslinking reaction without any extra crosslinking agent (Scheme 2b). The influence of organoclay on this self-crosslinking of the rubbers at various compositions is evidenced from the results of a rheometric study at 180°C (Fig. 47). The development of torque of different blends with time is given. This figure shows that all three compositions of the blends, containing 10-phr layered silicate, offer a superior state of cure as compared to their respective gum. The increase of the torque values by the organoclays can be explained by the presence of the hard filler particles and the modification of overall crosslinking density of the rubbers by the organoclay. To understand the self crosslinking between the carboxylic group of XNBR and the

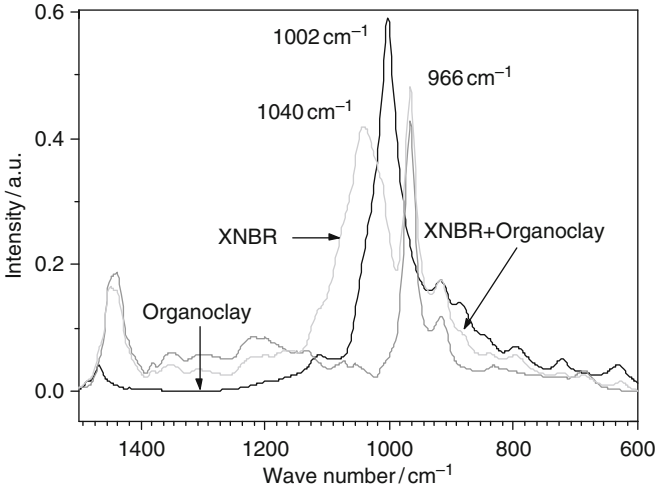

Fig. 46 ATR-IR spectra of pure XNBR, XNBR–organoclay, and organoclay

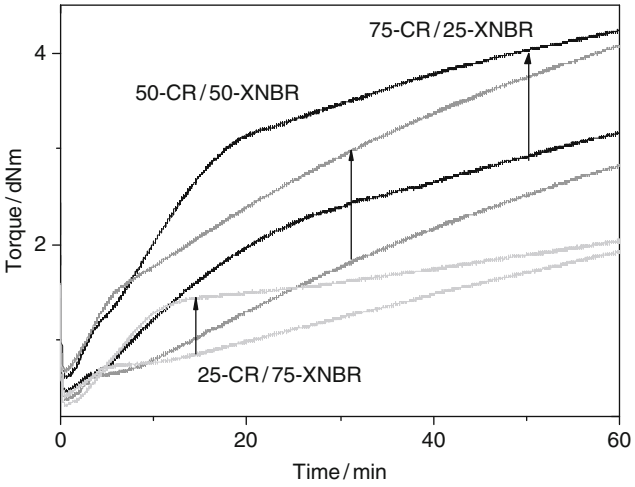

Fig. 47 Rheographs obtained from self-crosslinkable CR/XNBR blends of different composition at 180°C. *Arrows* indicate the development of torque after addition of 10 phr organoclay

tertiary allylic chloride of the CR chain, ATR–IR spectra were obtained. Figure 48 depicts the spectra obtained from two pure virgin rubbers and their blend (75 CR/25 XNBR) in the presence and absence of organoclay. The spectrum obtained from pure CR has some characteristic features, which include a C=C strong band at ~1,697 cm^{-1} and multiple C–H and C–C bending and stretching vibrations at

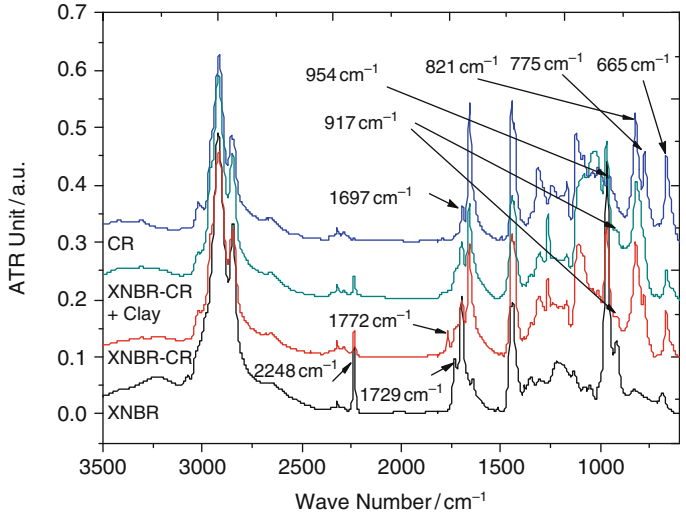

Fig. 48 ATR-IR spectra of CR and XNBR and their blends in the presence and absence of organoclay

~1,445, 1,431, 1,303, 1,202, 1,118, and 1,001 cm^{-1}. The C–Cl stretching and bending bands appear at 821, 775, and 665 cm^{-1}. A small band is also observed for $=CH_2$ out-of-plane vibration of the isomerized 1,2-units at 954 cm^{-1}. Obviously, there are some common bands with CR in the pure XNBR spectrum due to the existence of C=C, multiple C–H, and C–C bending and stretching vibrations. The characteristic absorbance of –C≡N of XNBR can be observed at 2,248 cm^{-1}. Peaks in the 1,729 cm^{-1} area stem from the >C=O group of the carboxylic part in the rubber. This band is shifted to higher wave number (1,772 cm^{-1}) in the spectrum of 75 CR/25 XNBR, which indicates the chemical interaction of carboxylic group of XNBR with the tertiary allylic chlorine of the isomerized 1,2-unit of CR. Interestingly, in the presence of organoclay the characteristic peak for >C=O in ester-type linkage is missing. However, in the area between 1,772 and 1,729 cm^{-1}, a broad shoulder-type peak appears or the organoclay-filled CR/XNBR blend. It is assumed that in the presence of organoclay either the surface of XNBR is blocked by the clay platelets or the carboxylic groups form hydrogen bonding with the silanol group of silicate particles without taking part in the crosslinking reactions. It is also observed that the band at 954 cm^{-1}, which is expected to come from the out-of-plane $=CH_2$ of CR, disappeared in the blends and a new peak appeared at 917 cm^{-1}. This shifting of peak in both cases indicates that most of the reactive tertiary allylic chloride groups react or that they are consumed by other reactive sites of rubber chains. So, it can be assumed that, in the presence of organoclay, the active groups of CR crosslink with each other rather than react with the XNBR phase, because the active carboxylic groups are

no longer available for this reaction. On the basis of these arguments, we conclude that organoclay promotes a phase-separated morphology of the blends without any chemical crosslinking between CR and XNBR. Discussion about the crosslinking density as well as the swelling index will be insightful in this case. The degree of the swelling (i.e., Q values) are given in the Table 10. With the increase of CR content in the blend, the Q values decrease, which means that CR is more solvent-resistant than XNBR. Another explanation could be given for this if the crosslinking density is correlated with the reciprocal of swelling index. The crosslinking density decreases with a decrease in the CR content in the self-crosslinked blends. This is also true for the blends containing layered silicates. Crosslinking density was determined by solvent swelling method and the values are given in Table 10. It is found from Table 10 that the crosslinking density of the vulcanizates follow the same trend with blend composition as revealed from the swelling study. However, what is more interesting, is that the crosslinking values of the filled sample are always less than the corresponding gum samples. That means that the layered silicates interrupt the self-crosslinking process between tertiary allylic chlorine of CR and the carboxylic group of XNBR. It should be mentioned here that the crosslinking density of the filled sample is estimated by considering the gum state equivalent and using the Einstein–Smallwood equation. If we consider the shape factor [91] of the anisotropic layered silicate particles in this equation, then the crosslinking value of the filled sample would be lowered further below that of the estimated values.

It is also of interest to see in the presence of nanoclay whether the phase-separated morphology of the blend affects the physical properties. As observed from Fig. 49, the 50% moduli of the organoclay-filled self-crosslinked rubber matrix remain more or less same compared to the corresponding unfilled rubber matrix at all blend ratios. Tensile strength is very badly affected by the addition of organoclay, especially in the case of 75 CR/25 XNBR. In order to get the beneficial effect of the layered silicate, the rubber blends were also cured by a sulfur vulcanization package. Remarkable improvements of the 50% modulus, as well as the tensile strength were observed. In addition to the extra self-crosslinks from XNBR and CR, the sulfur vulcanizing package leads to sulfur bridges between two different rubber chains in the blend, depending on the availability of allylic double bonds of the CR. However, in this case, one of the diene rubbers is CR and the fitness of sulfur vulcanization of CR is still a research topic and beyond the scope of the present discussion. However, it is concluded that the physical properties of such types of heterogeneous blends could be improved with layered silicate if sulfur vulcanization becomes one of the choices for crosslinking precursors.

It is evident from Fig. 50 that the self-crosslinked blend of 75 CR/25 XNBR containing 10 phr of organoclay shows no reflection in the 2θ range of 1–9°. The absence of any peak in the XRD patterns could be one indication of exfoliation of the organoclay. However, for the other two blends the presence of the characteristics peak of organoclay indicates an intercalated clay morphology in the matrix. The blend containing 50% CR exhibits higher gallery height as compared to the blend with 25% CR.

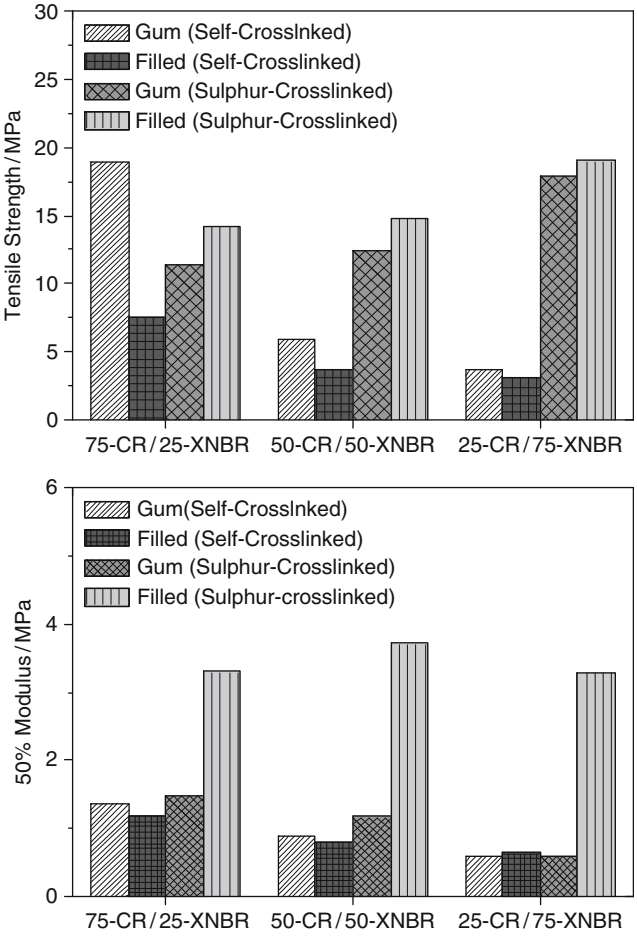

Fig. 49 Physical properties in terms of tensile strength (*top*) and 50% modulus (*bottom*) for CR-XNBR blends obtained from self-crosslinking and sulfur-crosslinking processes

Though the blends contain the intercalated clay structures, the tensile properties were not improved, as discussed in the previous section. The layers of the organoclay make the blends more immiscible and generate a heterogeneous phase morphology, which ultimately deteriorates the tensile properties of the blend composites. It is interesting to look into the intercalation of the clays in the blends if the rubber blends are efficiently cured by sulfur vulcanization packages. The XNBR–organoclay shows three peaks corresponding to the <001>, <002>, and <003> planes of the clay, whereas CR–organoclay shows only one peak corresponding to the reflection from the <001> plane of the clay (Fig. 50). The gallery height is 3.97 nm for XNBR and 4.85 nm for CR. The higher *d*-space of organoclay in pure CR may be due to higher surface energy of the CR, which

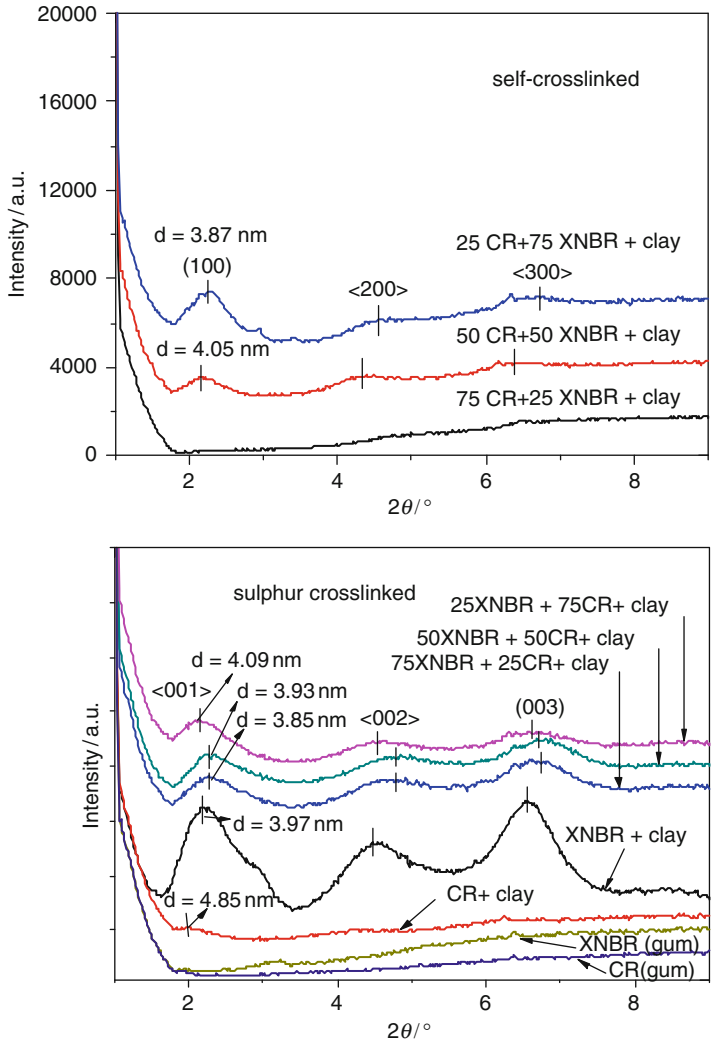

Fig. 50 WAXD patterns of CR and XNBR and their blends obtained from self-crosslinking (*top*) and sulfur crosslinking (*bottom*) processes

promotes higher intercalation of the CR chains. As far as the diffraction patterns of the blends are concerned, in all cases three distinct harmonic peaks are observed, which are the reflections of <001> plane and so on. It is shown that as the content of CR in blends increases from 25% to 75%, the interlayer *d*-spacing of the organoclay increases gradually from 3.85 to 4.09 nm, demonstrating that higher CR levels lead to better intercalation of the clay.

The T_g of a rubber or polymer depends on the structure and cooperative mobility of the chain segments. Only one glass transition is expected if two polymers are

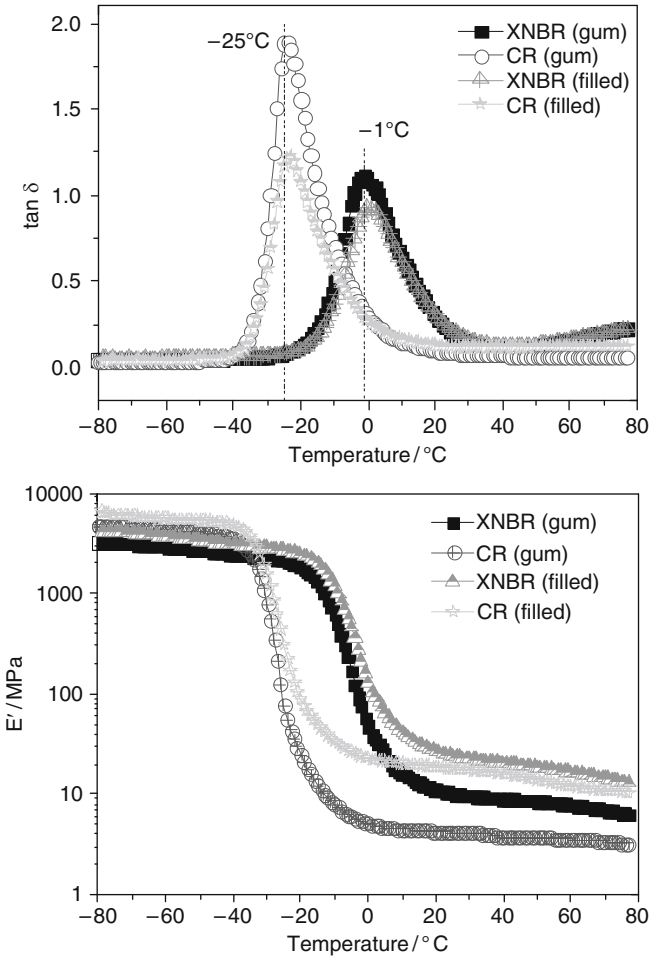

Fig. 51 DMTA plots of tan δ versus temperature (*top*) and storage modulus versus temperature (*bottom*) for XNBR and CR compounds vulcanized by sulfur

completely miscible. In the case of partially miscible blends, the T_g values of the blend components are separated but shifted towards each other as compared with the pure components. The T_g values remain largely unaltered for a completely immiscible blend. Figure 51 shows the tan δ dependencies on temperature for the pure CR and XNBR, crosslinked with sulfur and containing 10 phr organoclay. The results are compared with the corresponding gum rubber matrix without any filler. Gum as well as filled CR rubber matrices show a T_g at $-25°C$, whereas XNBR shows the transition at $-1°C$. In both cases, the incorporation of 10 phr organoclay remarkably reduces the peak heights, which indicates strong reinforcement by the organoclay. The presence of intercalated organoclays restricts the mobility of the

rubber chains due to their confinement between the layers. More precisely, it can be stated that the polar nature of CR and XNBR intercalates or exfoliates the silicate layers very efficiently and a strong rubber–filler interaction is established. Section 3.3.2 discusses an additional dielectric relaxation phenomenon, which was mainly governed by the chemical interaction of layered silicate with XNBR at higher temperature than T_g [39]. The plots of storage modulus (E') with temperature also indicate a strong reinforcement offered by the organoclay, since a considerable increase in E' of moderate temperatures is observed (Fig. 51). It is clear that two widely separated different T_g values primarily indicate the immiscibility of the phase if a blend is prepared with those rubbers. The damping behavior (tan δ) of the blends with increasing temperature delivers some interesting information about the miscibility of the rubber with two different T_g values. For easy understanding, the T_g values obtained from temperature sweep experiments are listed in Table 11. It can be seen from this table that with the increase of XNBR content the T_g values of CR and XNBR shift to a lower temperature in all composites. This decrease in T_g of the polymers may be explained if one considers the difference in the thermal expansion coefficient of the respective polymers in a blend, resulting in thermal stress across the boundary and development of a negative pressure within the rubber domains. Thus, the free volume of the rubber component increases and, consequently, the motion of the rubber chain becomes easier [92]. After analyzing the data in the table it is observed that the separation factor between the two T_g peaks is increased in all blends containing layered silicate, and that the difference between those T_g is maximum for the 50/50 rubber blend. For the clay-containing 50/50 blend, the separation is 26°K, whereas the separation is 20°K for the same blend without organoclay. So, presence of 10 phr organoclay makes the blends more heterogeneous as compared to their virgin composition. This finding also supports the inhibition action of layered silicate to self-crosslinking by blocking the carboxylic group from forming hydrogen bonds with the silanol group of the clay layers, rendering the carboxylic group passive to crosslinking. As far as the storage modulus (E') of the self-crosslinked blends is concerned, a relaxation at 40°C is observed in all the blends (Fig. 52). This relaxation arises due to melting of crystalline domains of the CR chains, and the effect is more prominent in blends of higher CR content without any filler. In the presence of organoclay, the

Table 11 Glass transition temperature of self-crosslinked CR/XNBR rubber blends

Rubber	Glass transition temperature (°C)					
	Without clay			With clay		
CR:XNBR	CR peak	XNBR	Separation between two peaks	CR peak	XNBR peak	Separation between two peaks
100:0	−25	*a*	–	−25	*a*	–
75:25	−23	−4	19	−24	−4	20
50:50	−26	−6	20	−28	−2	26
25:75	−29	−8	21	−30	−7	23
0:100	*a*	−1	–	*a*	–1	–

a absent for that particular case

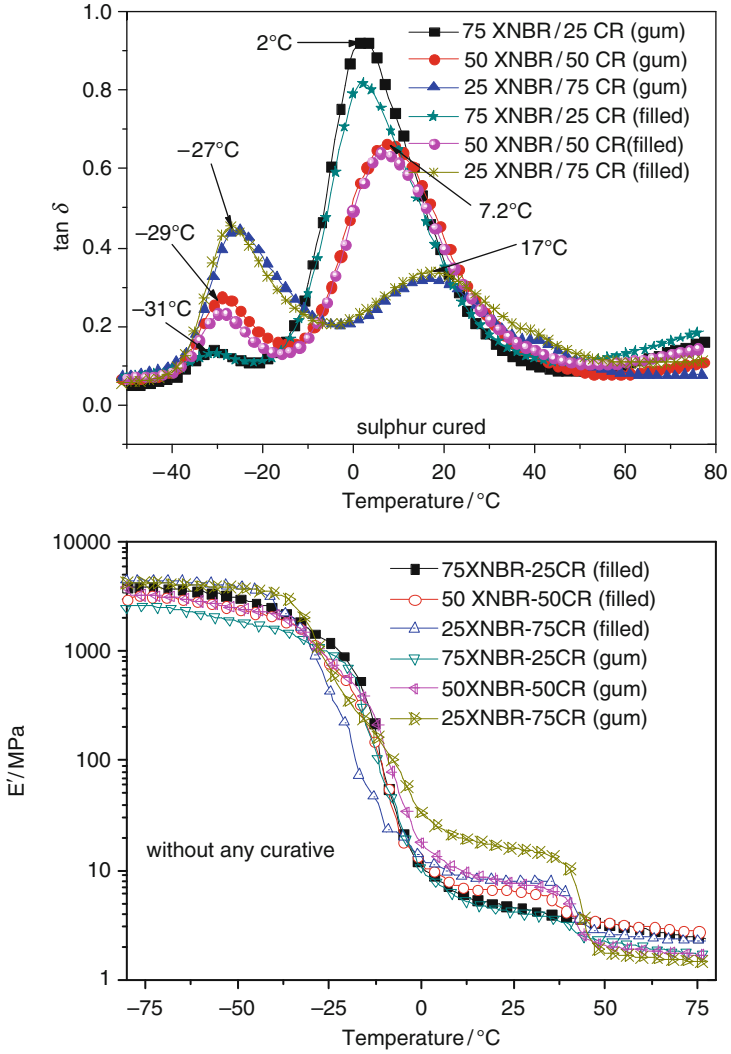

Fig. 52 Tan δ versus temperature plots of CR-XNBR blends vulcanized by sulfur (*top*). Storage modulus versus temperature plots of self-crosslinked CR-XNBR blends (*bottom*)

crystalline nature of the CR phase is reduced. It will be also interesting to discuss the damping behavior of those composites that are crosslinked by sulfur curatives. Figure 52 shows tan δ versus temperature curves obtained from sulfur-crosslinked CR/XNBR blends in the presence and absence of organoclay. All the curves possess two distinct relaxation peaks at different temperatures. It can be observed that with the increase of CR content in the blends, the T_g values corresponding to XNBR are shifted to a higher temperature to a remarkable extent; the T_g of XNBR in the

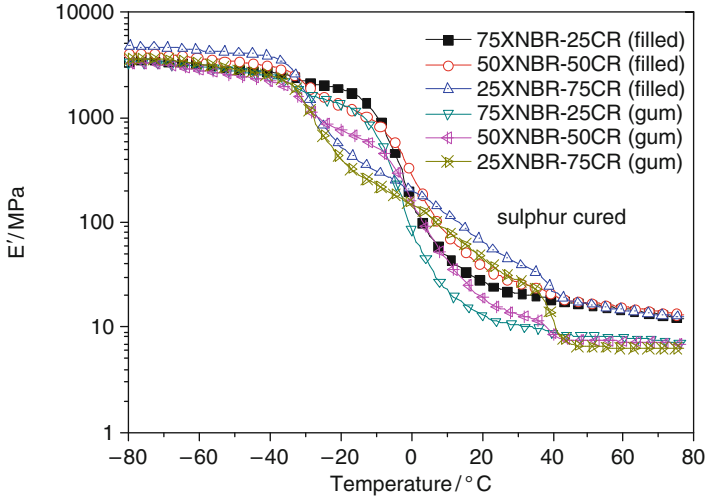

Fig. 53 Storage modulus versus temperature plots of CR-XNBR blends vulcanized by sulfur

25 XNBR/75 CR blend is shifted from –1 to 17°C as compared with pure XNBR. However, the shifting of T_g of the corresponding CR portion is only a few degrees. This may be explained by considering the polarity difference between XNBR and CR. Migration of curatives can take place from the less polar CR part to the more polar XNBR part and, ultimately, the XNBR phase becomes highly crosslinked. Thus, the mobility of the XNBR chains is greatly reduced and the T_g increases to a considerable extent. Any significant change in the damping behavior is not noticed after incorporation of the organoclay in the rubber blends. It is also evident from Fig. 52 that E' decreases with increasing temperature and that all the blends show a three-step relaxation process. The first two steps arise from the glass transition of the CR and XNBR phase and the third relaxation at ≈40°C is supposed to come from the microcrystalline phase of CR chain segments. At this temperature, the crystal structures disappear and an extra slippage within the crystal domain of the rubber chain takes place. The same behavior of E' against temperature can be observed from the sulfur-cured CR/XNBR blends. Figure 53 shows the temperature dependency of the storage modulus of those sulfur-cured samples. From this figure the clear crystalline nature of CR at the blend composition 75 CR/25 XNBR can also be observed. Morphological heterogeneity makes the CR phase more crystalline with the higher content of CR, in spite of a strong sulfur crosslinking network in the blend matrix. However, above 40°C the storage modulus of filled blends show a higher E' value as compared to the corresponding gum blends, demonstrating the apparent reinforcing ability of organoclay in all blends irrespective of their composition.

The micrographs obtained from scanning electron microscopy are shown in Fig. 54 for the tensile fractured surface of 50 CR/50 XNBR self-crosslinked blend filled with 10 phr layered silicate (Fig. 54a) and for the same blend without any

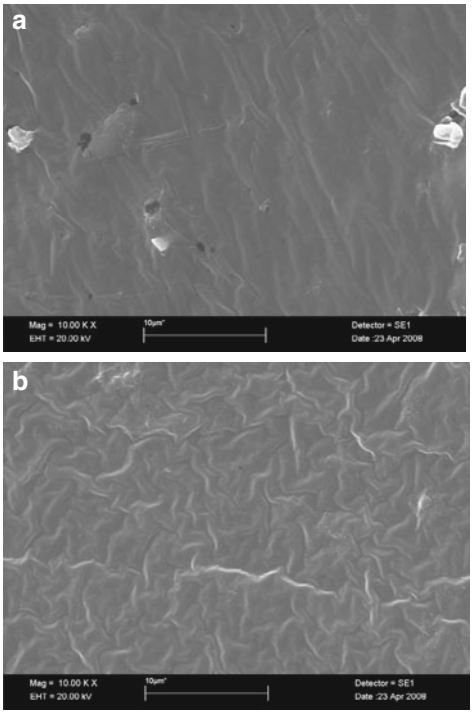

Fig. 54 Scanning electron micrographs of the tensile fractured surface of 50 CR/50 XNBR blends with modified layered silicate (**a**) and without any filler (**b**)

layered silicate (Fig. 54b). It is evident from Fig. 54a that some agglomerates of organoclay are pulled out from the matrix onto the fractured surface. As compared with Fig. 54b, there is a very clear difference in the texture of the surface. The surface of the gum rubber is more homogeneous and displays a knitting texture, which is a characteristic of a partially compatibilized rubber blend containing XNBR as one of the constituents [93]. In contrast, the surface of filled rubber does not have this texture. The inhomogeneous surface obtained from filled rubber vulcanizates clearly indicates the poor tensile properties. These findings confirm the negative influence of layered silicate on the compatibility of CR and XNBR phases.

6 Rubber–Anionic Clay Nanocomposites

During the past decade, rubber-layered silicate nanocomposites have been extensively studied for a variety of applications and in this review the preparation and characterization of such layered silicate–rubber composites is discussed. However, use of another type of clay, called anionic clay or LDH, in the rubber matrix is rather uncommon. In this section, rubber–LDH nanocomposites are described, including the synthesis and characterization of OLDH, preparation of rubber–LDH nanocomposites, and their special properties [94, 95].

6.1 Synthesis

It can be easily understood that the homogeneous and stable dispersion of LDH in rubber is a very difficult task because of organic–inorganic incompatibility and strong attractive forces between the two hydroxides layers. However, it is necessary to obtain a homogenous dispersion of nanoparticles in the rubber matrix to get a significant improvement in mechanical properties with a small filler concentration. As mentioned in the discussion in Sect. 2.3, to obtain good dispersion of LDH in the rubber matrix, the organic modification of LDH is necessary before using it as a filler. Generally, there are three main modification methods for preparing OLDH:

1. *Regeneration*: Many LDH materials show a unique phenomenon called "memory effect," which involves the regeneration of the layered crystalline structure from their calcinated form when the latter is dispersed in an aqueous solution containing suitable anions [96]. This property is often used to synthesize and modify LDH with different types of intercalating anions. The regeneration property shown by LDH is extensively reported in the literature [97, 98].
2. *Anion exchange*: This method takes the advantage of exchangeable interlayer anions present in LDH by other anionic species. Based on this property, the LDH containing one type of intercalating anionic species can be synthesized from the LDH containing another type of intercalating anion. Usually, the original LDH is dispersed in an aqueous solution of the desired anionic species and the dispersion is stirred at room temperature for several hours. However, some anionic species show more affinity for the intergallery region of LDH than others [99].
3. *One step synthesis*: This is an effective and easy method for preparation of OLDH and was developed recently. No additional measures other than controlling the pH of the medium are required to obtain a high degree of intercalation by the surfactant, retaining the high crystallinity independently of the presence of other anions, like NO_3^-, CO_3^{2-} and Cl^- [100, 101]. During synthesis, the pH value is kept constant by adding suitable amounts of base solution into the system solution containing the modifier agent. After addition of the mixed metal salt solution, the resulting slurry is continuously stirred at the same temperature for some time and then allowed to age in a heater for several hours. This method for modification of LDH is more effective than the other two methods.

6.2 Preparation and Characterization of Rubber–LDH Nanocomposites

There are few reports on rubber–LDH nanocomposites in which they have been prepared mostly by solution intercalation methods and not by a conventional technique for processing rubber-based composites [102, 103]. But, the melt

Table 12 Compound formulations for EPDM–LDH and XNBR–LDH nanocomposites [104]

Ingredient	Ingredient content (phr)	
	EPDM–LDH	XNBR–LDH
Elastomer	100	100
LDH-C10	X[a]	X[a]
ZnO	3.0	1.0
Stearic acid	1.5	1.0
Sulfur	1.5	0.5
MBT	1.5	2.0
TMTD	0.3	–

MBT mercaptobenzothiazole, *TMTD* tetramethyl thiuram disulfide

[a]The value of X is 0, 5, 7.5 or 10 phr. Accordingly, the EPDM/LDH system is designated as EL0, EL5, EL7.5 and EL10, and the XNBR/LDH system as XL0, XL5, XL7.5 and XL10

compounding method still remains promising to a large extent for preparing elastomer–LDH nanocomposites. Pradhan et al. [104] investigated how the matrix polarity and the presence of reactive functional groups on the rubber chain influenced the dispersion of LDH particles, the rubber–filler interfacial adhesion and the mechanical properties of the elastomer–LDH nanocomposites prepared by the melt compounding method. Two elastomer matrices widely differing in polarity and chemical nature such as a nonpolar elastomer, i.e., EPDM (surface energy about 34.0 mJ m^{-2}) and a polar functionalized elastomer, i.e., XNBR (surface energy about 52.0 mJ m^{-2}) were chosen as the base matrix. The EPDM–LDH and the XNBR–LDH nanocomposites containing different weight percentages of LDH-C10 (LDH modified by $C_{10}H_{21}SO_3Na$, called C10) were prepared via a melt compounding method. The compound formulations for each set of the nanocomposites are given in Table 12.

The WAXS patterns of two nanocomposites at different LDH concentrations are shown in Fig. 55. The similarity of these patterns between the two systems is that the first three Bragg's reflections of LDH-C10 can be detected in both. This means that the LDH particles are not fully exfoliated in any of the matrices.

However, these reflections were broad and not well defined, indicating that LDH particles in EPDM–LDH nanocomposites had a highly disordered structure. On the other hand, The WAXS patterns of XNBR–LDH nanocomposites (Fig. 55b) revealed distinct evidence of intercalation of the polymer chains in the LDH-C10 particles. The shifting of the first Bragg's reflection to a lower scattering angle corresponded to an increase of the interlayer distance by about 0.80 nm. This meant that a multiple number of XNBR chains were aligned within the interlayer space of LDH-C10. The polar/ionic interaction between the functionalities on XNBR and LDH particles might play a major role in easy intercalation of the XNBR chains within LDH-C10 layers without disturbing the crystalline order of the LDH-C10 particles. On the other hand, in an investigation of CR–LDH nanocomposites [23] it was observed that the first reflection from the nanocomposite showed at 3.17 nm, whereas the pure OLDH had a reflection of the same plane at 2.96 nm. However, in

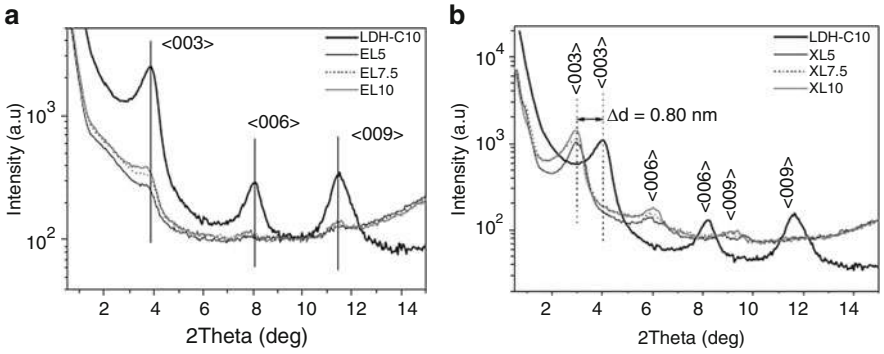

Fig. 55 WAXS patterns of the EPDM–LDH nanocomposites (**a**) and XNBRLDH nanocomposites (**b**) (the *number* at the end of sample designation EL and XL indicates the amount of LDH-C10 in phr) [104]

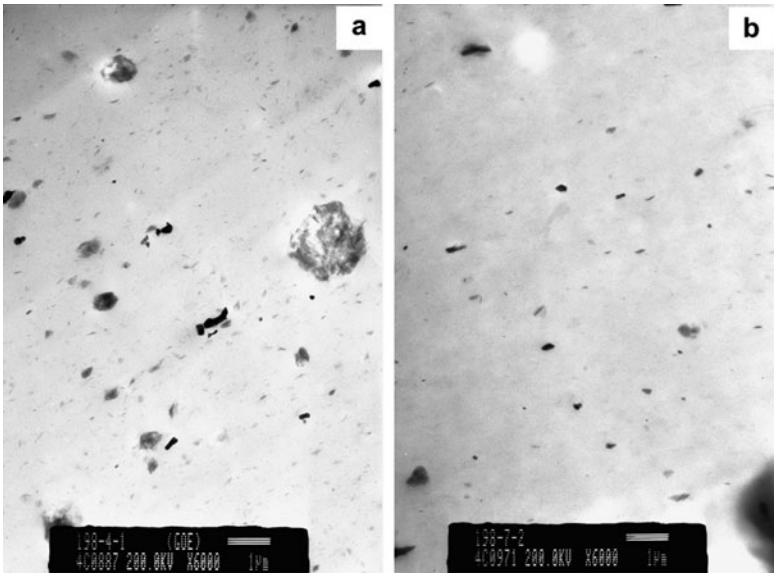

Fig. 56 TEM micrographs of EPDM–LDH (**a**) and XNBR–LDH (**b**) nanocomposites with LDH-C10 content of 5 phr. *Scale bars*: 1 μm [104]

the case of pure LDH there was no change in the peak position after incorporation of the LDH in the CR matrix.

The conclusions made from the WAXS patterns of the nanocomposites could be further established by analyzing the TEM micrographs of these materials. The micrographs for both the systems containing 7.5 phr of LDH-C10 are shown in Fig. 56. It is clear that in these nanocomposites, LDH-C10 particles were dispersed

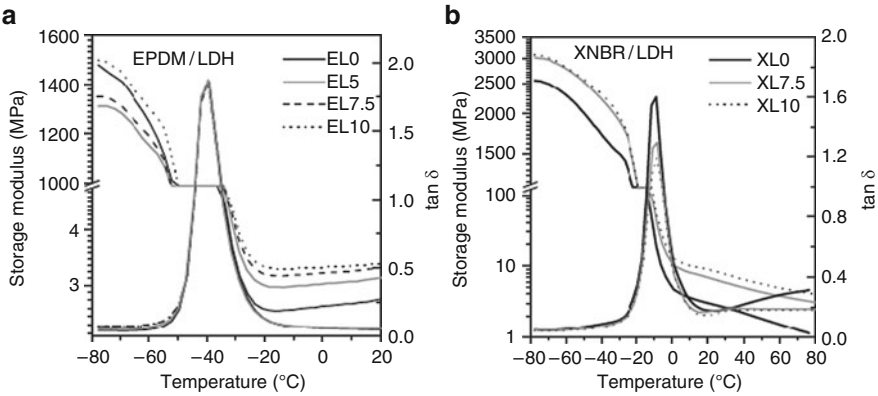

Fig. 57 Dynamic mechanical analyses of EPDM–LDH and XNBR–LDH nanocomposites [104]

in three different forms: as exfoliated fragments with lateral dimension below 100 nm, as primary particles with lateral dimension from a few hundred nanometers to 1−2 μm, and as soft clusters of the primary particles with lateral dimensions of over a few micrometers. In the case of the EPDM–LDH system, the proportions of the last two forms were much higher than the exfoliated fragments, whereas in XNBR–LDH the extent of the exfoliated fragments predominates with less or no cluster formation, showing the homogenous dispersion throughout the matrix, even at this magnification.

The addition of OLDH as nanofiller in rubber must affect significantly the materials properties in comparison to the pristine polymer or conventional composites, including enhanced mechanical properties, increased heat resistance, and decreased flammability.

Pradhan et al. [104] found that the trends in the variation of the storage modulus with increasing LDH-C10 concentration in the low temperature region (below the T_g of the respective system) were strikingly different between EPDM–LDH and XNBR–LDH systems (as shown in Fig. 57). For XNBR–LDH nanocomposites, the storage modulus increased with increasing LDH-C10 amount, whereas for EPDM–LDH it decreased first and then increased. The authors believed that at low LDH-C10 concentration, the EPDM–LDH nanocomposites showed a softening effect below T_g. Because LDH-C10 contains a large fraction of its weight as anionic surfactant, a part of this surfactant adhered on the outer surface of the LDH particles might be loosely bound and could eventually increase the mobility of the polymer matrix in the polymer–filler interfacial region. This interfacial plasticizing effect could be more influential when the reinforcing effect of the filler particle is low and when small or no secondary interaction occurr between the polymer and the filler. In the case of EPDM–LDH nanocomposites, there existed a weak interaction at the interface at low LDH-C10 concentration, resulting in a lower storage modulus value at low temperature. However, in the case of XNBR–LDH nanocomposites, due to strong interfacial interaction between LDH-C10 particles and the XNBR

Table 13 Summary of the mechanical properties of EPDM–LDH and XNBR–LDH nanocomposites [104]

Sample	LDH-C10 content (phr)	Tensile strength (MPa)	SD	200% modulus (MPa)	SD	Elongation at break (%)	SD
EPDM–LDH							
EL0	0.0	1.54	0.08	0.73	0.01	222	16
EL5	5.0	2.38	0.34	0.78	0.01	390	15
EL7.5	7.5	2.68	0.50	0.84	0.01	420	20
EL10	10.0	3.25	0.35	0.85	0.01	505	34
XNBR–LDH							
XL0	0.0	1.94	0.22	0.41	0.01	1,240	59
XL5	5.0	11.96	1.47	1.10	0.01	1,220	40
XL7.5	7.5	16.52	1.32	1.31	0.03	1,205	36
XL10	10.0	17.83	1.59	1.72	0.08	1,047	53

SD standard deviation

matrix, the reinforcing effect dominated over the whole temperature region used in the experiment. At temperatures above T_g, the segmental movements of the polymer chains become operative and hence the plasticizing effect due to small molecules at the interface becomes less significant. As a result, the storage modulus in both systems increased with increasing LDH-C10 concentration. Figure 57 also shows the variation of tan δ in the two systems with changing LDH-C10 concentration. In EPDMLDH no noticeable change in the maximum tan δ value was observed with increasing LDH-C10 concentration, indicating weak or no interaction between the EPDM matrix and the dispersed LDH-C10 particles. On the other hand, the tan δ maximum steadily decreased with increasing filler concentration in XNBR–LDH, showing once again the strong interaction at the interface. Similar conclusions can also be found in our recent report [105].

For both EPDM–LDH and XNBR–LDH nanocomposites, the various tensile properties are summarized in Table 13 and their typical stress–strain plots are shown in Fig. 58 [104]. In Fig. 58a, the gum vulcanizates of both rubber systems showed typical NR-like stress–strain behavior with a sharp upturn in the stress–strain plot after an apparent plateau region, indicating strain-induced crystallization. With the addition of LDH-C10 in the XNBR matrix, the stress value at all strains increased significantly, indicating that the matrix undergoes further curing (Fig. 58b).

The upturn in the stress–strain plot became more prominent and the plateau region diminished with increasing LDH-C10 concentration. On the other hand, in EPDM–LDH nanocomposites, the overall nature of the stress–strain plot was not changed much except for a significant increase in elongation at break and the tensile strength (Fig. 58c). At higher concentration of LDH-C10, a small upturn in the stress–strain plot could also be observed in EPDM–LDH system. Although in both EPDM and XNBR, LDH-C10 shows a reinforcing effect, the changes in mechanical properties in XNBR are much more significant. The polar/ionic interaction between XNBR and LDH-C10 particles can account for this difference. This means that the

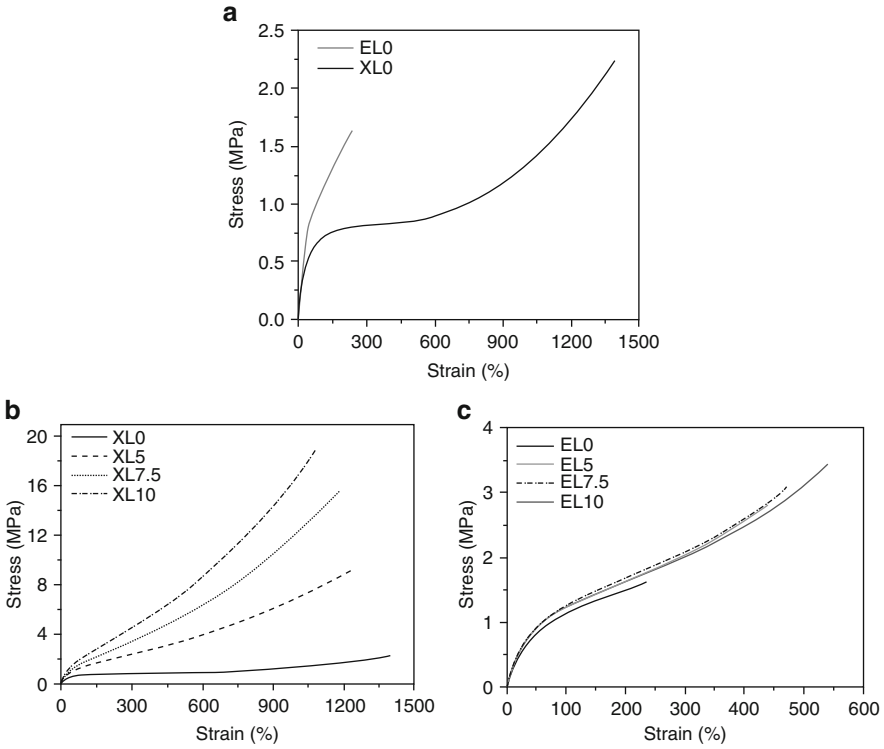

Fig. 58 Typical stress–strain plots of EPDM and XNBR gum vulcanizates (**a**), XNBR–LDH nanocomposites (**b**), and EPDM–LDH nanocomposites (**c**) [104]

differences in the dispersion of the nanoparticles and the interfacial adhesion directly influence the mechanical properties of the nanocomposites. In the report on rubber nanocomposites containing ethylene vinyl acetate (EVA) having 60 wt% of vinyl acetate content and OLDH as nanofiller, Kuila et al. [106] also found that EVA–LDH nanocomposites showed improved mechanical properties such as tensile strength and elongation at break in comparison with neat EVA.

Unquestionably, rubber materials are used in many applications. However, most rubber materials are flammable and produce large amounts of smoke on burning. In some special application fields, such as in building (flooring), transport, conveying belts, the fire retardancy of rubber materials is necessary. This disadvantage limits their usage in some areas. Usually, halogen-containing flame retardants such as decabromobiphenyl have been most widely used [107]. However, halogen-containing flame retardants produced large amounts of smoke and are corrosive on burning, and thus their use is limited. It was therefore worthwhile to investigate novel methods for improving the flame retardancy of rubber with the halogen-free flame retardants. Although the fire retardant properties of rubber materials are quite important, there are few reports on this aspect. LDH has promise as potential halogen-free flame-retardant for rubber.

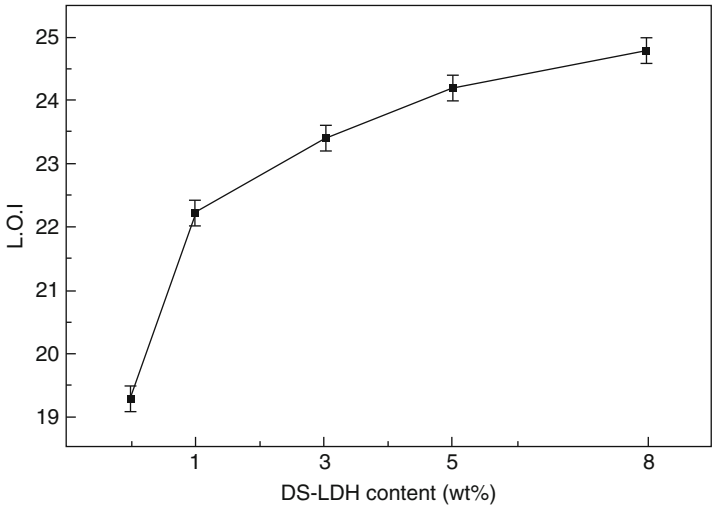

Fig. 59 Effect of LDH content on the limiting oxygen index values of nanocomposites of EVA-60 and DS-LDH [106]

Kuila et al. [106] studied the flammability of EVA–LDH nanocomposites with different LDH loading. The results shown in Fig. 59 represent the findings on the limiting oxygen index (LOI) of neat EVA and its nanocomposites.

During the burning test, it was observed that burning of pure EVA took place very rapidly in comparison to its corresponding nanocomposites. Calculation showed that the LOI values were relatively higher for the nanocomposites than for neat EVA (19.3). The maximum value of LOI (24.8) was noted for 8 wt% LDH content in EVA. The main reason was attributed to the presence of a char layer in the nanocomposites that impeded burning while acting as a barrier between the burning surface and supplied oxygen. For the nanocomposites with LDH content of 3 wt%, the thickness of the char layer looked thin and weak, whereas beyond 3 wt% of LDH loading, the formation of a thick char layer was likely to suppress the propagating downward flame by disrupting oxygen supply to the burning specimen. On the other hand, the authors also thought that the endothermic decomposition of LDH produced sufficient water vapor to account for the reduction of flammable characteristics in the case of nanocomposites as well as in the case of thermoplastic–LDH nanocomposites [108, 109].

7 Conclusion

We have presented several examples of the successful preparation of rubber nanocomposites with layered silicate as the inorganic phase. This review explores the idea that the designing and compounding are key factors in obtaining the

intercalated–exfoliated structure of the clay minerals in the rubber matrix, which ultimately governs the final physical properties of the composites. It has been realized that the melt-intercalation method is more effective if proper processing conditions and compounding techniques are carefully selected. Special attention is required in the selection of vulcanizing ingredients for the rubber formulation in order to achieve a superior degree of intercalation and exfoliation of the organoclay. Compatibility between two chemically dissimilar rubbers was understood by the accomplishment of the exfoliated–intercalated layers at the interface between the rubber phases. It is true that nanoclay does not always provide a positive effect in improving the compatibility between two dissimilar rubbers. In particular, the layered silicates are potentially unable to enhance or improve the compatibility, rather they induce more phase separation at the interface. In the presence of layered silicates, the self-crosslinking reactions between CR and XNBR were studied and the influence of the incorporation of the layered silicates on the physical properties was investigated. It was found that the presence of the intercalated silicate particles in the blend matrix does not improve the physical properties, especially in the case where the blend was vulcanized without the addition of any curatives.

References

1. Kojima Y, Usuki A, Kawasumi M, Okada A, Fukushima Y, Kurauchi T, Kamigaito O (1993) J Mater Res 8:1185
2. de Paiva LB, Morales AR, Diaz FRV (2008) Appl Clay Sci 42:8–24
3. Ibarra L, Rodríguez A, Mora I (2007) Eur Polym J 43:753
4. Wu YP, Zhang LQ, Wang YQ, Liang Y, Yu DS (2001) J Appl Polym Sci 82:2842
5. Goettler LA (2005) 63rd Annual Technical Conference by Society of Plastics Engineers, May 1–5, Boston
6. Das A, Jurk R, Stöckelhuber KW, Majumder PS, Engelhardt T, Fritzsche J, Klüppel M, Heinrich G (2009) J Macromol Sci Chem 46:7–15
7. Hwang WG, Wei KH, Wu CM (2004) Polymer 45:5729
8. Kim JT, Oh TS, Lee DH (2003) Polym Int 52:1203
9. Nah CW, Ryu HJ, Kim WD, Choi SS (2002) Polym Advn Technol 13:649
10. Hwang WG, Wei KH, Wu CM (2004) Polym Eng Sci 44:2117–2124
11. Liu L, Jia D, Luo Y, Guo B (2006) J Appl Polym Sci 100:1905–1913
12. Han M, Kim H, Kim E (2006) Nanotechnology 17:403–409
13. Kim JT, Lee DY, Oh TS, Lee DH (2003) Appl Polym Sci 89:2633–2640
14. Usuki A, Tukigase A, Kato M (2002) Polymer 43:2185
15. Varghese S, Karger-Kocsis J (2004) J Appl Polym Sci 91:813
16. Das A, Jurk R, Stöckelhuber KW, Heinrich G (2007) Express Polym Lett 1:17
17. Ma Y, Li QF, Zhang LQ, Wu YP (2007) Polym J 39:48
18. Das A, Jurk R, Stöckelhuber KW, Heinrich G (2008) Macromol Mater Eng 293:479–490
19. Das A, Debnath SC, De D, Naskar N, Basu DK (2004) Polym Advn Technol 15:551
20. Das A, De D, Naskar N, Debnath SC (2006) J Appl Polym Sci 99:1132
21. Yeh MH, Hwang WS, Cheng LR (2007) Appl Sur Sci 253:4777–4781
22. Wang Y, Zhang H, Wu Y, Wang J, Zhang L (2005) J Appl Polym Sci 96:318–323
23. Das A, Costa FR, Wagenknecht U, Heinrich G (2008) Eur Polym J 44:3456–3465

24. Wang DY, Costa FR, Leuteritz A, Schoenhals A, Anastasia V, Scheler U, Wagenknecht U, Kutlu B, Heinrich G (2010) Polyolefin nanocomposites with layer double hydroxides. In: Mittal V (ed) Advances in polyolefin nanocomposite. CRC, Boca Raton
25. Wang DY, Das A, Leuteritz A, Boldt R, Häußler L, Wagenknecht U, Heinrich G (2010) Polym Degrad Stab (in press) doi:10.1016/j.polymdegradstab.2010.03.003
26. Sae-Oui P, Sirisinha C, Thepsuwan U, Hatthapanit K (2007) Eur Polym J 43:185–9316
27. Ma J, Xu J, Ren JH, Yu ZZ, Mai YW (2003) Polymer 44:4619
28. Mousa A, Karger-Kocsis J (2001) Macromol Mater Eng 4:286
29. Jia QX, Wu YP, Wang YQ, Lu M, Zhang LQ (2008) Comp Sci Technol 68:1050–1056
30. Al-Yamani F, Goettler LA (2007) Rub Chem Technol 80:100–114
31. Jia QX, Wu YP, Xu YL, Mao HH, Zhang LQ (2006) Macromol Mater Eng 291:218–226
32. Jia QX, Wu YP, Wang YQ, Lu M, Yang J, Zhang LQ (2007) J Appl Polym Sci 103:1826–1833
33. Ma J, Xiang P, Mai YW, Zhang LQ (2004) Macromol Rapid Commun 25:1692–1696
34. Sadhu S, Bhowmick AK (2004) J Appl Polym Sci 92:698–709
35. Ganter M, Gronski W, Reichert P, Mülhaupt R (2001) Rubb Chem Technol 74:221235
36. Sadhu S, Bhowmick AK (2003) Rubb Chem Technol 76:860–874
37. Das A, Heinrich G, Jurk R, Stöckelhuber KW, Herrmann W, Recker C, Schmidt C (2007) German Patent File no. 10 2006 014 873.5
38. Das A, Jurk R, Stöckelhuber KW, Engelhardt T, Fritzsche J, Klüppel M, Heinrich G (2008) J Macromol Sci Chem 45:144–150
39. Fritzsche J, Das A, Jurk R, Stöckelhuber KW, Heinrich G, Klüppel M (2008) Express Polym Lett 2:373
40. Eisenberg A, Hird B, Moor RB (1990) Macromolecules 23:4098
41. Heinrich G, Klüppel M (2002) Adv Polym Sci 160:1–44
42. Kalgaonkar RA, Jog JP (2008) J Polym Sci Phys 46:2539–2555
43. Rao Y, Pochan JM (2007) Macromolecules 40:290
44. Hernandez MC, Suarez N, Martinez LA, Feijoo JL, Mocano SL, Salazar N (2008) Phys Rev E 77:051801
45. Page KA, Adachi K (2006) Polymer 47:6406
46. Psarras GC, Gatos KG, Karger-Kocsis J (2007) J Appl Polym Sci 106:1405
47. Steeman PAM, van Turnhout J (1997) Colloid Polym Sci 275:106–115
48. Wübbenhorst M, van Turnhout J (2000) Dielectric Newsletter 14:1–3
49. Morgan AB, Gilman JF (2003) J Appl Polym Sci 87:1327
50. Eckel DF, Balogh MP, Fasulo PD, Rodgers WR (2004) J Appl Polym Sci 93:1110
51. Herrmann W, Uhl C, Heinrich G, Jehnichen D (2006) Polym Bull 57:395
52. Katti KS, Sikdar D, Katti DR, Ghosh P, Verma D (2006) Polymer 47:403
53. Gatos KG, Százdi L, Pukánszky B, Karger-Kocsis J (2005) Macromol Rapid Commun 26:915–919
54. Gatos KG, Karger-Kocsis J (2005) Polymer 46:3069–3076
55. Vaia RA, Liu W (2002) J Polym Sci Part B Polym Phys 40:1590
56. Kim JT, Lee DY, Oh TS, Lee DH (2003) J Appl Polym Sci 89:2633
57. Liu L, Jia Y, Luo B, Guo B (2006) J Appl Polym Sci 100:1905
58. Das A, Debnath SC, Naskar N, Pal S, Datta RN (2005) Kautsch Gummi Kunstst 6:304
59. Ma Y, Wu Y-P, Zhang LQ, Li QF (2008) J Appl Polym Sci 109:1925–1934
60. Ishida H, Campbell S, Blackwell J (2000) Chem Mater 12:1260
61. Burrell H, (1995) Solubility parameter values. In: Bandrup J, Immergut EH (eds) Polymer handbook, 2nd edn. Wiley, New York, pp 337–359
62. Thielen G (2007) Kautsch Gummi Kunstst 60:389
63. Ghosh AK, Naskar N, Debnath SC, Basu DK (2001) J Appl Polym Sci 81:800
64. Das A, Ghosh AK, Pal S, Basu DK (2004) Polym Advan Technol 15:197
65. Das A, Ghosh AK, Basu DK (2005) Kautsch Gummi Kunstst 58:230
66. Vo LT, Giannelis EP (2007) Macromolecules 40:8271

67. Baghaei B, Jafari SH, Khonakdar HA, Rezaeian I, As'habi L, Ahmadian S (2009) Polym Bull 62:255–270
68. Fang Z, Harrats C, Moussaif N, Groeninckx G (2007) J Appl Polym Sci 106:3125
69. SinhaRay S, Bandyopadhyay J, Bousmina M (2007) Macromol Mater Eng 292:729
70. Kawazoe M, Ishida H (2008) Macromolecules 41:2931
71. Zhang P, Huang G, Liu Z (2009) J Appl Polym Sci 111:673
72. García-López D, López-Quintana S, Gobernado-Mitre I, Merino JC, Pastor JM (2007) Polym Eng Sci 47:1033
73. Arroyo M, Lópej-Manchado MA, Valentin JL, Carretero J (2007) Comp Sci Technol 67:1330–1339
74. Das A, Stöckelhuber KW, Heinrich G (2009) Macromol Chem Phys 210:189–199
75. Das A, Naskar N, Basu DK (2004) J Appl Polym Sci 91:1913
76. Deuri AS, Bhowmick AK (1987) J Appl Polym Sci 34:2205–2222
77. Ramesan MT, Mathew G, Kuriakose B, Alex R (2001) Eur Polym J 37:719–728
78. Good RJ, Girifalco LA (1960) J Phys Chem 64:561
79. Stöckelhuber KW, Das A, Jurk R, Heinrich G (2009) Proceedings of the 17. NDVak, Dresden, pp. 112–115. ISBN: 978-3-9812550-1-0
80. Göldel A, Kasaliwal G, Pötschke P (2009) Macromol Rapid Commun 30:423–429
81. Voulgaris D, Petridis D (2002) Polymer 43:2213
82. Li Y, Shimizu H (2004) Polymer 45:7381
83. Ramorino G, Bignotti F, Conzatti L, Riccol T (2007) Polym Eng Sci 47:1650
84. Fritzsche J, Klüppel M (2009) Kautsch Gummi Kunstst 62:16
85. Ganter M, Gronski W, Reichert P, Mülhaupt R (2001) Rubber Chem Technol 74:221
86. Antony P, De SK, Van Duin M (2001) Rub Chem Technol 74:376
87. Mukhopadhyay S, De SK (1991) J Appl Polym Sci 43:2283
88. Miyata Y, Atsumi M (1988) J Polym Sci Part A Polym Chem 26:2561
89. Johnson PR (1976) Rubber Chem Technol 49:650
90. Kovacis P (1955) Rubber Chem Technol 28:1021
91. Wolf S, Donnet JB (1976) Rubber Chem Technol 49:650
92. Tomova D, Kressler J, Radusch HJ (2000) Polymer 41:7773
93. Biswas T, Das A, Debnath SC, Naskar N, Das AR, Basu DK (2004) Eur Polym J 40:847
94. Sergey V, Ion D, Fan XW, Rigoberto A (2004) Macromol Rapid Commun 25:498
95. Wang DY, Wang YZ, Wang JS, Chen DQ, Zhou Q, Yang B, Li WY (2005) Polym Degrad Stab 87:171
96. Miyata S (1980) Clays Clay Miner 28:50
97. Meyn M, Beneke K, Legaly G (1990) Inorg Chem 29:5201
98. Stanimirova TS, Kirov G, Dinolova E (2001) J Mater Sci Lett 20:453
99. Khan AI, O'Hare D (2002) J Mater Chem 12:3191
100. Wang DY, Costa FR, Anastasia V, Leuteritz A, Scheler U, Jehnichen D, Wagenknecht U, Häußler L, Heinrich G (2009) Chem Mater 21:4490
101. Wang DY, Leuteritz A, Wagenknecht U, Heinrich G (2009) Trans Nonferrous Met Soc China 6:1470
102. Acharya H, Srivastava SK, Bhowmick AK (2007) Comp Sci Tech 67:2807
103. Acharya H, Srivastava SK, Bhowmick AK (2007) Nanoscale Res Lett 2:1
104. Pradhan S, Costa FR, Wagenknecht U, Jehnichen D, Bhowmick AK, Heinrich G (2008) Eur Polym J 44:3122
105. Thakur V, Das A, Mahaling RN, Rooj S, Gohs U, Wagenknecht U, Heinrich G (2009) Macromol Mater Eng 94(9):561
106. Kuila T, Srivastava SK, Bhowmick AK (2009) J Appl Polym Sci 111:635
107. Khattab MA (2000) J Appl Polym Sci 78:2134
108. Costa FR, Wagenknecht U, Heinrich G (2007) Polym Degrad Stab 92:1813
109. Costa FR, Saphiannikova M, Wagenknecht U, Heinrich G (2008) Adv Polym Sci 210:101